AMERICAN UNIVERSITY OF BEIRUT

MULTI SCALE PROBABILISTIC ANALYSIS OF THE ELASTIC MODULUS OF CONCRETE USING DIGITAL IMAGE PROCESSING

by
MAHA NASSER MRAD

A thesis
submitted in partial fulfillment of the requirements
for the degree of Master of Engineering
to the Department of Civil and Environmental Engineering
of the Faculty of Engineering and Architecture
at the American University of Beirut

Beirut, Lebanon
September 2016

AMERICAN UNIVERSITY OF BEIRUT

MULTI SCALE PROBABILISTIC ANALYSIS OF THE ELASTIC MODULUS OF CONCRETE USING DIGITAL IMAGE PROCESSING

by
MAHA NASSER MRAD

Approved by:

Dr. George Saad, Assistant Professor — Advisor
Civil and Environmental Engineering Department

Dr. Ghassan Chehab, Associate Professor
Civil and Environmental Engineering Department — Co-Advisor

Dr. Ibrahim Alameddine, Assistant Professor
Civil and Environmental Engineering Department — Member of Committee

Date of thesis defense: September 14, 2016

AMERICAN UNIVERSITY OF BEIRUT

THESIS, DISSERTATION, PROJECT RELEASE FORM

Student Name:	Mrad	Maha	Nasser
	Last	First	Middle

● Master's Thesis ○ Master's Project ○ Doctoral Dissertation

[X] I authorize the American University of Beirut to: (a) reproduce hard or electronic copies of my thesis, dissertation, or project; (b) include such copies in the archives and digital repositories of the University; and (c) make freely available such copies to third parties for research or educational purposes.

[ ] I authorize the American University of Beirut, **three years after the date of submitting my thesis, dissertation, or project,** to: (a) reproduce hard or electronic copies of it; (b) include such copies in the archives and digital repositories of the University; and (c) make freely available such copies to third parties for research or educational purposes.

September 23, 2016

Signature Date

ACKNOWLEDGEMENTS

I would first like to thank my thesis advisor Dr. George Saad of the Faculty of Engineering and Architecture at the American University of Beirut. The door to Prof. Saad office was always open whenever I ran into a trouble spot or had a question about my research or writing. He consistently steered me in the right the direction whenever he thought I needed it.

I would also like to thank my co-advisor Dr. Ghassan Chehab who guided me during these two years throughout all the experimental problems that I have faced. Dr. Chehab is truly a supportive professor and he pushed me always towards the best.

I would also like to acknowledge Dr. Ibrahim Alameddine as the second reader of this thesis, and I am gratefully indebted for his very valuable comments on this thesis.

I would like also to thank Mr. Helmi el – Khatib and Dima Hassanieh and the technicians Abdul Rahman and Bashir for their help in the laboratory experiments.

Finally, I must express my very profound gratitude to my parents, my sister Rayane, and my friends Sara, Hayssam, Zahwa, Angela and Grace for providing me with unfailing support and continuous encouragement throughout my years of study and through the process of researching and writing this thesis. This accomplishment would not have been possible without them. Thank you.

.

AN ABSTRACT OF THE THESIS OF

Maha Nasser Mrad for Master of Engineering
Major: Materials and Pavement Engineering

Title: Multi Scale Probabilistic Analysis of the Elastic Modulus of Concrete Using Digital Image Processing

In the design of concrete structures, knowledge of the materials properties is required to conduct a proper, safe, and economical design. Young's modulus of concrete, denoted as (E), is in particular a key mechanical parameter utilized by engineers in the design and analysis of concrete structures. Design codes provide the engineers with relationships to estimate the elastic modulus of concrete of different strengths; these formulas relate (E) to its 28 day compressive strength. However, concrete is a highly heterogeneous material and extensive research shows that its mechanical properties are effected by the properties of its constituents. Several researchers provided composite models that relate the elastic modulus of concrete to the elastic modulus and volumetric fractions of aggregate, mortar, and interfacial zone (ITZ). However, these models interpret concrete as a homogeneous medium and use deterministic values for the elastic properties of the input variables (aggregate, mortar, and ITZ); thus, neglecting the effects of the spatial distribution of aggregates and the natural variation in the elastic properties of the input variables on the elastic modulus estimation.

This study presents a probabilistic framework for estimating the modulus of elasticity of concrete while taking into consideration the uncertainties associated with the mix constituents and their spatial distribution. The variability of the characteristic of the mix constituents, i.e. elastic modulus and Poisson's ratio, is quantified by experimentally testing cylindrical core specimens of limestone and mortar. The tested specimens originate from different local sources for the case of the limestone and correspond to different mix design proportions for the mortar. This is specifically done to capture the possible range of variability for the input parameters. The spatial distribution of the aggregates and the volumetric fractions are captured by utilizing digital image correlation techniques to process scanned images of sections cut from concrete cylinders. Using Monte Carlo simulations, the probabilistic volumetric characterization of the mix constituents along with the quantified uncertainty in the mix constituent's characteristics are employed to stochastically predict the corresponding modulus of elasticity utilizing empirical models such as the Hirsch and Ramesh and Hashin models. The probabilistic representation of the elastic modulus of concrete is then compared to the elastic modulus measured experimentally in the laboratory.

CONTENTS

ILLUSTRATIONS

Figure Page

TABLES

Table Page

CHAPTER 1

INTRODUCTION

1.1 Problem Statement

In the design of concrete structures, knowledge of the materials properties is required to conduct a proper, safe, and economical design. Young's modulus of concrete, denoted as (E), is in particular a key mechanical parameter utilized by engineers in the design and analysis of concrete structures. Design codes provide the engineers with relationships to estimate the elastic modulus of concrete of different strengths; these formulas relate (E) to its 28-day compressive strength. However, concrete is a highly heterogeneous material and extensive research shows that its mechanical properties are effected by the properties of its constituents. Several researchers provided composite models that relate the elastic modulus of concrete to the elastic modulus and volumetric fractions of aggregate, mortar, and interfacial zone (ITZ). However, these models interpret concrete as a homogeneous medium and use deterministic values for the elastic properties of the input variables (aggregate, mortar, and ITZ); thus, neglecting the effects of the spatial distribution of aggregates and the natural variation in the elastic properties of the input variables on the elastic modulus estimation.

1.2 Research Objective

This study presents a probabilistic framework for estimating the modulus of elasticity of concrete while taking into consideration the uncertainties associated with the mix constituents and their spatial distribution. The variability of the characteristic of the mix

constituents, i.e. elastic modulus and Poisson's ratio, is quantified by experimentally testing cylindrical core specimens of limestone and mortar. The tested specimens originate from different local sources for the case of the limestone and correspond to different mix design proportions for the mortar. This is specifically done to capture the possible range of variability for the input parameters. The spatial distribution of the aggregates and the volumetric fractions are captured by utilizing digital image correlation techniques to process scanned images of sections cut from concrete cylinders. Using Monte Carlo simulations, the probabilistic volumetric characterization of the mix constituents along with the quantified uncertainty in the mix constituent's characteristics are employed to stochastically predict the corresponding modulus of elasticity utilizing empirical models such as the Hirsch, Ramesh and Hashin models. The probabilistic representation of the elastic modulus of concrete is then compared to the elastic modulus measured experimentally in the laboratory.

1.3 Research Outline

This thesis is structured into seven chapters. Chapter 2 presents first a brief description of concrete, its composition and properties. Second, it defines concrete's Young's modulus, its significance, and discusses in-depth the various methods used to determine it. Chapter 2 also highlights the importance of the elastic properties of the constituents of concrete i.e. aggregates and mortar with a particular emphasis on limestone as a main source of aggregates and the variability associated with its elastic modulus measurement. Finally, Chapter 2 presents a thorough description of Digital Image Processing Techniques, their origin, applications and components. Chapter 3 describes the research approach and provides a general insight on the methodology adopted.

Chapter 4 shows the experimental program carried out to propose suitable probabilistic distributions for the elastic modulus of limestone and mortar. Chapter 5 elaborates on the equipment and techniques used in the Digital Image Processing. The chapter also provides suitable probabilistic distribution for the volumetric fraction of aggregates and mortar. Chapter 6 studies the effect of the end of the specimens on the elastic modulus measurement. Chapter 7 compares the values obtained using experimental results and the tool proposed and also compares it to the empirical relationships provided by several design codes such as American Concrete Institute, Eurocode, and others. Finally Chapter 8 presents the main findings of this study.

CHAPTER 2

LITERATURE REVIEW

2.1 Concrete and Its Constituents

ASTM C125 defines concrete as “a composite material that consists essentially of a binding medium within which are embedded particles or fragments of aggregate” [2]. Moreover, ACI CT-13 defines concrete as a “mixture of hydraulic cement, aggregates, and water, with or without admixtures, fibers, or other cementitious materials”. Thus, concrete can be regarded as a multi-phase and heterogeneous composite material that provides strength to engineering structures [3].

Aggregates occupy approximately 75% to 80% of the volume of concrete [3] and can be divided into two categories: coarse and fine aggregates. Coarse aggregates are gravel or crushed stone particles that are retained on a 4.75 mm sieve size and are usually between 9.5 mm and 37.5 mm in diameter [4]. Fine aggregates consist of natural sand or crushed stone that are smaller in diameter than 4.75 mm and usually retained on the 75 μm sieve size [5]. Since aggregates are the least expensive component of concrete, they are mainly used as filler that provides concrete with volume stability and increases its strength.

Cement paste is a byproduct of the reaction between Portland cement clinker and water. The reaction between cement clinker and water is known as the hydration process, it forms the cement paste which hardens and binds all the constituents of concrete together.

2.2 Concrete Young's Modulus

2.2.1 Definition and significance

In the design of concrete structures, knowledge of the materials properties is required to conduct a proper, safe, and economical design. In particular, the elastic properties which relate stress to strain are the ones needed to allow professional engineers to proportion sections, compute the quantity of steel reinforcement needed [6], control deflections, and provide satisfactory serviceability. Young's modulus of concrete, denoted as (E), is in particular a key mechanical parameter utilized by engineers in the design and analysis of concrete structures [7]. It is defined in the region of the stress-strain curve where the ratio of stress over strain obeys Hooke's law [8].

Throughout the past decades, researchers have extensively investigated different methods for determining the Young's modulus of concrete. These methods presented in Section 2.2.2 could be classified under experimental, analytical, and numerical approaches.

2.2.2 Young's Modulus determination

2.2.2.1 Experimental methods

Experimentally, the methods that are followed to determine Young's modulus are either based on destructive or non-destructive testing [9]. Destructive testing allows the measurement of the static Young's modulus, thus known as the static method. Non-destructive testing is also known as the dynamic method since it allows measuring the dynamic Young's modulus.

Static Method

The most common destructive method is the standard compression test, where concrete cylinders are subjected to a static uniaxial compressive load [10, 11]. Cylinders are loaded until failure and the strength of concrete is recorded as the stress achieved at failure. During testing, the axial strain is recorded, and the static Young's modulus is defined as the slope of the linear range of the stress-strain curve i.e. up to approximately 40% of the strength [12]. The standard compression test is common in situations where the structure is under construction and testing the properties of the material such as compressive strength, tensile strength, and Young's modulus is part of Quality Assurance/Quality Control (QA/QC). However, this traditional method does not provide immediate results and in some cases, the quality of the concrete cast in cylinders is different from that placed in the structure. Moreover, this method is time-consuming since ASTM C469 requires that the specimen must be loaded at least three times in order to record the average Young's modulus. Other destructive methods include measuring the tensile Young's modulus. It can be obtained either by performing direct tension test on bone shaped specimens or three – point bending test on rectangular beams. However, all of these tests are complex, time-consuming and require skilled technicians; therefore, researchers resort to non-destructive testing for their advantages.

Dynamic Method

Non–destructive testing holds several advantages as compared to destructive testing. It does not impair the function of the structure, hence it is utilized to assess the structural integrity of old and new structures and monitor long term changes in the properties of concrete [13]. It gives immediate results with higher precision. Moreover, it is simple

and easy to handle, and measurements can be repeated on the same specimen, etc. [14, 12, 15]. Moreover, it can be utilized to determine different parameters in concrete such as chloride concentration, corrosion rate, and permeability, etc. [14] . Non-destructive testing is dynamic in nature and is divided into resonant and ultrasonic methods [15]. The resonant method depends on the vibration of an elastic body if struck a blow [16, 17] , while the ultrasonic method is based on the transit time of a wave within a body [18, 19]. Although non-destructive testing is advantageous, findings show that the dynamic Young's modulus is always larger than the static one [20] As a result, researchers attempted to find different relations between the static and dynamic Young's modulus as listed below:

- $E = 0.83 * E_d$ [13]
- $E_d/E_s = 1 + 0.0875\lg(\dot{\varepsilon}/\varepsilon_s)$ [21]
- $E = 1.25 * E_d - 19$ British Standard Code of Practice, BS 8110

Where E_d: Dynamic Young's modulus, E: Static Young's modulus, $\dot{\varepsilon}$: Current strain and ε_s: Static strain.

2.2.2.2 Analytical

Empirical Equations

Concrete is typically specified according to a compressive strength class i.e. low strength, medium strength, and high strength concrete. Testing the compressive strength of concrete is considered relatively an easy and quick test; therefore, researchers established relationships that correlate the compressive strength of concrete at 28 days to the elastic modulus. All established relations are empirical and derived based on

experiments carried under controlled conditions. Table 2.1 provides a summary of some of the commonly used empirical relations.

Table 2.1: List of empirical relations adopted by design codes

Formula	Source	Type of Concrete	Units
$E_c = 9.5f'c^{0.3}$	NS 3473 [20]	High Strength	E_c in (GPa) $f'c$ in (MPa)
$E_c = 3.32\sqrt{f_c'} + 6.9$	ACI 363 [21]	$21 < f_c{}' < 73$	
$E_c = 22\left(f_c'/10\right)^{0.3}$	BS EN1992 [22]	With Quartzite Aggregates	
$E_c = 0.4E_a + 200f_c'$	Parrot , L. J [23]	$20 < f_c{}' < 70$	E_c in (MPa) $f'c$ in (MPa)
$E_c = 2.15 \times 10^4(f'c/10)^{1/3}$	CEB [24]	Normal Weight	
$E_c = 33{w_c}^{3/2}\sqrt{f'c}$	ACI 318-11 [25]	$90 < w_c < 160$	E_c in (psi) $f'c$ in (psi) w_c in (pcf)
$E_c = 57000\sqrt{f'c}$	ACI 318-11 [25]	Normal Weight	E_c in (psi) $f'c$ in (psi)
E_c *and* f_c' are the modulus of elasticity and compressive strength of concrete at 28 days after casting, respectively, and w_c is the unit weight of the concrete.			

Composite models

Voigt (1889) and Reuss (1929) studied concrete as a composite material composed of two phases: aggregates and mortar [26, 27]. Both researchers relied on the law of mixtures, which defines the properties of any composite as the weighted average of the properties of the constituents, to relate the elastic modulus of concrete to the volume fractions, elastic modulus, and the arrangement of the two phases. The model proposed

by Voigt (1889) assumes that the two phases are arranged parallel to the loading axis and the displacement exhibited by the concrete sample is equal to the displacement exhibited by each phase [28]. While, that proposed by Reuss (1929) assumes that the phases are arranged perpendicular to the loading axis, and the stress experienced by each phase is equal to that experienced by the overall composite [28]. Based on the arrangement of the phases, Voigt and Reuss models were named the "parallel" and "series" models respectively. However, experiments have shown that the parallel and series models do not give exact solutions for the elastic modulus but rather give the upper and lower bounds [29].

Hirsch (1962) argued that stresses in both phases of the series model are not equal; each phase experiences a stress equivalent to the volume fraction of that phase multiplied by a stress coefficient [30]. In addition, the displacement of the concrete is equal to the sum of the displacement of the phases. After conducting an experiment for different mixes varying: aggregate type (limestone, lead drops, steel punching, Ottawa sand, etc...) and volume fraction of aggregate (0.2 to 0.57), Hirsch proposed that the elastic modulus of concrete is the weighted average of both the series and parallel models, and is a function of an empirical constant. Counto (1964) reported that all the three mentioned models show limited agreement with experimental results, therefore Counto proposed a model where the aggregates are represented as a rectangular prism placed in the center of the concrete cylinder [31]. Figure 2.1 schematically presents the four two-phase models.

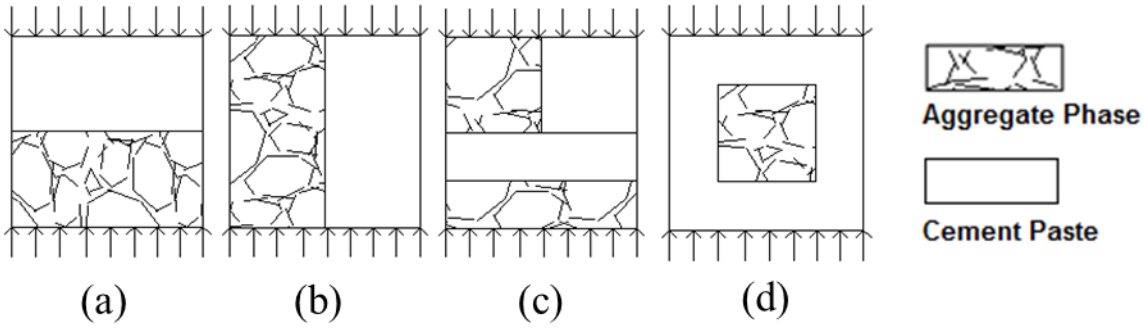

Figure 2.1: Two-phase composite models: (a) Reuss model, (b) Voigt Model, (c) Hirsch Model, and (d) Counto Model

Hashin and Shtrikman (1963) used the variational principles in the linear theory of elasticity to derive upper and lower bounds for the effective elastic modulus of heterogeneous materials [28, 29, 32]. The Hashin-Shtrikman bounds were narrower than those provided by the parallel and series models, however the bounds become wider as the ratio of the elastic modulus of one phase to another increases [29, 32].

Further investigations on the behavior of concrete showed that a thin film of cement paste surrounds the aggregates and has different properties than the cement paste away from it [33, 34]. This phase known as the interfacial zone (ITZ) greatly influences the behavior of concrete as it is considered the weakest link in concrete [33, 34, 35, 36, 37, 38]. Therefore, Hashin et al. (1962), Ramesh et al. (1996), and other researchers formulated theoretical four phase models to incorporate the effect of ITZ in the study of the elastic modulus [34, 39, 40]. These models are based on the linear theory of elasticity and unlike the previous mentioned two-phase models; they do not assume a specific arrangement for the phases. Four phase composite models are thought to provide a realistic representation for the elastic modulus as it accounts for the interfacial

zone. However, quantification of the thickness and properties of the interfacial zone and its influence on the elastic modulus of concrete is still an active research area. In addition, the assumptions underlying these models overlook the effect of several factors: the shape of aggregate since it is assumed spherical; and the heterogeneity of concrete since it is represented by only one spherical aggregate surrounded by a layer of ITZ and cement paste, which is embedded in an equivalent homogeneous medium that replaces all other aggregates. Therefore, with the abundance of computational resources, researchers started employing numerical simulations to generate the internal structure of concrete, which allow for a better characterization of the heterogeneity of concrete. Table 2.2 presents the list of the commonly used empirical and theoretical composite models.

Table 2.2: List of composite models

Model	Relation
Voigt [26]	$E_c = E_m V_m + E_a V_a$
Reuss [27]	$E_c = \frac{V_m}{E_m} + \frac{V_a}{E_a}$
Hirsch [30]	$\frac{1}{E_c} = (1-x)\left(\frac{v_a}{E_a} + \frac{v_m}{E_m}\right) + x\,(\frac{1}{v_a E_a + v_m E_m})$
Counto [31]	$\frac{1}{E_c} = \frac{1-\sqrt{v_a}}{E_m} + \frac{\sqrt{v_a}}{\sqrt{v_a} * E_a + (1-\sqrt{v_a})E_m}$
Ramesh et al. [34]	$K_{eff} = \frac{\gamma_1 + \gamma_2}{\gamma_3 + \gamma_4}$ $\gamma_1 = (v_a + v_{ITZ})(3K_a + 4G_{ITZ})[K_m(4G_m + 3K_{ITZ}) + 4(v_a + v_{ITZ})G_m(K_{ITZ} - K_m)]$ $\gamma_2 = 4v_a(K_a - K_{ITZ})[3K_m(G_{ITZ} - G_m) + (v_a + v_{ITZ})G_m(3K_m + 4G_{ITZ})]$ $\gamma_3 = (v_a + v_{ITZ})(3K_a + 4G_{ITZ})[(4G_m + 3K_{ITZ}) - 3(v_a + v_{ITZ})(K_{ITZ} - K_m)]$ $\gamma_4 = 3v_a(K_a - K_{ITZ})[3(G_{ITZ} - G_m) + (v_a + v_{ITZ})(3K_m + 4G_{ITZ})]$
Hashin [40]	$K_{eff} = K_m + \frac{v_m + v_a}{\frac{1}{K_e - K_m} + 3v_m/(3K_m + 4G_m)}$ $K_e = K_{ITZ} + \frac{v_a/(v_m + v_a)}{\frac{1}{K_a - K_{ITZ}} + \left[\frac{3v_{ITZ}}{v_m + v_a}\right]/(3K_m + 4G_m)}$
The subscripts *c, a, m, ITZ* stand for concrete, aggregates, cement paste, and interfacial zone respectively. v represents the volume fraction, E the elastic modulus, and x the ratio of phases in parallel arrangement to total volume. G and K represent the shear modulus, and bulk modulus respectively.	

Numerical Approach

To overcome the limitations of previous models, numerical methods such as the Finite Element Method (FEM) and Discrete Element method (DEM) have been used to predict

the performance of concrete. As input to either method, two mechanisms have been extensively employed for an accurate representation of the internal structure of concrete: computer-generated geometry and actual geometry acquisition.

The concept of computer-generated geometry is based on random simulation of aggregate particles, which are then positioned inside a container that represents the cement paste. Computer-generated geometry models can be divided into static and dynamic methods. The "take and place" method is a common static method, where aggregates according to a specific gradation are generated and placed randomly into the container starting with the largest size aggregate to the smallest [50]. Whenever an overlap between the particles exists, rejection occurs and the generation process is continued. The main drawbacks of this method is that first it excludes the effect of mutual particle interaction; second, it becomes unpractical when dealing with high volume fractions of particles due to the increasing number of rejections [51]. Therefore, dynamic methods were introduced to account for the particle interaction. The process in the dynamic methods is different: first, a 3D dilute aggregate skeleton is generated within a container using the static method. Second, motion vectors are assigned to the aggregate particles and the aggregate skeleton undergoes a mixing process known as the dynamic stage. In the dynamic stage, the location of the aggregates is changed in an iterative process, and the walls of the container move to reach the specified volumetric fraction of aggregate [51]. Both methods generate a representative internal structure of concrete; however, both require high computational efforts particularly when dealing with high volumetric fractions of aggregates.

Actual geometry acquisition is based on digital image analysis of existing and realistic images of the internal structure of concrete. Images are captured by means of several

imaging devices: high-resolution flatbed scanners, digital cameras, microscopes, and X-ray computed tomography [52]. Digital image analysis is a three-step process: image acquisition, processing, and analysis. Image acquisition can be performed using any of the devices mentioned earlier. Processing of images consists of first converting the original image into a digital image, and then enhancing it (contrast adjustment, filtering, noise removal, and others) in order to identify the aggregates accurately. Image analysis consists of identifying the shape, location, orientation, and distribution of the aggregates, the volume fractions of aggregates, cement paste. Several researchers utilized digital image techniques to relate the internal structure of asphalt concrete and the effect of several factors to its performance [52]. Digital image techniques have several advantages: characterizing the internal structure with high-resolution details [53], availability of imaging devices and software, and low computational cost; therefore, these techniques have become widely applied in the engineering field.

To avoid the high computational costs associated with numerical models and yet get an accurate representation of the variability of the elastic modulus within a concrete mix; this study aims at combining low cost composite models with high resolution scanning and data correlation techniques for predicting the stochastic elastic characteristics of concrete mixes.

2.3 Elastic Modulus of Aggregates

Aggregates are intact rock fragments obtained by quarrying and processing natural rocks. They differ by their mineralogical composition, physical and chemical properties depending on the source of origin of rocks. Therefore, basic mechanical properties such

as uniaxial compressive strength (UCS), Young's modulus and Poisson's ratio vary for different aggregate types. Knowledge of these properties is important since they play a major role in determining the properties of concrete [41, 42, 43]. Several studies highlight the effect of aggregate types on the mechanical properties of PCC; among these studies are the following:

1. Aitcin and Mehta (1990) studied the effect of four aggregates types (granite, limestone, diabase and gravel) on the mechanical properties of high strength concrete. For similar mix proportions, concrete mixes incorporating diabase and limestone aggregates exhibited higher strength and elastic modulus than those with granite and gravel [44].
2. Hamad et al. (2000) investigated the effect of limestone aggregates from different sources in Lebanon on concrete properties. All concrete mixes were designed using a common gradation and based on a water to cement ratio of 0.5. Mixes produced with limestone collected from Berquayel and Sibline areas gave lower strength than those produced with limestone from other sources [45].
3. Al-Oraimi et al. (2006) used aggregates from five different areas in Oman to study the effect of their minerology on the strength of concrete. For the same size of aggregate, the strength of concrete varied according to the source of aggregate [3].
4. Shamsad and Al-Ghamdi (2012) studied the effect of two types of coarse aggregates (crushed calcareous limestone and basaltic) on the performance of concrete. The study showed that at low water to cementitious materials ratio, the quality of aggregates controls the performance of concrete [43].

5. Other studies also include the effect of aggregate sizes on the strength of normal and high strength concrete; the effect of aggregate content on the compressive strength and fracture of concrete.

Given the effect exerted by aggregates on the properties and performance of concrete, it is important to have an accurate knowledge of their properties to better understand and quantify the relation between the properties of aggregates and concrete. Since rocks are the origin of aggregates, then it is essential to study the properties of rocks in order to obtain information about the aggregates.

2.3.1 Classification of rock mass

Early research dates back to 1946, when Terzaghi proposed the first descriptive and behavioristic rock mass classification system. The classification system was mainly developed for the design of tunnel supports [47]. Different systems were then developed to estimate rock mass behavior and quality. Below is a brief description of the approaches:

- Rock Quality Designation (RQD): It was introduced in the mid-1960s as an index for rock quality [48] . RQD represents the number of intact cores that are larger than 100 mm in a borehole as a percentage of the length of the borehole. So, a higher RQD percentage implies a higher number of intact cores larger than 100 mm, and thus a higher rock quality.
- Rock Structure Rating (RSR): Developed by Wickham, Tiedmann, and Skinner in the period of 1972 and 1974; the RSR is a quantitative method for describing

the quality of rock mass. It is the sum of three parameters A, B, and C; where A characterizes the rock type, hardness, and geological structure, B measures the effect of joint spacing and orientation, and C measures the effect of groundwater inflow [49].

- Rock Mass Rating (RMR): It is an index based on six parameters: uniaxial compressive strength, RQD, groundwater conditions, spacing, condition, and orientation of discontinuities [51].
- Quality (Q) scheme: Barton et al. (1974) analyzed 212 tunnel case histories and proposed a tunneling quality index (Q) for the determination of the characteristics of rock mass and tunnel support requirements. The index is based on six parameters: RQD, number of joint sets and joint roughness, degree of alteration, and water and stress reduction factors.

These classifications systems have been widely applied in the United States, Canada, Japan and other countries [53] since they are of key importance in rock engineering projects such as the design of tunnels in rocks, mining operations, and deep rock foundations and slopes. However, rock masses are in-situ medium that consist of intact rock blocks separated by discontinuities, and often researchers are interested in the physical characteristics and mechanical properties of those intact rock blocks. Therefore, researchers established engineering classification systems for intact rocks to characterize their properties.

2.3.2 Classification of intact rocks

An intact rock is defined as a polycrystalline solid that consists of an aggregate of minerals or grains. The properties of the solid are governed by the physical properties of the constituting materials and the type of bond between those materials [54] . There exist three classifications for intact rocks: geological, elementary, and engineering classifications.

Geologically, intact rocks are classified according to the minerals that compose the rock. There is a wide range of minerals; however, there exist 14 common rock forming-minerals such as calcite, dolomite, quartz, biotite, etc. The elementary classification is related to the rock formation process which is igneous, metamorphic, or sedimentary. Igneous rocks are formed by the cooling and solidification of molten magma. The structure of the igneous rocks is affected by the mode of crystallization, rate of cooling, and mode of occurrence. Metamorphic rocks undergo the metamorphism process which is the solid state conversion of pre-existing rocks. Sedimentary rocks are formed from the consolidation of sediments.

In order to understand the behavior of intact rocks in engineering projects, Coates (1964), Hansagi (1965), Deere and Miller (1966), Stapledon (1968), Franklin et al. (1971), Bieniawski (1978), and ISRM (1978, 1981) have established approaches to classify rocks based on their engineering properties (Reference Book). The engineering classification is based either on the unconfined uniaxial compressive strength (UCS), modulus of deformation, or both. Depending on the value of the unconfined UCS, intact rocks are classified into five classes: very low, low, moderate, high, and very high strength. Also, the deformability of rocks ranges from very low to very high depending on the modulus of deformation. However, a classification system based only on one measurable property is not always realistic since there are several factors that influence

the engineering behavior of rocks. Therefore, Deere and Miller (1966) proposed a classification system based on the combined influence of the UCS and the tangent modulus of elasticity at 50% of the ultimate UCS. The system designates two letters to describe the behavior of rocks. The first letter describes the class of the UCS and the second letter designates the modulus ratio where it is defined as the ratio of elastic modulus to the UCS [52] . Figure 2.2 shows the classification system adopted by Deere and Miller (1966) that has been widely used since it takes into account two main engineering properties at a time.

According to the classification proposed by Deere and Miller (1966), each type of rock falls in a specific zone. Each strength zone covers a range of strength values i.e. E-strength zone implies that the strength of rocks is smaller than 25 MPa while an A-strength zone implies that the strength of rocks ranges between 200 MPa and 400 MPa and the same applies to the modulus ratio. For example, basalt lies in the A-strength category and towards the lower portion of the average modulus ratio; dolomite falls in the region between average and high modulus ratio and limestone plots similar to dolomite and etc. [55]. This system is considered useful and workable since it identifies the class for each type of rock. However, often the mineralogical composition, texture, pore geometry, presence of miniature cracks and other factors vary for the same type of rock, consequently affecting its strength and elastic modulus. Thus, the need for an accurate experimental characterization rather than a classification system arises.

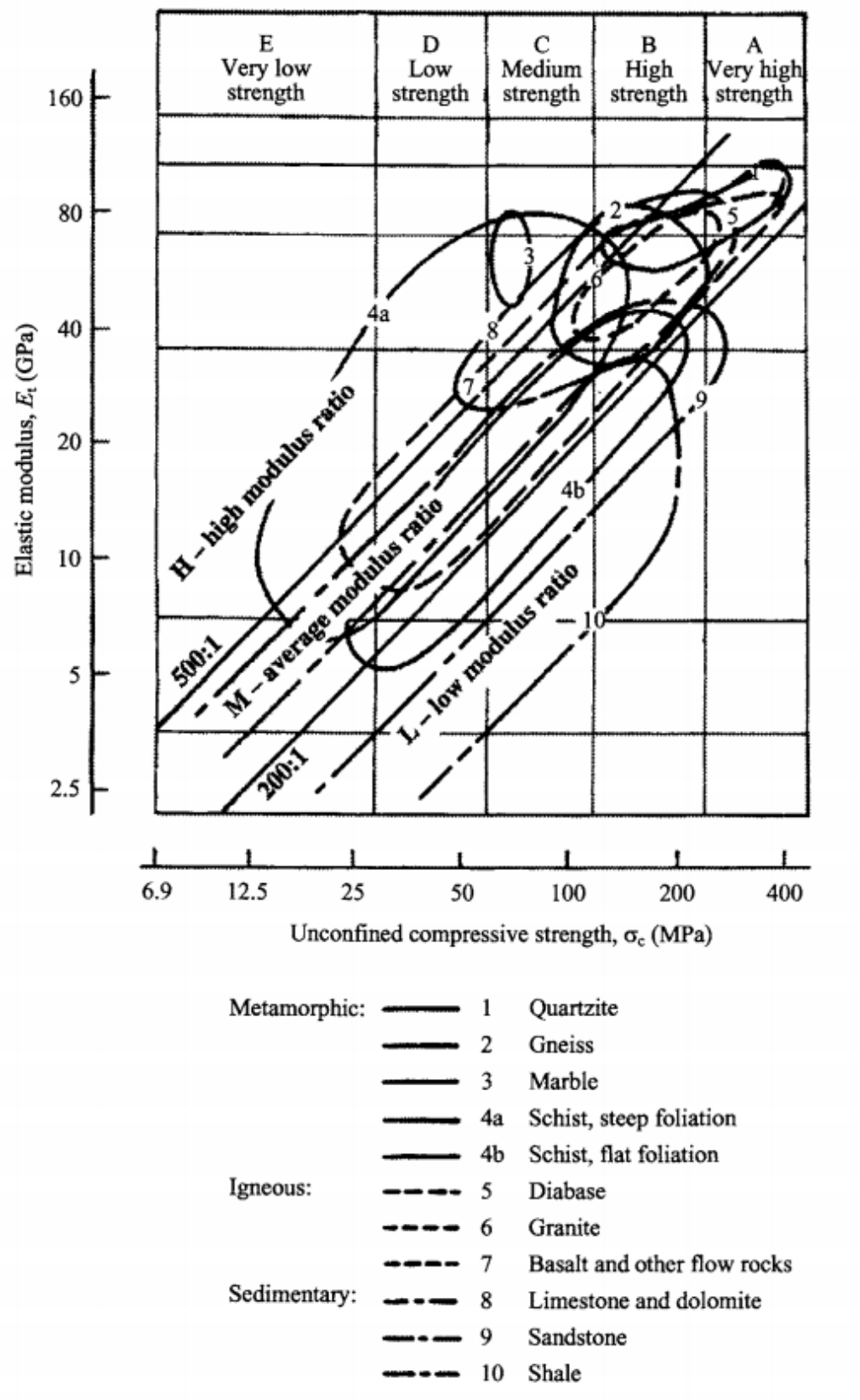

Figure 2.2: Rock classification based on the approach proposed by Deere and Miller (1966)

2.3.3 Variability in the elastic modulus of limestone

Several researchers attempted to measure the elastic modulus of different types of rocks. The reported range in the literature is 20-200 GPa [59]. In particular, the elastic modulus of limestone ranges between 16.548 GPa and 66.882 GPa [60, 61] . Other studies in Southeastern Mexico, Turkey, China, and Canada reported averages of 8.34 GPa, 13.6 GPa, 17.77, and 31.5 GPa respectively for limestone [62, 63, 64, 65]. Therefore, it is evident that the elastic modulus of limestone is affected by lithological variations. Also, the presence of impurities, fractures, and pores are additional causes of scatter in the values of the elastic modulus.

2.4 Digital image processing

2.4.1 What is digital image processing (DIP)?

A digital image is an electronic representation of a scene that can be produced in several ways using digital cameras, scanners, x-ray computed tomography, and radar and ultrasound imaging, etc. The electronic representation is a two dimensional grid of dots or pixels where each has a particular location and value. Depending on the value of the pixels, digital images can be colored, grayscale, or black and white. Often an image needs adjustments in order to improve its quality; therefore, digital image processing has been introduced as a tool to manipulate images. Digital Image Processing (DIP) is the use of mathematical algorithms and digital computers to alter and perform operations on digital images. There exist three types of DIP techniques:

- Image to image transformation: In this process, both the input and output are digital images; however, the output image is usually of a higher quality. Examples of such transformation include noise removal, image enhancement and restoration, contrast and brightness, color processing and others.
- Image to information transformation: This transformation is mainly known as image analysis. It uses a digital image as an input and yields the information correlated with it. Image segmentation, feature extraction, pattern recognition, image compression and statistics illustrate this type of transformation.
- Information to image transformation: This process mainly includes reconstruction of images and creation of computer graphics and animations.

Thus, it can be concluded that digital image processing is simply the manipulation of digital images in an attempt to improve their quality, extract specific information, or use information to construct digital images.

2.4.2 History of DIP

In the early 1920s, the idea of digital images originated at the newspaper industry where they were transmitted through the Bartlane Cable picture transmission service [48]. Images were coded and transferred by submarine cable and then reconstructed at the receiving end using specialized printing equipment. Later, improvements to the Bartlane system resulted in higher quality images. These improvements included adopting a new reproduction system based on photographic techniques and increasing the number of tones in the reproduced images [49]. Although it may look like the origin of digital image processing is directly correlated to the invention of digital images; however, it is

tied to two other factors -- namely, the journey to the space and the development of the first electronic computer in 1946.

The first major application of digital image processing was carried in the early 1960s at the Jet Propulsion Laboratory in the United States of America [56]. Due to the advancement in the performance and capacity of digital computers, the first image of the moon taken and transmitted by the U.S aircraft Ranger 7 was processed to correct for the distortions. This event was marked as the benchmark for digital image processing. Since then, DIP techniques have been used in other space missions such as the Apollo landings on the moon, Surveyor missions to the moon and Mariner series to Mars [57].

In the late 1960s, DIP techniques gained popularity and the field witnessed a continuous and significant expansion. These techniques were incorporated in medical applications and the invention of the Computerized Axial Tomography (CAT) scanner in 1979 was considered a breakthrough in medical imaging. In recognition for their invention, the electrical engineer Sir Godfrey Hounsfield and the nuclear physicist Allan Cormack shared the Nobel Prize in Medicine [58].

Beside medical imaging and space applications, DIP techniques have been used in a broad range of applications since the 1970s. These applications include and are not limited to: remote sensing, office automation, industrial automation, face and fingerprint detection, traffic monitoring, automatic target recognition, meteorology, printing graphics, and others [51].

2.4.3 Applications of DIP in civil engineering

Recently, digital image processing techniques have been widely implemented in civil engineering applications [52]. In rock mechanics, Reid and Harrison (2000) used the brightness of a digital image to trace the discontinuities in rock mass surfaces and have proven that DIP is efficient in discontinuity trace detection [53]. Chen et al. (2004) developed a two-dimensional digital image-based numerical model to obtain the actual mineral distribution within granite and predict the failure behavior of inhomogeneous rocks [54]. Li (2001), Hadjigeorgiou et al. (2003), Tham et al. (2003) and other researchers employed DIP techniques to study the cracking behavior of rocks and investigate discontinuity network [54].

Moreover, DIP techniques are widely used in the field of Asphalt Concrete (AC) characterization and design [55, 52]. The first study on the characterization of AC mixtures using DIP techniques was conducted by Eriksen and Wegan in 1993 [56]. In AC characterization, the focus was mainly on the internal structure of aggregates as it provides the skeleton for AC mixture [57]. Yue et al. (1995) is among the researchers who evaluated the orientation, gradation, distribution, and shape of the aggregate skeleton using DIP techniques [52, 56]. Also, Masad et al. (1999) proposed a computer-automated image analysis procedure to quantify the effect of different compaction methods on the internal structure of AC [58]. Arasan et al. (2011) used DIP techniques to measure the physical parameters of different types of coarse aggregates. The influence of those parameters such as aspect ratio, elongation, roundness, and others on the behavior of AC was later investigated [59]. Bruno et al. (2012) analyzed planar images of asphalt slices using different segmentation methods. The study aimed at finding the most suitable segmentation method for determining the aggregate gradation

of asphalt [60]. Moreover, Arshadi and Bahia (2015) utilized image based simulation to predict the mechanical response of asphalt mixtures [61].

In addition, researchers used DIP techniques to study the mechanical properties and behavior of Portland Cement Concrete (PCC). Wu et al. (2011) utilized these techniques to measure the development and properties of the fracture process zone in PCC [62]. Başyiğit et al. (2012) aimed at determining if image processing can be considered as an alternative method to destructive and non-destructive methods for testing the compressive strength of concrete [63]. Moreover, the study attempted at finding the percentages of aggregates, air voids, and cement matrix in concrete. Razmjoo (2013) employed scanned images of the internal structure of concrete along with finite element analysis to model chloride diffusion in concrete. Furthermore, Duarte et al. (2015) conducted a study on the mechanical behavior of rubberized concrete and showed that DIC techniques provide an excellent visualization of the heterogeneous material [64].

Given the broad applications of DIP techniques, it can be seen that they are considered powerful tools in studying the composition of heterogeneous materials such as AC and PCC. These techniques avoid researchers the use of algorithms that are typically associated with high computational costs, in order to generate aggregates of random shapes and sizes to simulate its effect on the behavior of AC and PCC.

2.4.4 Components of DIP

In general, digital image processing comprises of three steps: image acquisition, processing, and analysis.

- Image acquisition: This step aims at obtaining the actual geometry of the internal structure of any composite material. Images can be captured by means of several imaging devices: high-resolution flatbed scanners, digital cameras, microscopes, and X-ray computed tomography [65]. Once the image is obtained, it is stored as a rectangular array of pixels [66]. The resolution of the image depicts the dimensions of the pixels i.e. width and length. A higher resolution results in a higher number of pixels, thus smaller dimensions. Also, pixels can vary between 0 and 1or 0 and 256, if the image is black and white or greyscale respectively. If the image is colored, then each pixel is a combination of three numbers which indicate the variations in red, green, and blue.
- Image processing: Often a raw digital image requires manipulation. Manipulation includes image enhancement, contrast adjustment, filtering, noise removal, restoration, and segmentation. This is performed to differentiate the aggregates from one another, detect particles boundaries, and etc.
- Image analysis: This step can be termed object recognition since it helps in identifying the different components of an image. It consists of identifying the shape, location, orientation, and distribution of the aggregates, the volume fractions of aggregates, cement paste.

Digital image processing techniques have several advantages, and therefore have become widely applied in the engineering field.

CHAPTER 3

RESEARCH APPROACH AND METHODOLOGY

The aim of this section is to present a general overview of the approach undertaken to complete the objective of the study. It will also help in setting a clear idea for the reader on the path followed for: collecting and preparing the needed materials, conducting experimental procedures, performing statistical analysis on the data obtained, and finally presenting and the results of the study.

3.1 Methodology

A probabilistic estimation of the elastic modulus of concrete using composite models requires two major inputs:

1. Knowledge of the elastic properties of the concrete constituents. This is attained by setting a full experimental program to measure the elastic modulus of both aggregates and mortar. Once the variability in the measurements is captured, a probabilistic characterization of the elastic modulus is then created. The details of this step are presented in Chapter 4.
2. Knowledge of the spatial distribution of the volumetric fractions of the constituents and that is acquired using Digital Image Correlation techniques. It is important to observe the spatial distribution of aggregates since they are randomly dispersed in a concrete mix. This parameter is studied with respect to a Representative Volume Element (RVE). A proper RVE size shall be small enough to model the volumetric concentrations of aggregates and mortar in a

concrete mix, yet large enough to yield values representative of the whole. The process is detailed in Chapter 5.

These two inputs are then incorporated into three composite models: Hirsch, Ramesh, and Hashin models and a Monte Carlo simulation is performed as explained in section 3.2

3.2 Monte Carlo Simulation

The main input to the three composite models (Hirsch, Hashin and Ramesh) is the volumetric fractions and elastic properties of aggregate, mortar and interfacial zone. Since the volumetric fractions and elastic modulus are modeled as probability distributions, then the input to these models is random numbers that are generated from the probability distributions. For the case of Hirsch model, the random numbers for the volumetric fractions of aggregates and voids were sampled from their corresponding distributions. Since the volume fraction of the three phases should sum up to a unit value, then, the volumetric fraction of mortar was obtained by subtracting the sum of the volumetric fractions of aggregates and void obtained from one. For the case of Hashin and Ramesh models, a third parameter is introduced and it is the interfacial zone. Therefore, the volumetric fractions of aggregates, void and interfacial zone are first sampled from their corresponding distributions and the volumetric fraction of mortar was obtained by subtracting the sum of the three sampled numbers from one.

After having sampled the random numbers corresponding to the volumetric fractions of all the phases, these numbers were entered into the equations of the composite models and the calculated elastic modulus was recorded. The process was repeated until the standard deviation of the average elastic modulus converged to a value of 0.005.

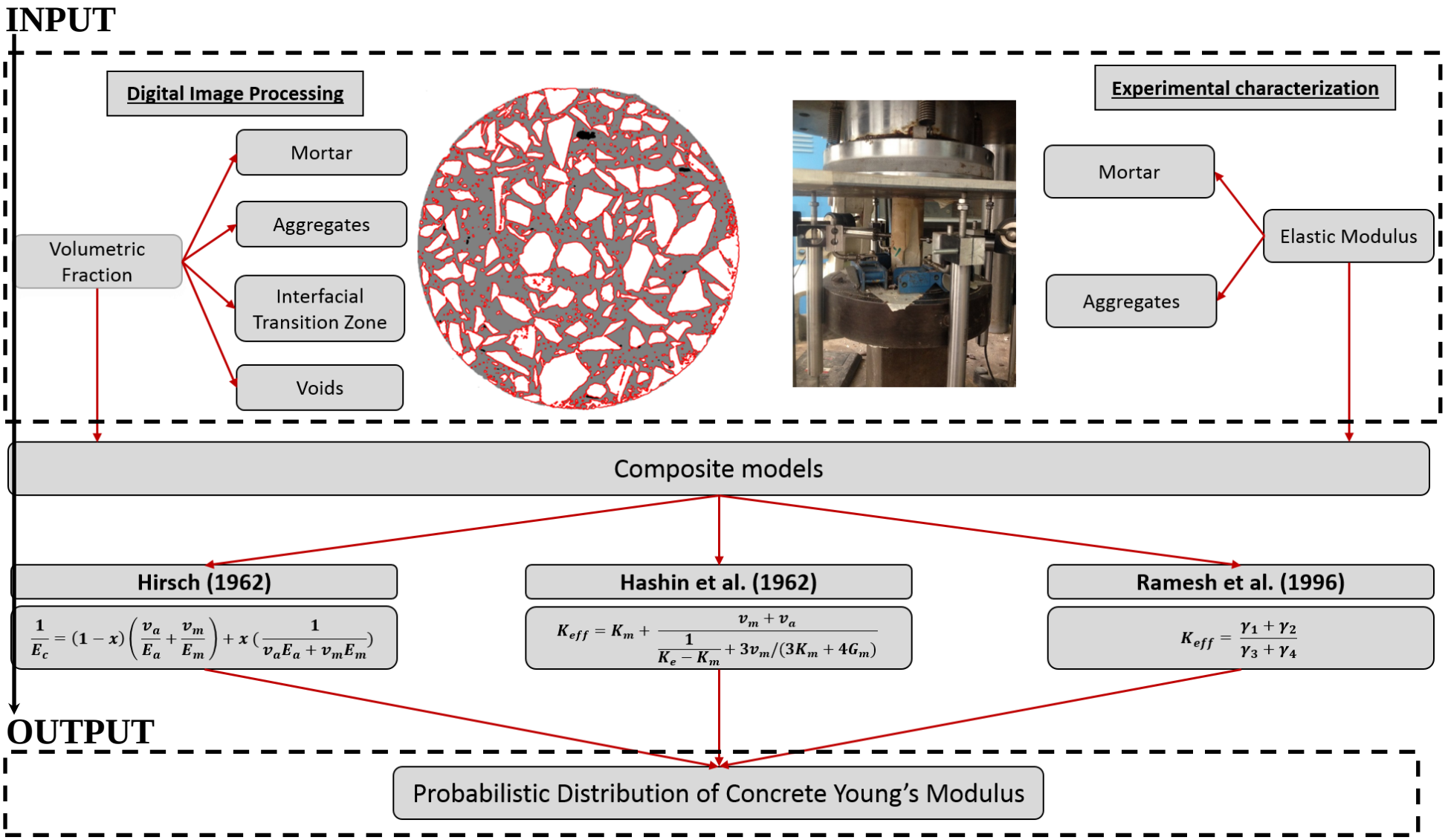
INPUT
Digital Image Processing
Mortar
Aggregates
Volumetric Fraction
Interfacial Transition Zone
Voids
Experimental characterization
Mortar
Aggregates
Elastic Modulus
Composite models
Hirsch (1962)
$\frac{1}{E_c} = (1-x)\left(\frac{v_a}{E_a} + \frac{v_m}{E_m}\right) + x\left(\frac{1}{v_a E_a + v_m E_m}\right)$
Hashin et al. (1962)
$K_{eff} = K_m + \frac{v_m + v_a}{\frac{1}{K_e - K_m} + 3v_m/(3K_m + 4G_m)}$
Ramesh et al. (1996)
$K_{eff} = \frac{\gamma_1 + \gamma_2}{\gamma_3 + \gamma_4}$
OUTPUT
Probabilistic Distribution of Concrete Young's Modulus

CHAPTER 4

EXPERIMENTAL CHARACTERIZATION OF THE ELASTIC MODULUS OF CONCRETE CONSTITUENTS

This chapter presents in detail the experimental program developed to measure the elastic modulus of aggregates and mortar. Then, it discusses thoroughly the statistical tests and analysis performed on the experimental data to fit a probabilistic distribution for the elastic moduli.

4.1 Experimental Program

The experimental program discusses the details of the process adopted in obtaining the materials required for the preparation of PCC mixes. The materials include limestone aggregates, cement, and sand. It is important to mention that the coarse aggregates used in the construction industry are mainly limestone; therefore, this study focuses on the elastic properties of limestone as a source of aggregates only. The experimental program also includes information on specimen preparation, fabrication, mortar mix proportions, and testing methods. Briefly, the experimental program targets the following variables:

1. The effect of lithological properties of rocks on the elastic properties of limestone aggregates.
2. The effect of water to cement ratio (0.4, 0.55, and 0.7) on the elastic properties of mortar and concrete
3. The effect of aggregates shape (flaky versus angular) on the elastic properties of concrete.

4.1.1 Materials and specimen preparation

4.1.1.1 Limestone cores

To measure the elastic properties of limestone aggregates, ASTM D7012-14 recommends using rock cores with a minimum diameter of 47 mm and a length to diameter ratio between 2:1 and 2.5:1 [84]. Therefore, to satisfy the requirements, 40 rectangular limestone prisms were obtained from rock beds from three different quarries in the Beqaa region in Lebanon. Given that the elastic properties of limestone differ due to the variability in their lithological properties, the quarries were chosen to cover the entire Beqaa region. Hence, the quarries are located in Aarsal, Tamnine, and Kelya and they cover the Eastern, Middle, and Western Beqaa areas respectively as seen in Figure 4.1.

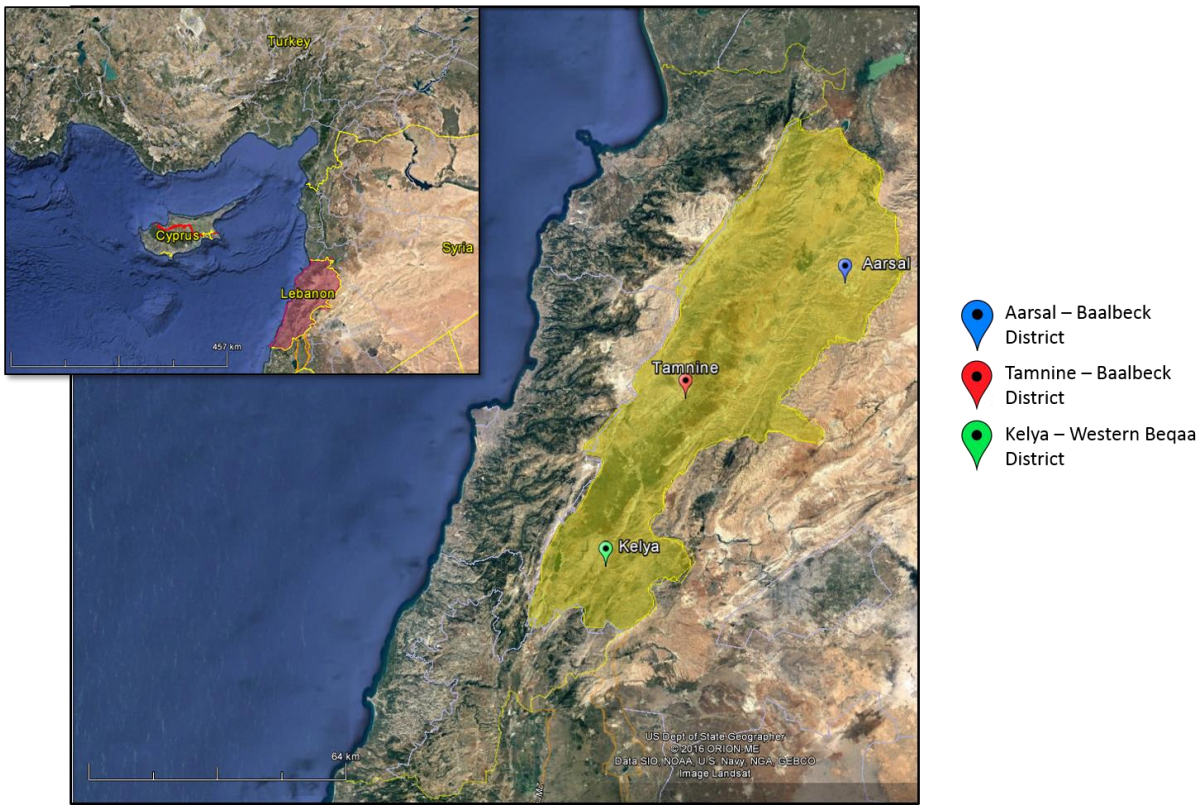

Figure 4.1: Location of three different quarries in the Beqaa region

The dimensions of the prisms were 15 cm* 15 cm * 20 cm. 10 prisms were obtained from Tamnine, the other 10 from Aarsal, and the remaining 20 are obtained from Kelya. From each prism, two cores of diameter 50 mm and length 125 mm were drilled using a DD 120 Hilti diamond coring machine. The length of the cores was then adjusted by cutting the edges from both sides of the core in order to ensure that the length to diameter ratio falls in the recommended range. This was performed using the saw available in the laboratory. The cores were capped to remove any irregularities in the end surfaces and to ensure that they are smooth and parallel. A total of 80 limestone cores were drilled and sawed and their length to diameter ratio ranged between 2:1 and 2.88:1. The cores were later tested for the unconfined uniaxial compressive strength (UCS) and the elastic modulus (E). Figure 4.2 shows the preparation process of the limestone cores for testing.

(a) (b) (c) and (d)

Figure 4.2: (a) Rectangular limestone prisms, (b) drilling of limestone cores, (c) limestone cores, and (d) capping of limestone cores.

4.1.1.2 Mortar

The elastic properties of mortar are highly dependent on the water to cement ratio since mortar is a mix of cement, sand and water. Three water to cement ratios are considered: 0.4, 0.55, and 0.7. Four mortar cylinders were prepared for each water to cement ratio. The diameter and length of the cylinders were 50 mm and 125 mm respectively. The mass proportions of mortar were prepared in accordance with the proportions of the concrete mixes. Type I Portland cement and sand with a fineness modulus of 1.4 available in the local market were used. Table 4.1 shows the proportions used for the preparation of mortar cylinders.

Table 4.1: Proportions used for mortar preparation

	Mix Proportions (kg/m^3)		
Material	Mix 1	Mix 2	Mix 3
Cement	915	805.5	718.2
Sand	915	805.5	718.2
Water	384	458.2	516
Water to Cement Ratio (w/c)	0.4	0.55	0.7

4.1.1.3 Concrete cylinders preparation

27 Concrete Cylinders are prepared for two purposes: Nine cylinders containing flaky aggregates were prepared to be used in the Digital Image Processing where the volumetric fractions of the constituents were obtained. The other 18 were divided to two sets: 9 cylinders having flaky aggregates and 9 having regular shaped aggregates. The 18 cylinders were used to measure experimentally the elastic modulus of concrete; this aims at validating the numerical results obtained by the tool proposed against the

experimental measurements. The 27 cylinders were in replicates of three, each group corresponding to a water to cement ratio (0.4, 0.55, and 0.7).

In order to incorporate the measured elastic properties of the constituents in the numerical tool and validate its suitability against experimental measurement of the concrete modulus, it is essential to incorporate the same type of aggregates and mortar proportions in the concrete mixtures. The materials and the mix proportions used in preparing the concrete cylinders are listed below:

Limestone aggregates – flaky

The aggregates used in the preparation of the concrete cylinders were obtained from the prisms used for drilling the limestone cores. After drilling the limestone cores, the surplus from the prisms was used to obtain the aggregates. The prisms were crushed into coarse and fine aggregates using the crusher in the laboratory. The aggregate grain size ranged between 19 mm and 75 μm. The aggregates were also sieved into two categories: coarse and fine aggregates. Figure 4.3 shows the process of crushing the limestone cores into coarse and fine aggregates and sieving the aggregates.

Figure 4.3: Crushing of limestone cores and sieving of limestone aggregates.

The absorption and saturated surface dry density (SSD) for the crushed coarse and fine aggregates are needed when computing the proportions of aggregates, cement and water for PCC mixes. These properties were measured according to ASTM C127 and ASTM C128 respectively and they are presented in Table 4.2.

Table 4.2: Recorded absorption and SSD values for crushed coarse and fine aggregates

	Absorption (%)	Saturated Surface Dry Density
Crushed Coarse Aggregate	1.4	2.63
Crushed Fine Aggregate	2	2.65

Moreover, ASTM C33 specifies the grading requirements for both fine and coarse aggregates in concrete. The gradations of coarse and fine aggregates individually should fall between the upper and lower limits in order to maintain a workable concrete. Figure 4.4 (a) and (b) show the upper and lower limits along with the gradations for coarse and fine aggregates. However, in concrete, aggregates are a combination of coarse and fine, and therefore a blended gradation is adopted. The blended gradation combines 60% of the coarse aggregates and 40% of the fine aggregates. The percentages were chosen to achieve a blended gradation that falls within the limits specified by BS EN 12620:2002 as shown in Figure 4.4 (c).

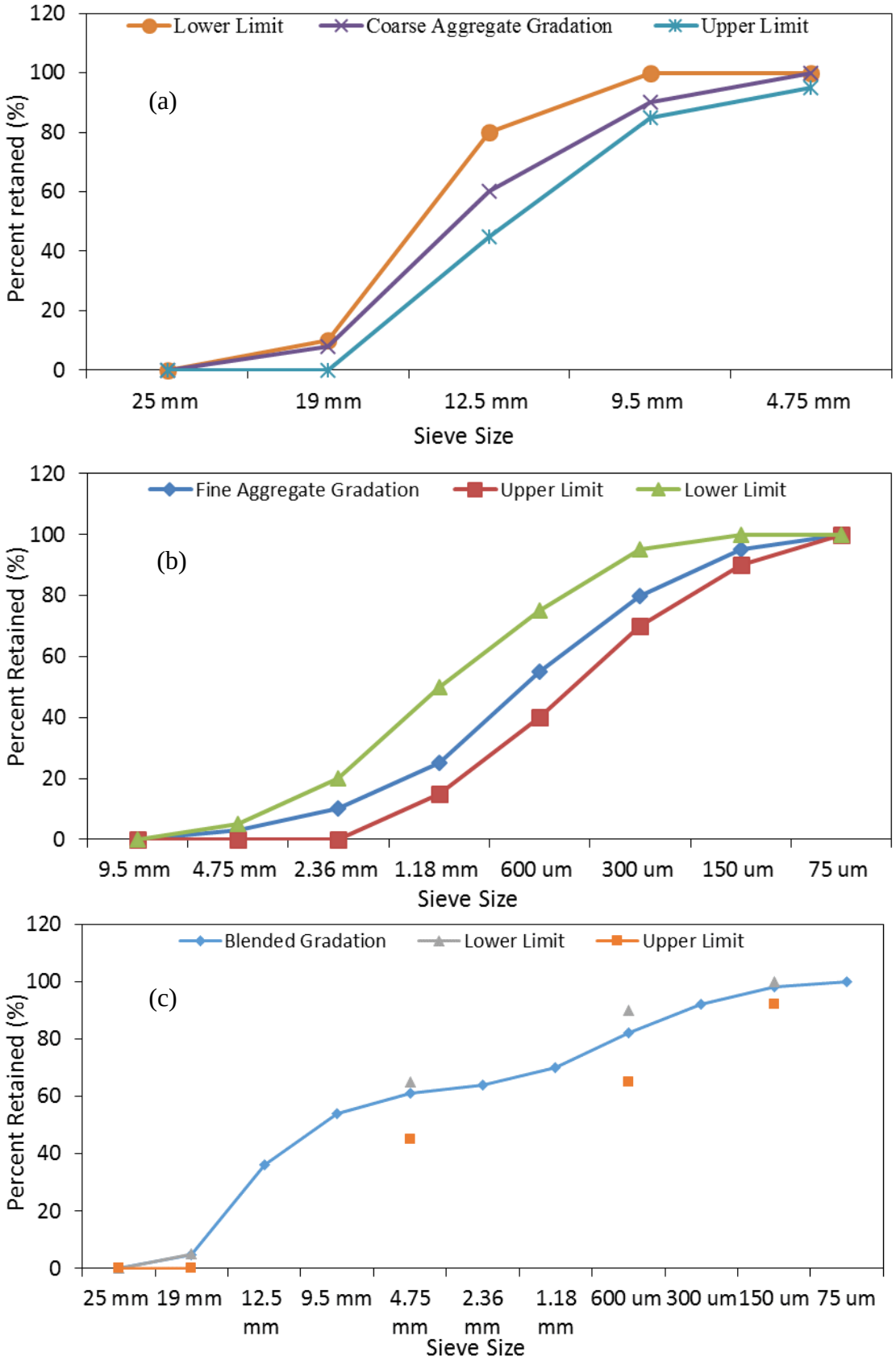

Figure 4.4: Gradation charts for (a) crushed coarse aggregates, (b) crushed fine aggregates, and (c) blended gradation

Limestone aggregates – regular

Regular aggregates were used to study the effect of the shape of aggregates on the elastic properties of concrete. The regular aggregates were obtained crushed, directly from the quarry as the limestone prisms. The elastic properties of the regular aggregates were not measured since they are obtained from the same source as the flaky aggregates; thus it is assumed they have the same properties.

PCC Mix Proportions and Fabrication

The following materials were used in the PCC mixes:

1. Crushed coarse aggregates (Flaky/Regular aggregates)
2. Fine aggregates as a mix of crushed fine aggregates and natural sand. The crushed fine aggregates are either flaky or regular. The natural sand was obtained from a local source in Lebanon.
3. Type I Portland Cement.

The fineness modulus of the crushed fine aggregates and the natural sand were 2.68 and 1.4 respectively. The maximum aggregate size (MAS) was kept constant throughout all the mixes. The MAS used is 19 mm. The mixes were cast in cylinders of diameter 150 mm and length 300 mm in three lifts. Each lift was rodded 25 times according to ASTM C192. After 24 hours, the cylinders were removed from the molds and cured for 28 days in a curing room. The proportioning method was done according to ACI 211. Table 4.3 presents the proportions and volumes of constituents for the three mixes.

Table 4.3: Mix proportions and volumes for three concrete mixes

Material	Mix Proportions (kg/m^3)			Volumes (in 1 m^3 of concrete)		
	Mix 1	Mix 2	Mix 3	Mix 1	Mix 2	Mix 3
Cement	475	346	272	0.15	0.11	0.09
Water	218	220	221	0.218	0.22	0.221
Crushed Coarse Aggregates	1011	1011	1011	0.38	0.38	0.38
Crushed Fine Aggregates	203.5	442	577	0.07	0.16	0.22
Natural Sand	475	346	272	0.16	0.12	0.10
w/c ratio	0.4	0.55	0.7			
Target Air Content				0.02		

4.1.2 Test methods

It is important to note that ASTM C39 and C42 require that the end surfaces of cylindrical specimens are perpendicular to the applied axis load during compressive strength testing. Therefore, in this study, limestone cores, mortar specimens, and concrete cylinders tested in compression for the elastic modulus were capped using sulfur mortar.

Limestone cores and mortar cylinders were tested for the uniaxial compressive strength and the elastic modulus. The protocols followed during testing for each material are listed in Table 4.4. The machine used for testing is a servo hydraulic closed loop machine with a capacity of 200 tons. Four vertical linear variable differential transformers (LVDT) were used to measure the axial strain of the cores. Each pair of vertical LVDTs was placed diametrically opposite to each other. The setup used for testing is shown in Figure 4.5.

Table 4.4: Testing specifications for the different material types.

Material	ASTM	Gage Length	Loading Type/ Rate
Limestone Cores	D7012-14	75 mm	Loading type: Displacement control Rate: 1 mm/min
Mortar cylinders	C469/C469M-14*	75 mm	
Concrete Cylinders	C469/C469M-14	150 mm	

*This standard applies to the static elastic modulus and Poisson's ratio of concrete in compression; however, in this study it is also adopted for finding the properties of mortar.

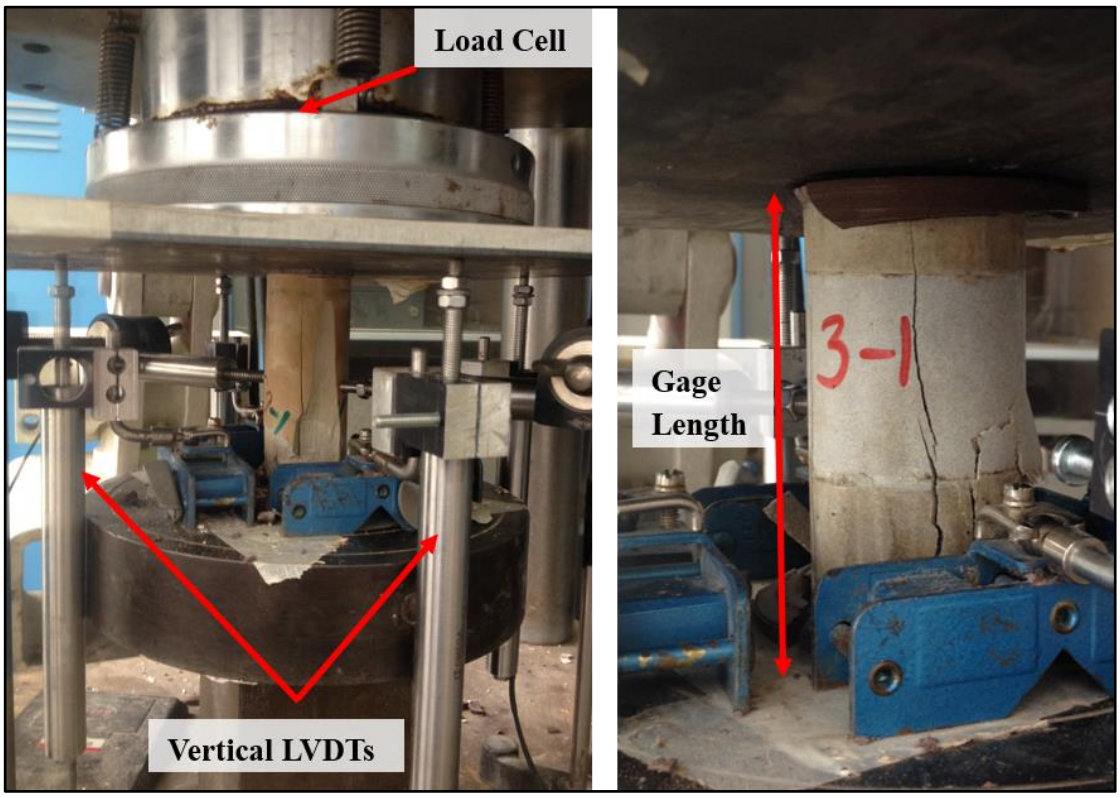

Figure 4.5: The setup prepared for testing concrete cylinders, limestone cores, and mortar specimens.

4.2 Probabilistic Fitting

4.2.1 Limestone

The elastic modulus of 80 limestone cores was measured and recorded. Given that the limestone cores were obtained from three different regions, the effect of source is discussed and a probabilistic distribution to the data is proposed.

4.2.1.1 Effect of source

The elastic modulus varied between 31.1 GPa and 67.3 GPa, 34 GPa and 72.9 GPa, 28.3 GPa and 68.7 GPa for Arsal, Kelya, and Tamnine respectively. Figure 4.6 shows the distribution of the elastic modulus with the minimum, first quantile, median, third quantile and maximum for each source. A one way analysis of variance on the means of the elastic modulus at a confidence interval of 0.95 yields a p-value of 0.9. This indicates that there is no statistical difference between the means of the different sources and it is primarily due to the fact that the variability within each source is larger than the variability between the sources as seen in Figure 4.6. This variation is primarily caused by the heterogeneity of each sample such as the presence of impurities, longitudinal cracks, and quartz, which all weakens the sample. Also, the heterogeneity in the mineralogical composition of the samples lead to a larger variability in the elastic modulus values. Figure 4.7 shows the factors leading to a variability in the elastic modulus of limestone.

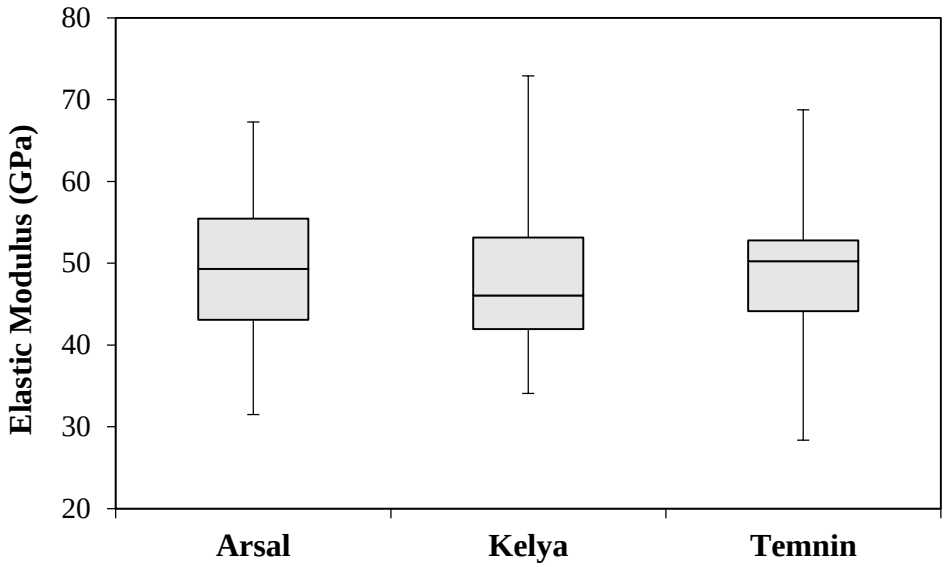

Figure 4.6: Box and Whisker plot for Elastic Modulus of limestone (10 cores obtained from Aarsal, 20 cores obtained from Kelya, and 10 cores from Temnine)

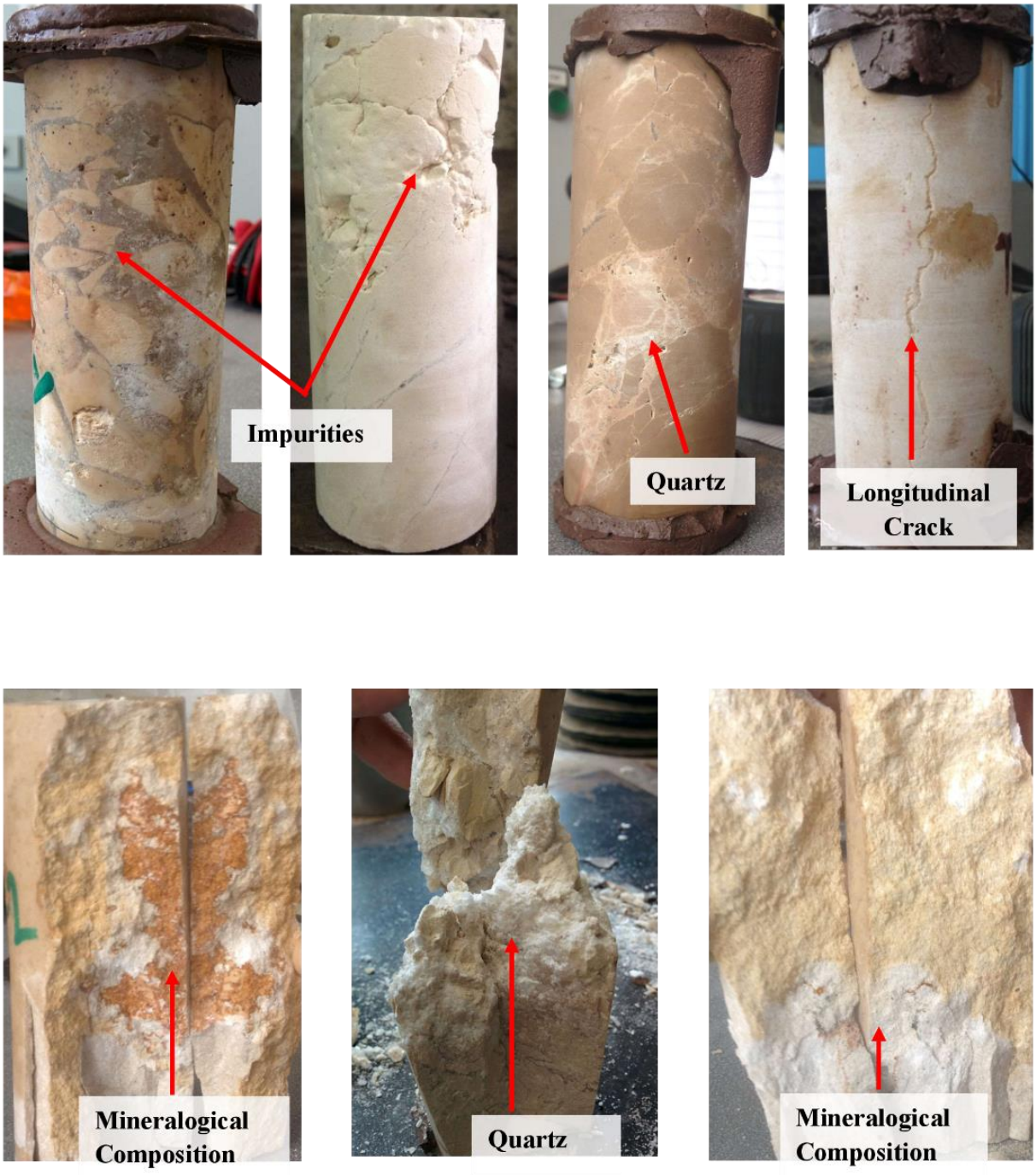

Figure 4.7: Factors affecting the elastic modulus of limestone and causing large scatter in the results.

4.2.1.2 Probabilistic distribution

The results for the three sources were combined and analyzed as one sample since in this study the source does not affect the elastic modulus. Figure 4.8 shows that E_a can be

best described by a lognormal distribution with a log mean of 3.85 and a log standard deviation of 0.186. A Chi-Square test was used to measure the goodness of fit of the lognormal distribution to the experimental data. At a confidence interval of 95%, the chi-square test resulted a p-value of 0.436 indicating that the lognormal distribution is a good fit to the data (E_a~LN(3.86,0.186)).

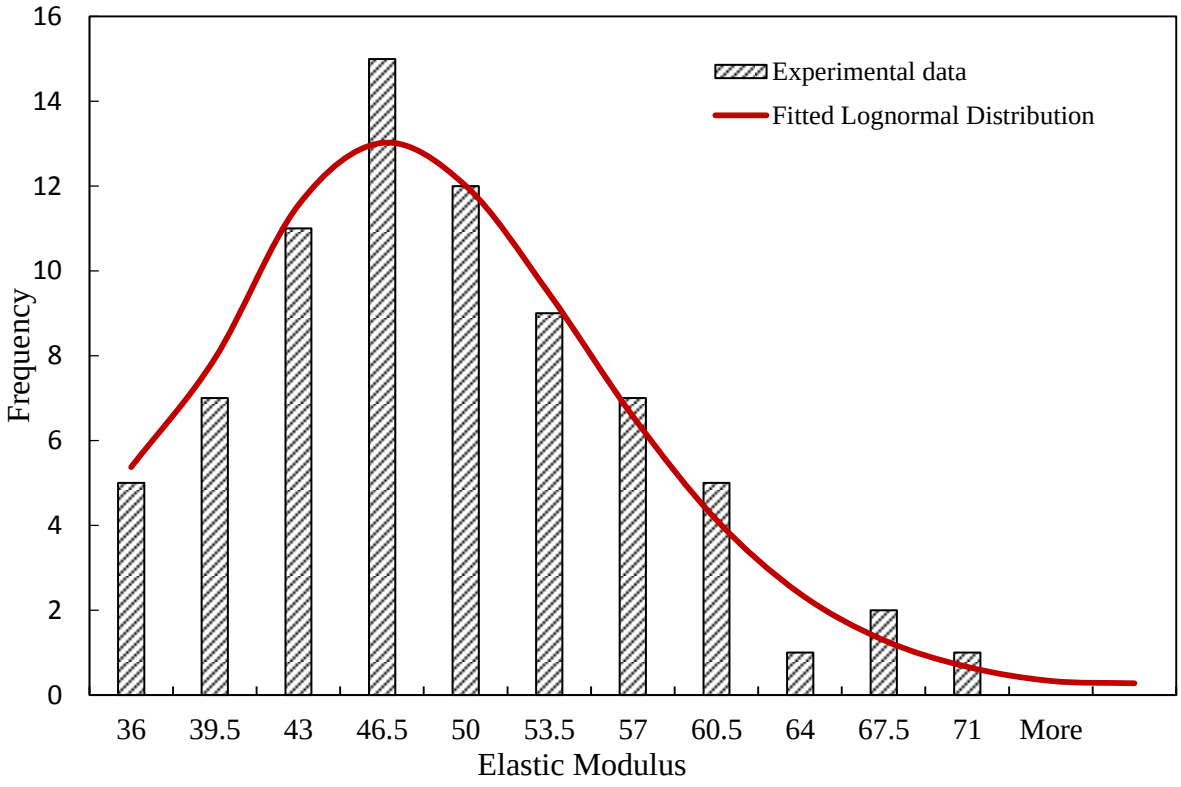

Figure 4.8: Histogram and Probability distribution for the elastic modulus of Limestone in Lebanon

Table 4.5 provides a summary of the values of the elastic modulus of limestone found in the literature. The experimental data obtained ranges between 28.3 GPa and 72.9 GPa. Therefore, the average elastic modulus of tested limestone falls within the reported range.

Table 4.5: Comparison of elastic modulus of limestone with literature reported values.

Authors	Location	Average E* (GPa)	Standard Deviation/ Range
(Deere & Miller, 1966) [57]	Bedford, Indiana	27.09	1.35
	Carthage, Missouri	49.5	10.54
	Solenhofen, Bavaria	63.84	14.55
(Santi, Holschen, & Stephenson, 2000) [77]	East Tennessee, United States	64.99	-
	Indiana, United States	25.76	
(Palchik & Htazor, 2002) [78]	Negev, Israel	30.96	15.12
(Al-Shayea, 2004) [79]	Gassim, Saudi Arabia	60.392(1)	-
		50.11(2)	
(Lam, Martin, & McCreath, 2007) [80]	Ontario, Canada	31.5	10-67 GPa
(Turgut, Yesilnacar, & Bulut, 2008) [81]	Sanliurfa, Turkey	13.9	2.6
(Zhang, AiHong, & Lu, 2009) [82]	Xuzhou, China	17.77	-
(MayCrespo, et al., 2012) [83]	Peninsula of Yucatan, Mexico	8.34	0.22
This Study	Beqaa, Lebanon	48.2	8.8 / 28.3 – 72.9

*Elastic Modulus of limestone.

(1)Tangent modulus measured at 50% of stress level for sample 1 and (2) for sample 2

4.2.2 Mortar

Given that the mortar is considered to behave as a homogeneous medium, it is expected that the variation among the replicates for each water to cement ratio is minimal. Therefore, only four replicates were used to measure the elastic modulus. Table 4.6

presents the average and standard deviation of the elastic modulus measurement. It can be seen that the elastic modulus of mortar decreases as the water to cement ratio increases from Mix 1 to Mix 3. This is typical since the water content increases and reduces the properties of mortar. The decrease is approximately 6% when the water to cement ratio increases from 0.4 to 0.55, however it increases to 24% when the water to cement ratio increases from 0.55 to 0.7. This indicates that the relation between the elastic modulus of mortar and water to cement ratio is not linear.

Table 4.6: Experimental values for the elastic modulus of mortar

	Mix 1	Mix 2	Mix 3
Average Elastic Modulus	19.47	18.27	13.8
Standard Deviation	1.74	0.77	1.87

CHAPTER 5

PROBABILISTIC DISTRIBUTION FOR THE VOLUMETRIC FRACTION OF CONCRETE CONSTITUENTS

As mentioned earlier, DIP techniques consist of three components: image acquisition, processing, and analysis. This chapter presents in details the steps undertaken in the digital image process.

5.1 Digital Image Processing Setup

5.1.1 Image acquisition

Concrete cylinders were first cut transversally (along the short axis) into 15 sections with a thickness of 2 cm each. Then, each section was scanned in gray scale color using an HP ScanJet G3110 photo scanner with a resolution of 1200 dpi. This step was performed for each of the three cylinders of the three mixes.

5.1.2 Image processing

The first step was to digitize the scanned images by transforming the real images into digital images. This was achieved by storing each image in MATLAB software as a matrix consisting of coefficients termed pixels. Given that the images were captured in gray scale, the value of each pixel ranges between 0 and 255 indicating the intensity of the gray color. The values 0 and 255 indicate the colors black and white respectively.

After storing the images, each image undergoes the following set of operations to enhance its quality:

- Median filtering: This algorithm was applied for noise removal identified as "salt and pepper" noise. In this case, noise was defined as any particle that has a diameter smaller than the diameter specified by the user.
- Filling operation: This step was carried to fill all the holes found in the image. Holes were defined as an area of dark pixels surrounded by lighter pixels. However, this step excludes the voids (identified as black holes in the gray colored matrix).
- For Hashin and Ramesh models, the volumetric fraction of the Interfacial zone is needed. This was obtained by calculating the perimeter of each aggregate in an image and then multiplying it by a thickness of 20 μm which is assumed to be the thickness of the interfacial zone. Figure 5.1 (a), (b), and (c) show the steps of the enhancement process.

5.1.3 Image analysis

To identify the three phases of concrete (void, aggregate, mortar, and ITZ), an algorithm was applied to convert the matrix of the image to a standard matrix consisting of 0, 0.5, and 1 which represent the void, mortar and aggregate phases respectively. The last step was discretizing each image into 2D square elements. In each element, the area fraction of aggregates, mortar, and voids were obtained by counting the number of pixels corresponding to each phase and then dividing it by the total number of pixels in each element.

An appropriate size of the 2D square element was called an RVE. The size of the RVE in this study varied between 20*20 mm and 105*105 mm at an increment of 15*15 mm, and its effect on the volumetric fractions of the constituents was examined. The smallest element size was set approximately equal to the MAS which is 19 mm. Also, the smallest dimension of the cylinder is 150 mm; therefore, the maximum element size was set to 105*105 mm to eliminate the effect of the boundary conditions. Figure 5.1 (d) shows the effect of the RVE size on the concentrations of the constituents in a RVE.

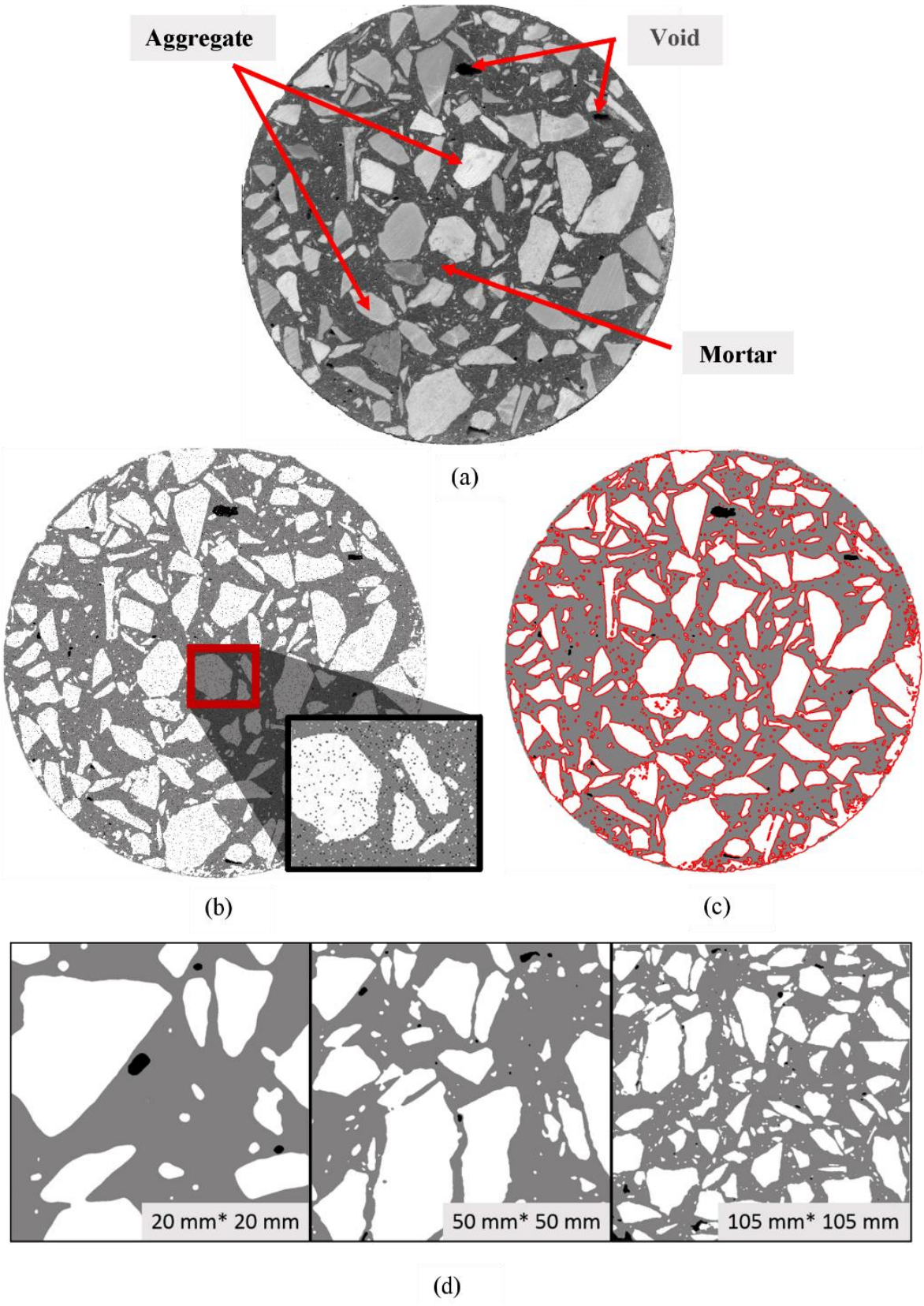

Figure 5.1: (a) Grayscale scan of a concrete section, (b) Salt and Pepper noise, (c) Detection of interfacial zone, and (d) Effect of RVE size

5.2 Probabilistic fitting

5.2.1 Aggregates

Figure 5.2 presents the volumetric fraction of aggregates for Mix 1. The results indicate that the mean volumetric fraction of aggregate is not affected by the RVE size (Figure 5.2 (a)). However, the variation in the volumetric fraction diminishes as the RVE size increases, and this indicate that as the RVE size increases the element becomes a better representation of the concrete section. A one-way analysis of variance (ANOVA) with Welch correction for unequal variance was performed to check if the means were statistically different. The test returned a p-value of 0.9 indicating that the mean is not affected by the RVE size. Figure 5.2 (a) also shows the difference between the volume of aggregates employed in the concrete mix according to ACI and the volume of aggregates obtained by the use of the digital images. The difference was approximately 6%, which was considered negligible due to the loss of information when converting from the real scanned images to the digitized images.

Figure 5.2 (b) shows the probability density function for the aggregate volume fraction. The standard deviation appears to decrease as the size of the RVE increased. The MAS is 19 mm and therefore a RVE size of 20 mm is not a suitable representation of the concrete mix given that it will only display an aggregate particle excluded from mortar. Figure 5.2 (b) also shows that the standard deviation drops from 0.126 at a RVE of 20 mm to 0.046 at a RVE of 75 mm, after which the standard deviation slightly changes. This indicates that the RVE size of 75 mm or higher can be used to represent the properties of a concrete mix. It is important to mention that the volumetric fraction of

aggregates was modeled as a normal distribution with a mean of 0.469 and a standard deviation of 0.046 – N (0.469, 0.046).

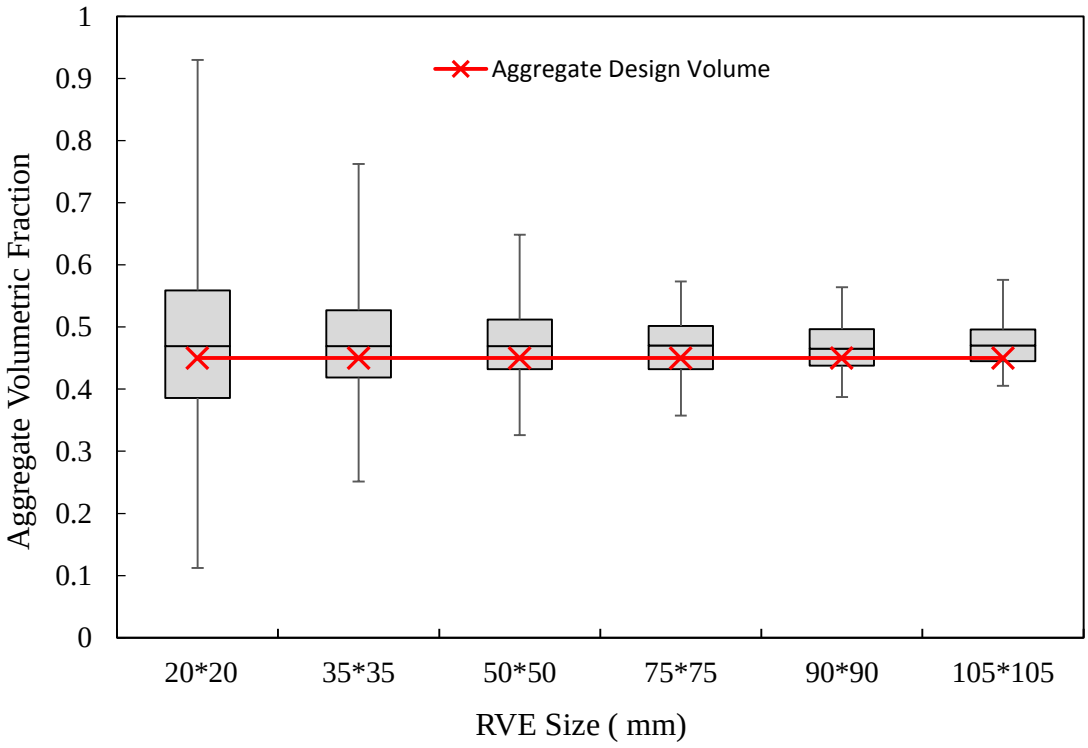

(a)

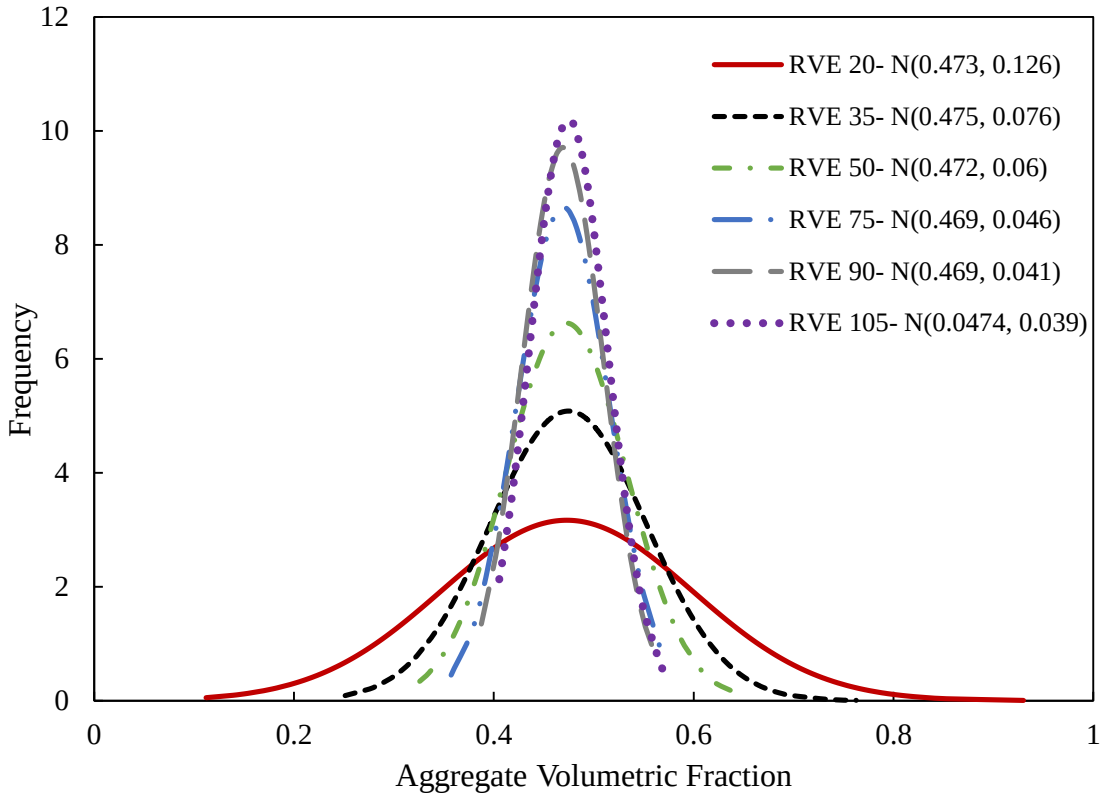

(b)

Figure 5.2: (a) Box and Whisker plot and (b) Probability density function for the volumetric fraction of aggregates in Mix 1.

5.2.2 Mortar

For a RVE of 75 mm * 75 mm, Figure 5.3 shows that also the volumetric fraction of mortar in Mix 1 can be modeled as a normal distribution with a mean of 0.528 and a standard deviation of 0.045 – N (0.528, 0.045). As the RVE size increased the standard deviation approximately decreased by 30% from a RVE size of 20 mm to a RVE size of 75 mm. However, from a RVE size of 75 mm and onward the standard deviation decreased only by 9%. As previously mentioned this indicates that a RVE size of 75 mm and higher can be considered a proper representation of the concrete constituents.

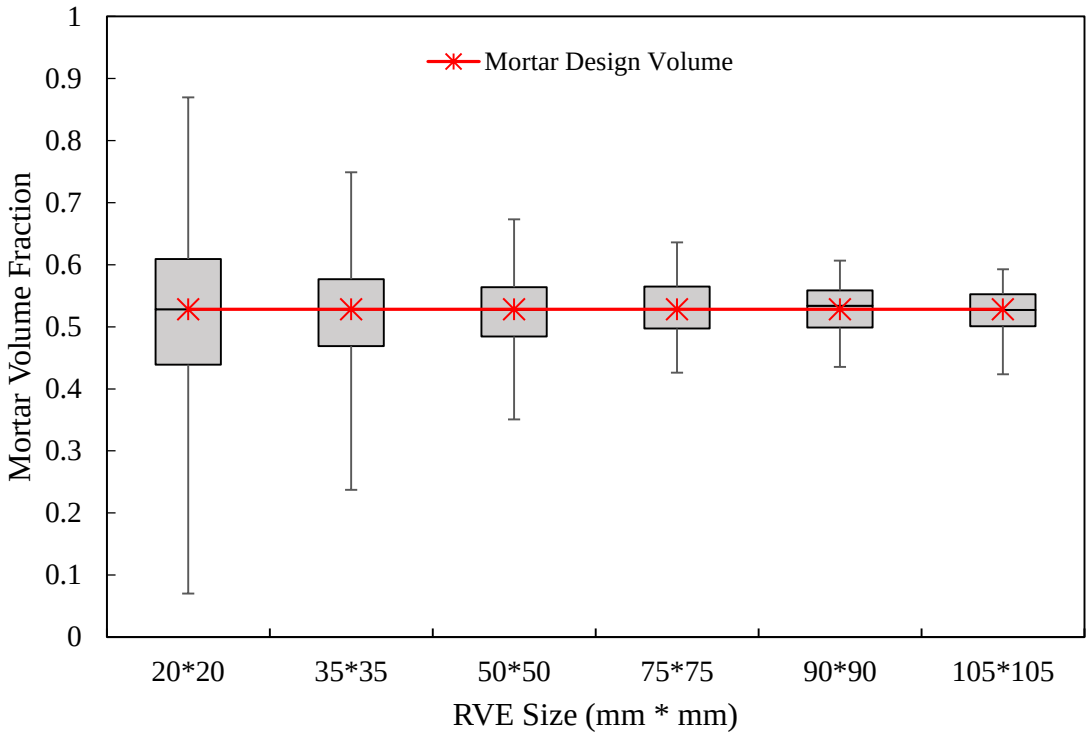
Mortar Design Volume
Mortar Volume Fraction
1
0.9
0.8
0.7
0.6
0.5
0.4
0.3
0.2
0.1
0
20*20
35*35
50*50
75*75
90*90
105*105
RVE Size (mm * mm)

(a)

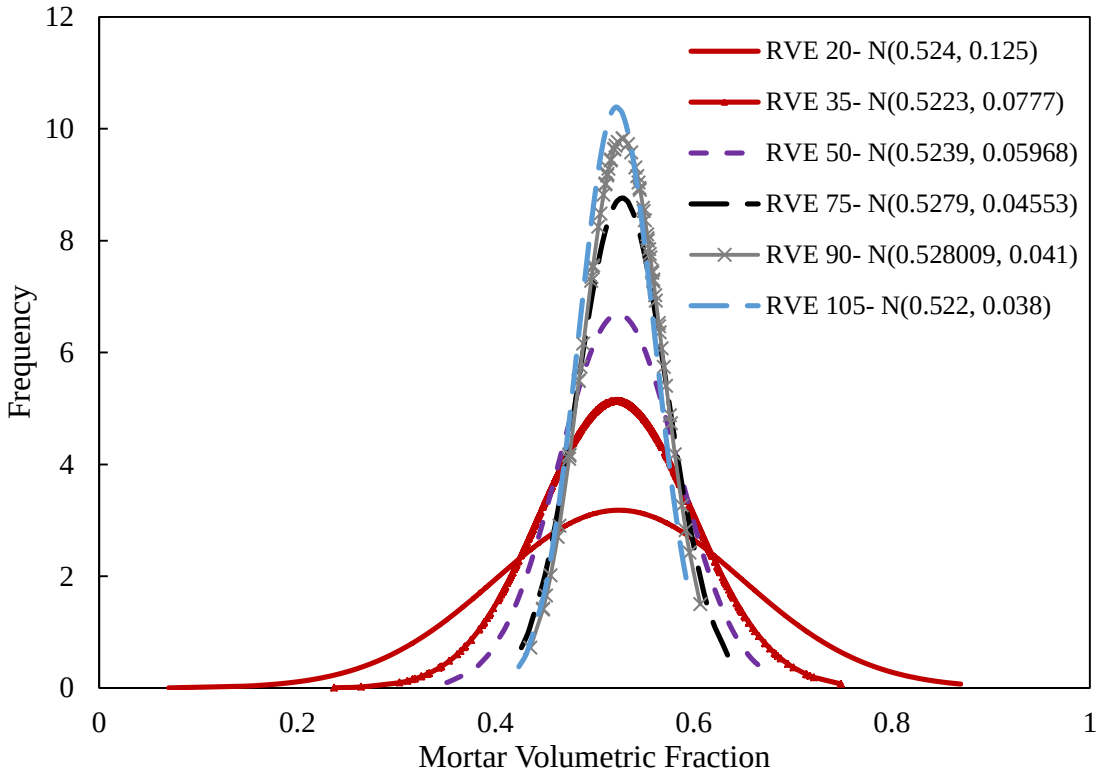

(b)

Figure 5.3: (a) Box and Whisker plot and (b) Probability density function for the volumetric fraction of mortar in Mix 1.

Table 5.1 presents a summary of the distributions for the volumetric fractions of aggregates and mortar for Mix 1. Appendix A shows the distributions for Mixes 2 and 3 along with the interfacial zone volumetric fractions.

Table 5.1: Summary of the probabilistic distributions for the volumetric fractions of aggregates, mortar, and void in Mix 1.

RVE Size	Type of Mix		
	Mix 1	Mix 2	Mix 3
	Aggregate		
20 mm* 20mm	N(0.473, 0.126)	20 mm* 20mm	N(0.473, 0.126)
35 mm * 35 mm	N(0.475, 0.076)	35 mm * 35 mm	N(0.475, 0.076)
50 mm * 50 mm	N(0.472, 0.06)	50 mm * 50 mm	N(0.472, 0.06)
75 mm * 75 mm	N(0.469, 0.046)	75 mm * 75 mm	N(0.469, 0.046)
90 mm * 90 mm	N(0.469, 0.041)	90 mm * 90 mm	N(0.469, 0.041)
105 mm * 105 mm	N(0.474, 0.039)	105 mm * 105 mm	N(0.474, 0.039)
	Mortar		
20 mm* 20mm	N(0.524,0.125)	N(0.482, 0.135)	N(0.408, 0.114)
35 mm * 35 mm	N(0.522,0.077)	N(0.479, 0.098)	N(0.405, 0.084)
50 mm * 50 mm	N(0.523,0.059)	N(0.481, 0.076)	N(0.408, 0.068)
75 mm * 75 mm	N(0.527,0.045)	N(0.483, 0.056)	N(0.416, 0.055)
90 mm * 90 mm	N(0.528,0.041)	N(0.484, 0.053)	N(0.414, 0.055)
105 mm * 105 mm	N(0.522,0.038)	N(0.479, 0.05)	N(0.405, 0.054)

CHAPTER 6

END EFFECT STUDY

The objective of this chapter is to investigate the effect of the end conditions of the specimen along with the LVDTs gage length on the elastic modulus measurement. This chapter describes the process that helped in developing the setup adopted for testing the elastic modulus of limestone cores, mortar, and concrete cylinders.

6.1 Setup I

ASTM C469 specifies that the effective gauge length of the LVDTs, when testing the elastic modulus of concrete, shall not be less than "three times the MAS in the concrete nor more than two thirds the height of the specimen" [10]. Also, it specifies that a preferred gauge length is one half the height of the specimen. Moreover, ASTM D7012 specifies that the gauge length shall be close to mid height. It is important that the LVDTs do not encroach on the ends of the specimen because the contact between the steel plates of the machine and the surfaces of the specimen causes restraints at those surfaces. In addition, sulfur mortar capping restricts the horizontal movement of the ends of the specimen and hence creates stress concentrations at the edges of the specimens. Both phenomena create non-uniformity in the strain distribution in the specimen, and the strain at the edges are different from strain elsewhere in the specimen. This is known as the "End Effect".

Given that the length of concrete cylinders in this study was 300 mm and the MAS used was 19 mm, then the gauge length shall be between 57 mm and 200 mm, and preferably

150 mm. However, in this case the LVDTs were not mounted directly on the specimens and were encroaching on the ends (

Figure 6.1) for the following reasons:

- First, when testing the limestone and mortar cores, the lengths of the specimens were small compared to the size of the LVDTs; thus the LDVTs could not be attached directly to the specimen.
- Second, when testing the concrete cylinders, the weight of the four LVDTs was large and the designed steel circular plates could not hold the LVDTs on the specimen.

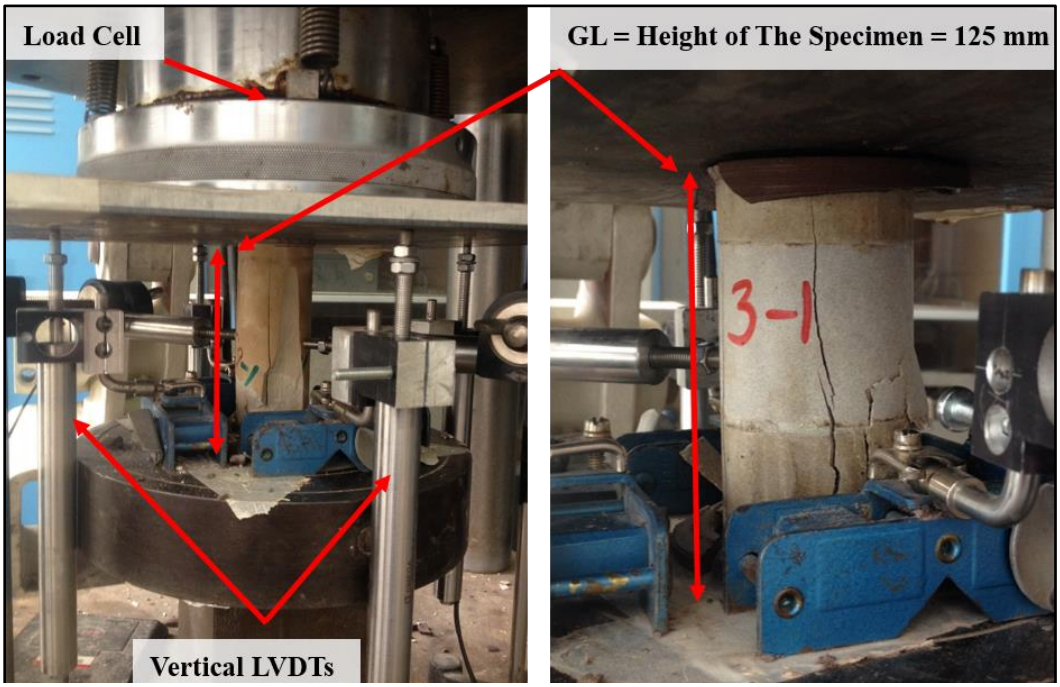

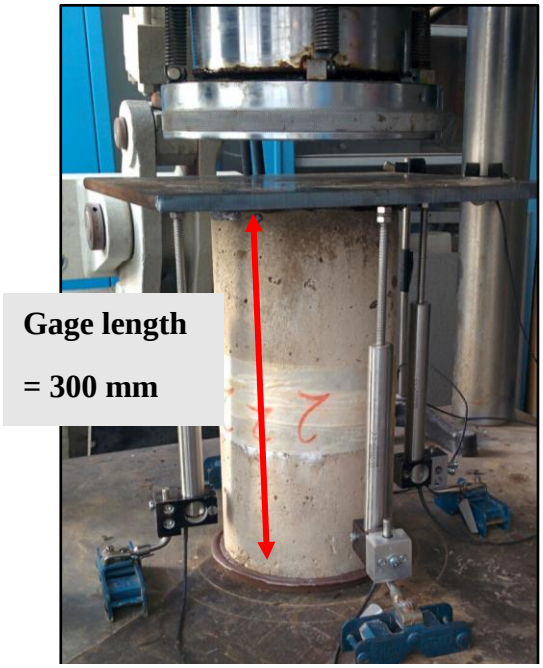

Figure 6.1: Setup I showing the configurations of the LVDTs and the gage lengths.

During testing, it was noticed that as the load applied to the cylinder increases, minor deviations from planeness in the end surfaces caused the steel plate to tilt leading to unequal readings in the LVDTs as shown in Figure 6.2. This phenomenon decreased the recorded strength and elastic modulus of all the specimens. Since the setup did not fully adhere to the requirements set for the gauge lengths and due to the rotation of the steel plate, a finite element analysis was conducted in order to understand the end effect mechanism and its influence on the vertical strain distribution.

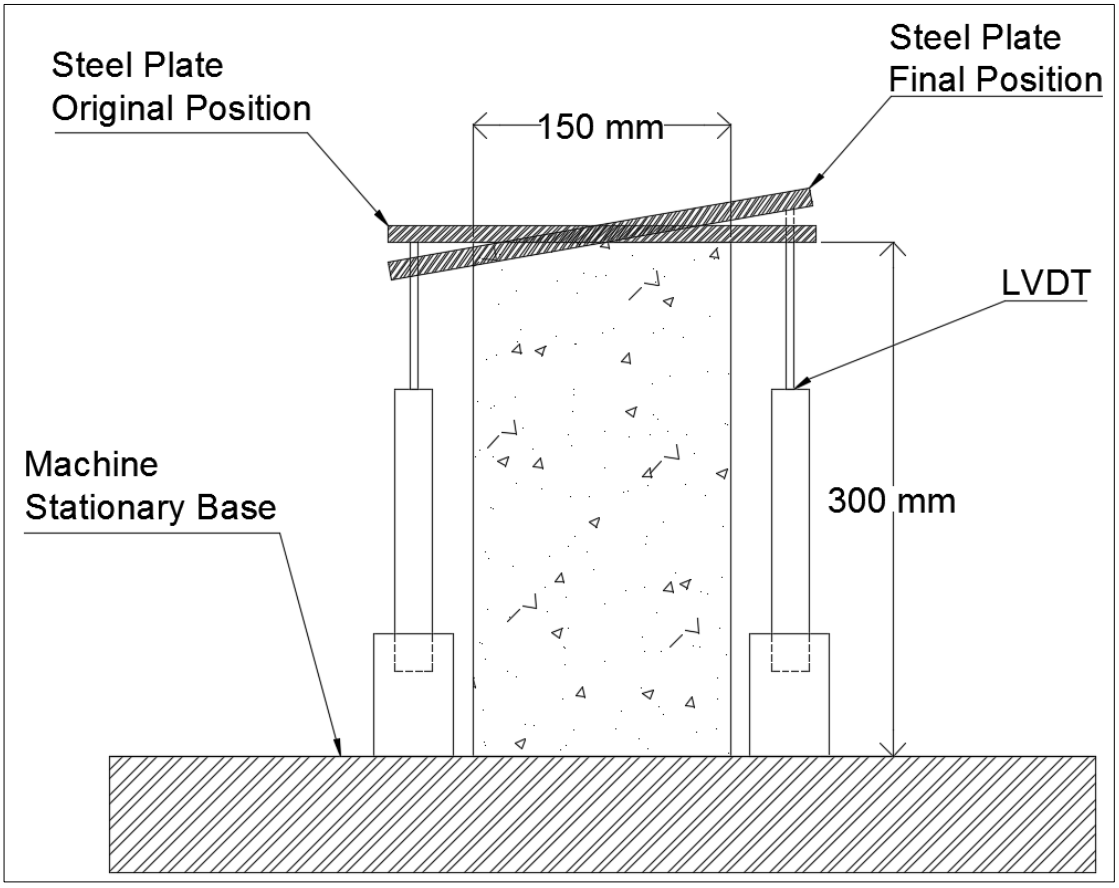

Figure 6.2: Tilting angle of the steel plate causing reduction in the strength and elastic modulus measurement.

6.2 Finite Element Analysis

A 3-Dimensional Finite Element Model was developed to understand the stress and vertical strain distributions along the height of a specimen. This was essential to accurately estimate the region where the stress was constant and therefore the strain was uniform. A finite element software ADINA was utilized to conduct the analysis [86]. The analysis was conducted in the linear elastic state, therefore, only the elastic modulus and Poisson's ratio were used to describe the material of the model. The

boundary conditions and the displacement load were chosen to mimic the conditions of the experimental tests and they were as follows:

- ***Boundary Conditions:*** The movement at the bottom surface of the solid body was restrained in the lateral and vertical directions; while only in the lateral direction at the top surface.
- ***Load Type and Rate:*** A displacement Control load at a rate of 1 mm/min was applied to the top surface of the solid body.

Figure 6.3 (b) shows that the stress in the model is the highest at the edges of the top and bottom surfaces (indicated in blue color). Given that stress and strain are directly proportional, strains reach also their maximum value at the ends. As the load propagates through the specimen shown in Figure 6.3 (a), stress reaches a constant value at mid height of the specimen. Therefore, strain in a specimen is only uniform at mid height of the specimen where the stress is constant as shown in Figure 6.3 (c). Based on the region where the strain is uniform, a gage length of 150 mm was adopted. The gage length is 75 mm away from both surfaces of the specimen.

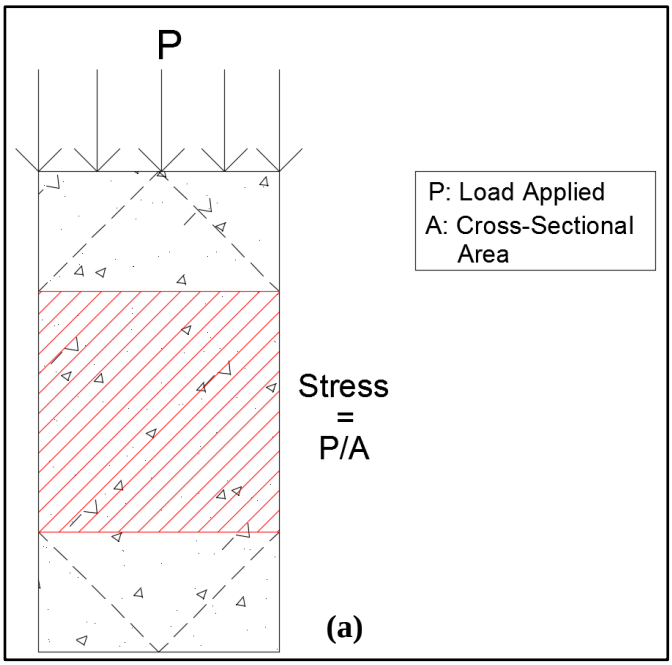

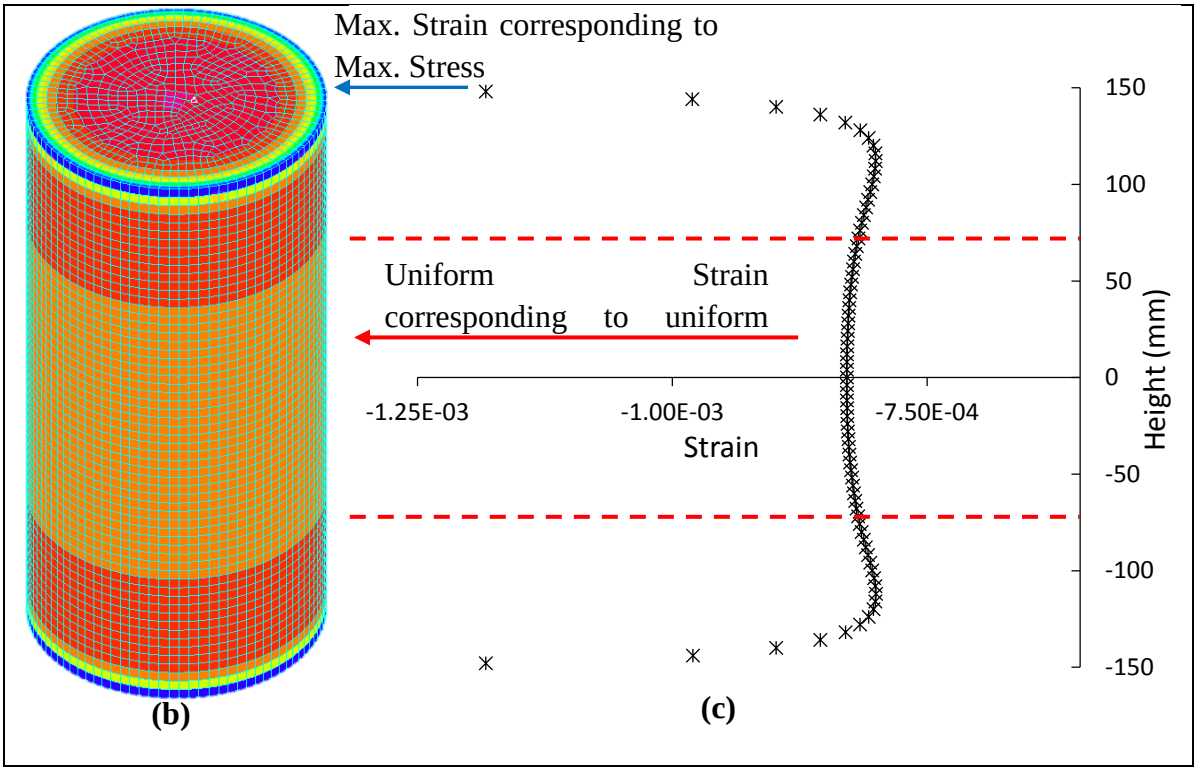

Figure 6.3: (a) Load Propagation in a cylinder, (b) Stress distribution in a 3D solid body and (c) Strain distribution along the height of the solid body.

6.3 Setup II

As a result of the finite element analysis, a new setup was developed that comprises of two steel rings which allow the LVDTs to be mounted directly on the specimen with a gage length of 150 mm. This setup was used for the concrete cylinders.

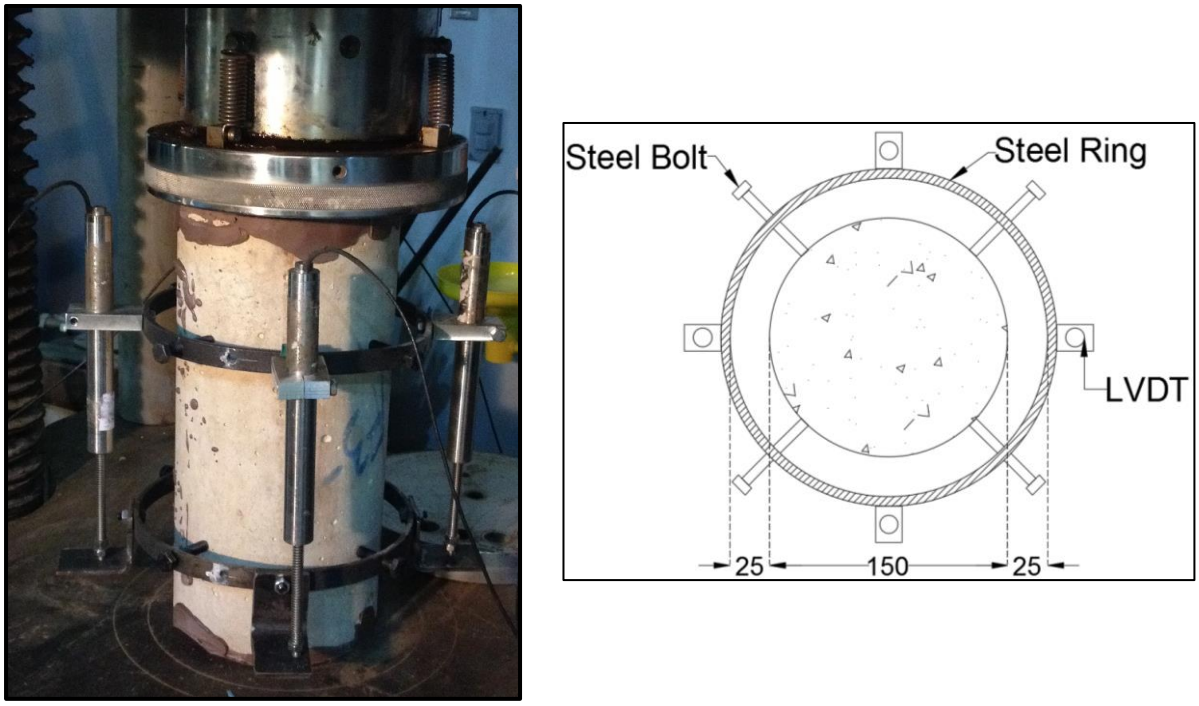

Figure 6.4: Setup II configuration

6.4 Correction factor

A correction factor was obtained by measuring the elastic modulus for 7 cylinders using Setup I and Setup II. The ratio of the elastic modulus measured using Setup II to that measured using I was considered as the correction factor. Figure 6.5 shows the effect of the gage length and the conditions of the end specimen on the elastic modulus measurement. It was noticed that a higher elastic modulus was obtained when the LVDTs do not encroach the end of the specimens and the gage length was equal to half the height of the specimen.

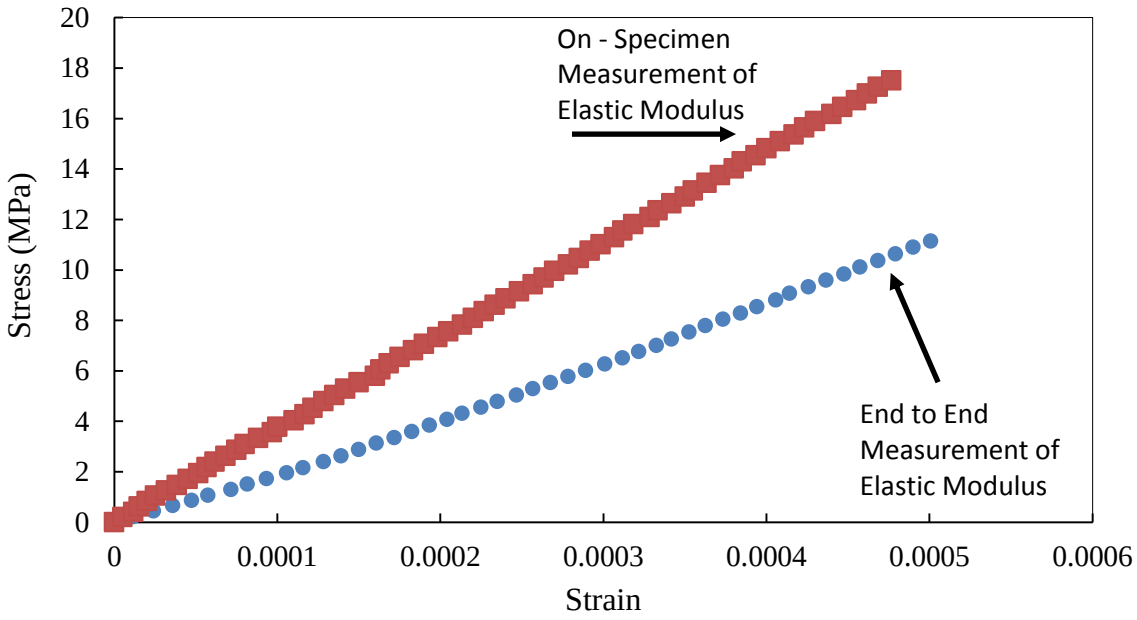

Figure 6.5: End to End and On-Specimen Stress- Strain curves

Table 6.1 shows the correction factor obtained for seven cylinders. On average the elastic modulus measured at a gage length equal half the length of the specimen is approximately 1.8 times that measured from the end of the specimens. This was in close agreement with ASTM which recommended using a correction factor of 2 [6].

Table 6.1: Correction Factor for 7 cylinders

Cylinder No.	Elastic Modulus – Setup I	Elastic Result – Setup II	Correction Factor
1	38.486	22.145	1.74
2	34.21	21.53	1.6
3	36.725	22.212	1.65
4	36.207	22.119	1.64
5	36.462	18.509	1.97
6	38	18.19	2.08
7	33.36	17.723	1.88
Average			1.79

CHAPTER 7

VALIDATION

This chapter presents the results of the experimental investigation of the elastic modulus of concrete conducted for 18 cylinders divided into two sets: the first set incorporating flaky aggregates and the second incorporating regular angular aggregates. The results of the numerical tool proposed are then validated against the experimental measurement. Finally, both the numerical and experimental results are compared to the values obtained by the empirical formulae proposed by the design codes.

7.1 Experimental Measurement

Typically, the uniaxial strength of concrete decreases as the water to cement ratio increases due to a higher water content. Table 7.1 shows that the uniaxial strength decreases from 44.2 MPa to 30 MPa and from 46.3 MPa to 27 MPa as the water to cement ratio increases from 0.4 to 0.7 for flaky and regular aggregates respectively. At a water to cement ratio of 0.4, the strength is higher for the mix incorporating regular aggregates than for that incorporating flaky aggregates. A concrete mix is classified as a high strength concrete if its strength exceeds 40 MPa, and the strength is controlled by the strength of the aggregate. Although the flaky and regular aggregates are from the same source so their strength was assumed to be identical, flaky aggregates were thin, elongated and tend to break faster when the load was applied. Therefore, regular shaped aggregates can withstand a higher load increasing the load carried by the concrete cylinder. Normal strength concrete mixtures are mixes with a water to cement ratio

greater than 0.4, which is the case for Mixes 2 and 3. The strength of normal strength concrete is dominated by the strength of mortar and the bond between the mortar and the coarse aggregate. Given that Mixes 2 and 3 for both flaky and regular aggregates incorporate the same type and strength of mortar, then Mixes 2 and 3 with flaky aggregates exhibited higher strengths due to the bond between the mortar and the coarse aggregate. Flaky aggregates have a higher surface area compared to regular shaped aggregates, thus an increased area for bonding with the paste. According to Goble and Cohen (1999) an increase in peak stress is witnessed as the aggregate surface area increases [85], thus the increased strength of Mixes 2 and 3 incorporating flaky aggregates.

Table 7.1: Experimental results for the uniaxial strength and elastic modulus of concrete

	Uniaxial Strength (MPa)		Elastic Modulus (GPa)	
	Mean	Standard Deviation	Mean	Standard Deviation
Flaky Aggregates				
Mix 1	44.2	2.61	35.5	1.78
Mix 2	38.9	1.73	36.3	0.18
Mix 3	30.08	1.02	35.6	3.28
Regular Aggregates				
Mix 1	46.3	0.76	37.9	0.81
Mix 2	37.2	0.64	33.2	0.67
Mix 3	27.2	1.08	30.8	0.93

Figure 7.1 (b) shows the stress strain curves for the concrete mixes with regular shaped aggregates. The elastic modulus was measured as the secant modulus between two intervals (Zero Stress and 45% of the maximum uniaxial strength). It was noticed that

the elastic modulus of concrete decreased as the water to cement ratio increased. This decrease is associated with the decrease in the elastic modulus of the mortar. However, the elastic modulus remained constant for the case of the mixes having flaky aggregates. This observation can be attributed to several factors:

1. The packing density of flaky aggregates is higher than that of regular shaped aggregates. A higher packing density requires less amount of cement paste to fill the voids between the aggregates, thus a higher amount of cement paste is coating the aggregates and increasing the elastic modulus of concrete.
2. The surface texture of flaky aggregates is rougher which results in a greater adhesion between the cement paste and the aggregates.
3. The surface area of flaky aggregates is higher than that of regular shaped aggregates. Aggregates with a higher surface area exhibit a higher water absorption, thus decreasing the water to cement ratio of the concrete mix. The effect of water to cement ratio in Mixes 1, 2, and 3 is not remarkable due to the surface area of the flaky aggregates. The surface area of the aggregates is causing additional water to be absorbed, thus lowering the water to cement ratio of the cement paste. Hence a constant elastic modulus for the three mixes with flaky aggregates is obtained [87] .

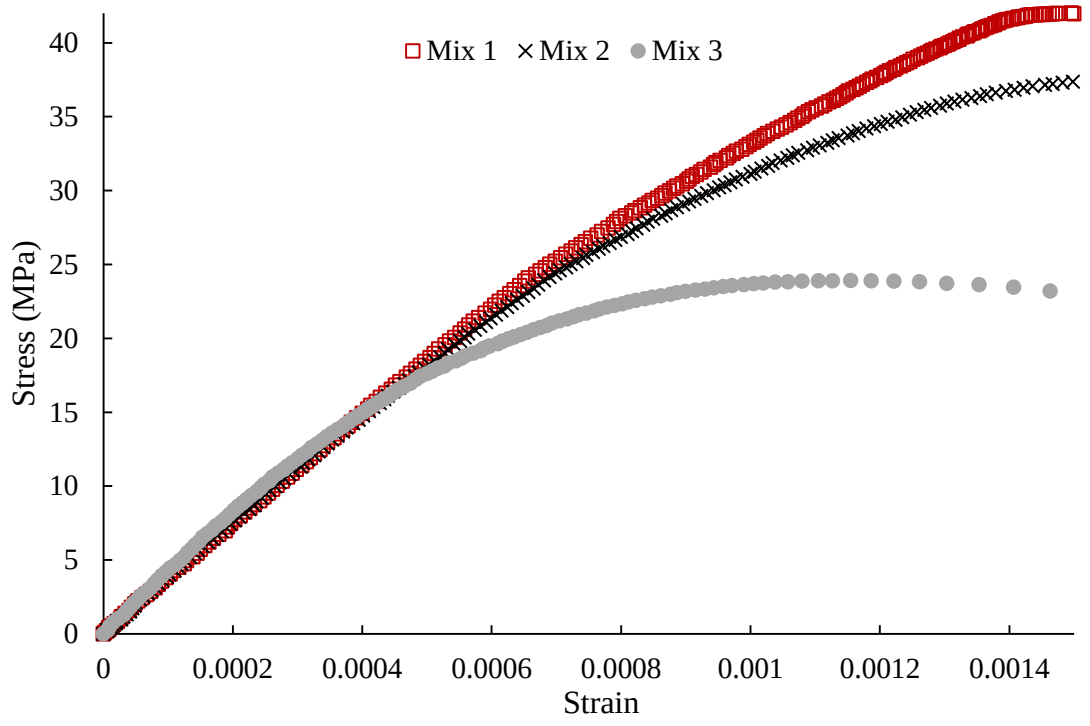

(a)

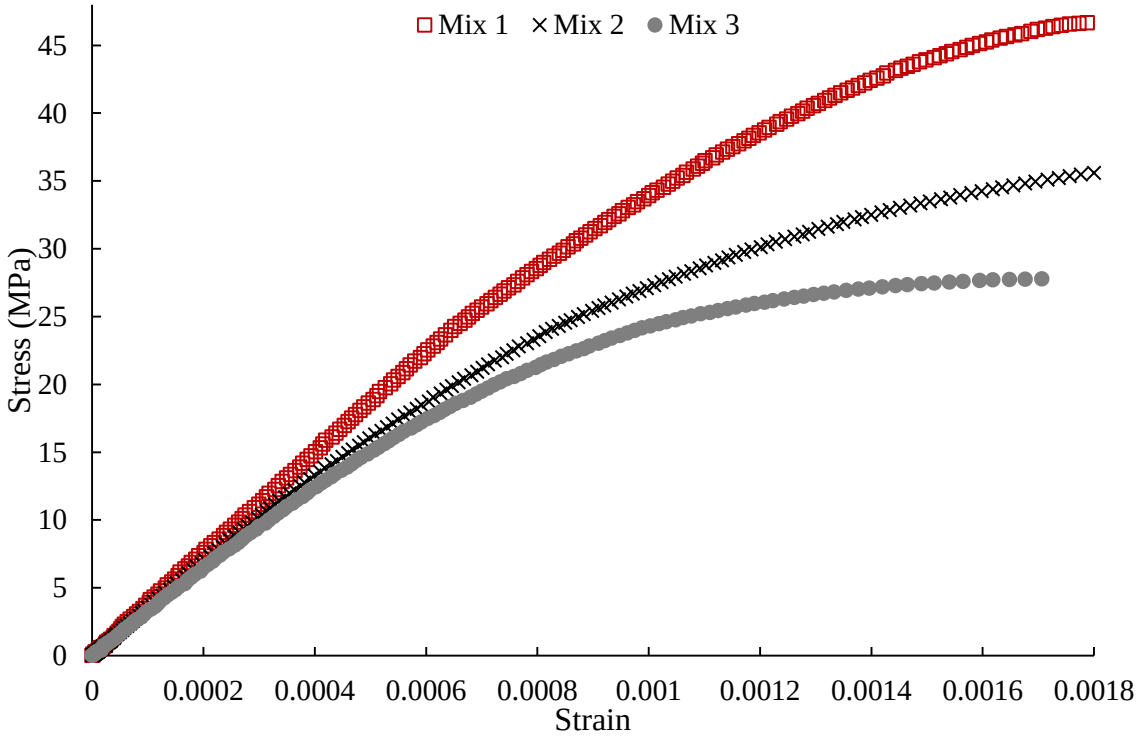

(b)

Figure 7.1: Stress – Strain curves for concrete mixes with (a) flaky and (b) regular aggregates

7.2 Numerical Tool

The elastic modulus of concrete was computed by using the composite models Hirsch, Ramesh and Hashin. The input to these models was the volumetric fraction and elastic moduli of aggregates, mortar, voids, and the interfacial zone. The interfacial zone was an additional parameter for the case of Ramesh and Hashin models. The results shown in Table 7.2 presents the elastic moduli computed using the proposed tool for the three concrete mixes incorporating the flaky aggregates.

Table 7.2: Results for the elastic modulus of concrete using the numerical tool proposed in the study

	Hirsch Model		Ramesh Model		Hashin Model	
	Mean (GPa)	Standard Deviation	Mean (GPa)	Standard Deviation	Mean (GPa)	Standard Deviation
Mix 1	29.4	2.87	27.4	2.55	27.1	3.1
Mix 2	29.5	2.78	27.5	2.41	27.4	3.12
Mix 3	27.4	3.25	25.1	2.9	25.9	3.3

It was noticed that the numerical tool returned the same elastic modulus for mixes 1 and 2 using the three proposed models. Given that the elastic modulus of aggregates incorporated in mixes 1 and 2 is identical, then the controlling factors are the elastic modulus of mortar, volumetric fraction of mortar and aggregates. However, the difference in the elastic modulus of mortar between mixes 1 and 2 was relatively small (19.5 and 18.3 GPa) respectively. Moreover, Figure 7.2 shows that the distributions for the volumetric fraction of aggregates for mixes 1 and 2 are overlapping with a slight difference (4%) in the mean. Since the elastic moduli of aggregates and mortar along with the volumetric fraction of aggregates for mixes 1 and 2 were similar, the elastic modulus computed using the numerical tool were equal. However, the elastic modulus decreased between Hirsch model and Hashin and Ramesh from 29.4 GPa to 27 GPa due

to the incorporation of the interfacial zone. The volumetric fraction of interfacial zone is associated with that of the aggregates since the interfacial zone is very thin films that surround the aggregate. Therefore, the volumetric fraction of mortar decreased when a layer of interfacial zone was added. Moreover, the elastic modulus of the interfacial zone was 70% times the elastic modulus of the mortar which led to an overall decrease in the elastic modulus of the mortar leading to a decrease in the elastic modulus of the concrete itself.

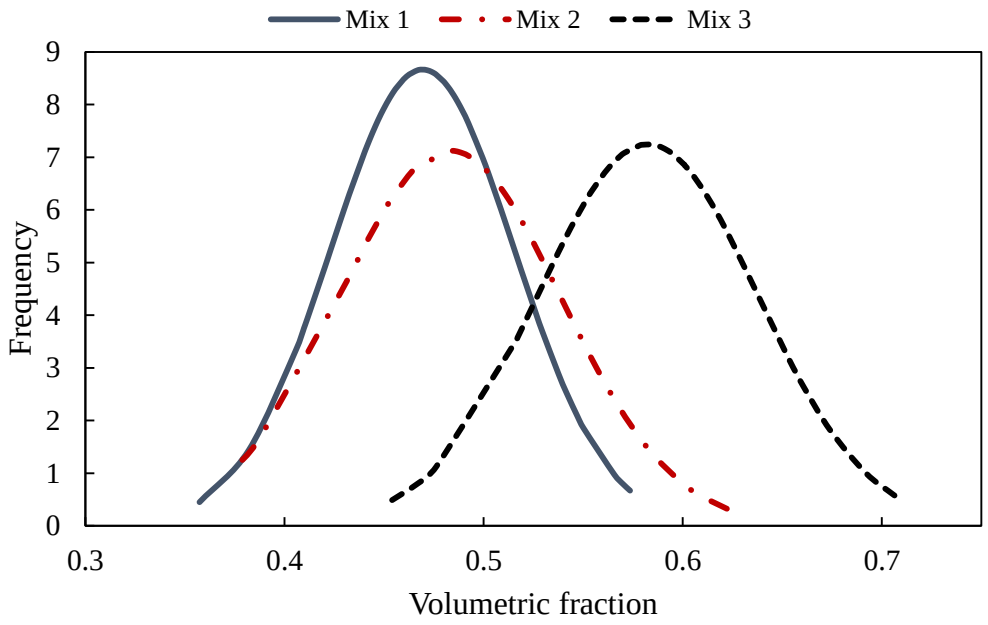

Figure 7.2: Volumetric fraction of aggregates for RVE size 75 mm * 75 mm

On the other hand, Figure 7.2 shows that the volumetric faction of aggregates is higher (0.6) for Mix 3. Typically, an increase in the volumetric fraction of aggregate should lead to an increase in the elastic modulus of concrete. However, the elastic modulus of mortar dropped from an average 18.7 GPa for both mixes 1 and 2 to 13.8 GPa for mix 3 (standard deviation=1.9 GPa). Therefore, the elastic modulus of mortar could range between 11.9 GPa and 15.7 GPa, and its effect was more pronounced on the elastic

modulus of concrete. This led to a decrease in the elastic modulus of concrete for mix 3 using Hirsh Model. The same trend is seen using the Hashin and Ramesh models for mix 3. The drop in the elastic modulus of concrete from 27 GPa for both mixes 1 and 2 to 25 GPa for mix 3 was not only due to the drop in the elastic modulus of mortar, but also due to the increase in the volumetric fraction of interfacial zone which is associated with the increase of the volumetric fraction of aggregates. Table 7.3 shows the percentage error between the experimental and numerical measurements for the elastic modulus of concrete. It is clear that the error increases when the interfacial zone is incorporated in the elastic modulus computation. This can be attributed to several factors:

1. The thickness of the interfacial zone which is assumed to be 20 μm. Decreasing the value of the thickness will increase the value of the elastic modulus of concrete.
2. The elastic modulus of the interfacial zone is assumed as 70 % times the elastic modulus of mortar. Increasing this value will increase the modulus of concrete.
3. Error accompanied with the computation of the volumetric fraction of interfacial zone. Since the interfacial zone surrounds the aggregates, then the volume of interfacial zone is obtained by calculating the perimeter of the aggregate and then adding to it the thickness of the interfacial zone. The process of calculating the perimeter of the aggregate is not extremely accurate and may over predict its value, thus increasing the volume of interfacial zone.

Table 7.3: Percent error between the experimental and numerical measurements of the elastic modulus of concrete

	Hirsch	Ramesh	Hashin
Mix 1	17%	22.8%	23.6%
Mix 2	18.7%	24.6%	25%
Mix 3	23%	29%	26.8%

7.3 Comparison with Design Codes

Figure 7.3 shows the elastic modulus for the experimental results as compared to the ones predicted using relationships provided by Design codes. The least observed difference was the one between the values predicted by Eurocode and the experimental. On average the difference for regular shaped aggregates was 5%, while for flaky aggregates the difference was 11%. It was also evident that the remaining design codes under predict the elastic modulus of concrete for both regular shaped and flaky aggregates.

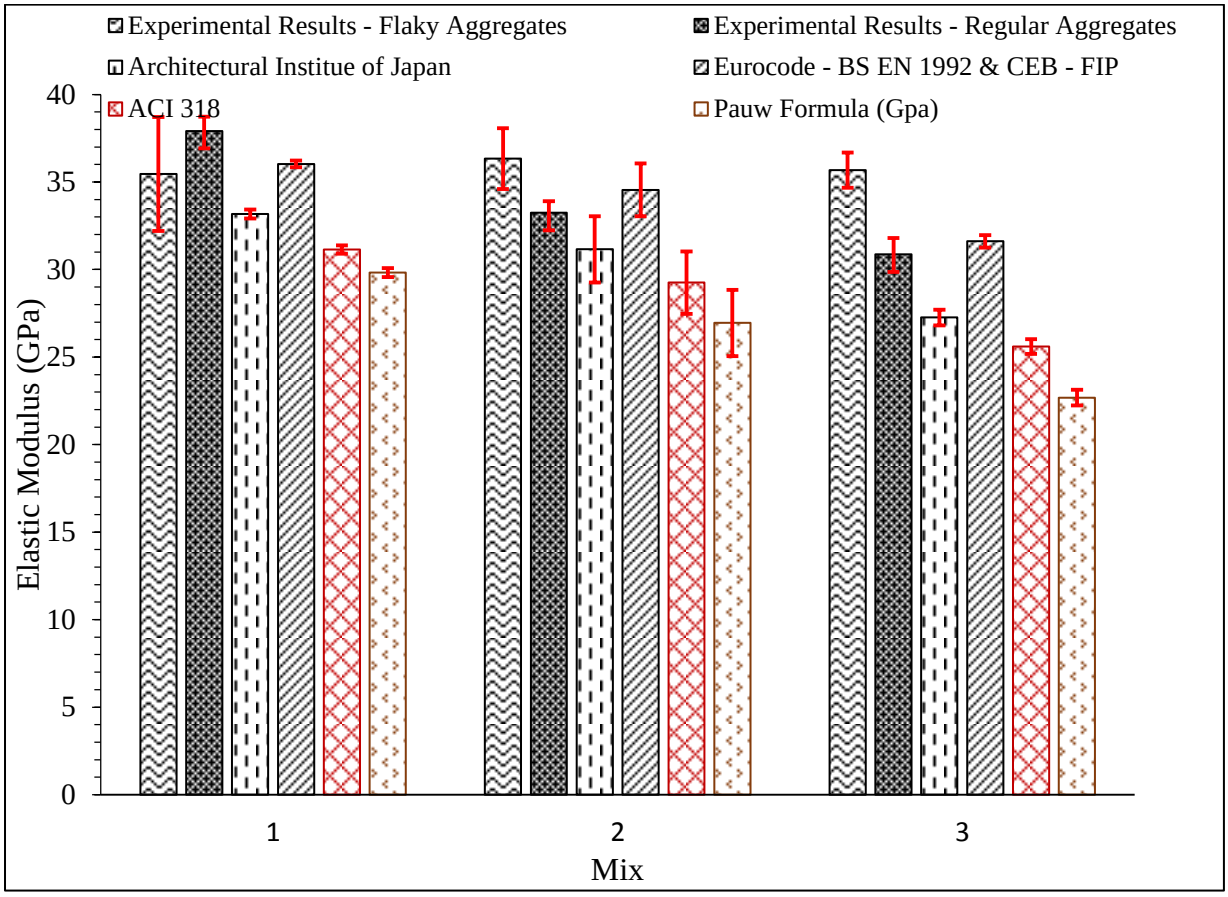

Figure 7.3: Comparison between experimental results and design codes

Figure 7.4 shows the lower and upper bounds provided by ACI for the prediction of the elastic modulus of concrete. These bounds correspond to 80 % and 120 % of the estimated value respectively. The values predicted by the proposed tool fall within the lower and upper bounds, proving that the tool was a suitable method for estimating the elastic modulus of concrete. An additional observation is that the values tend to fall more towards the lower bound.

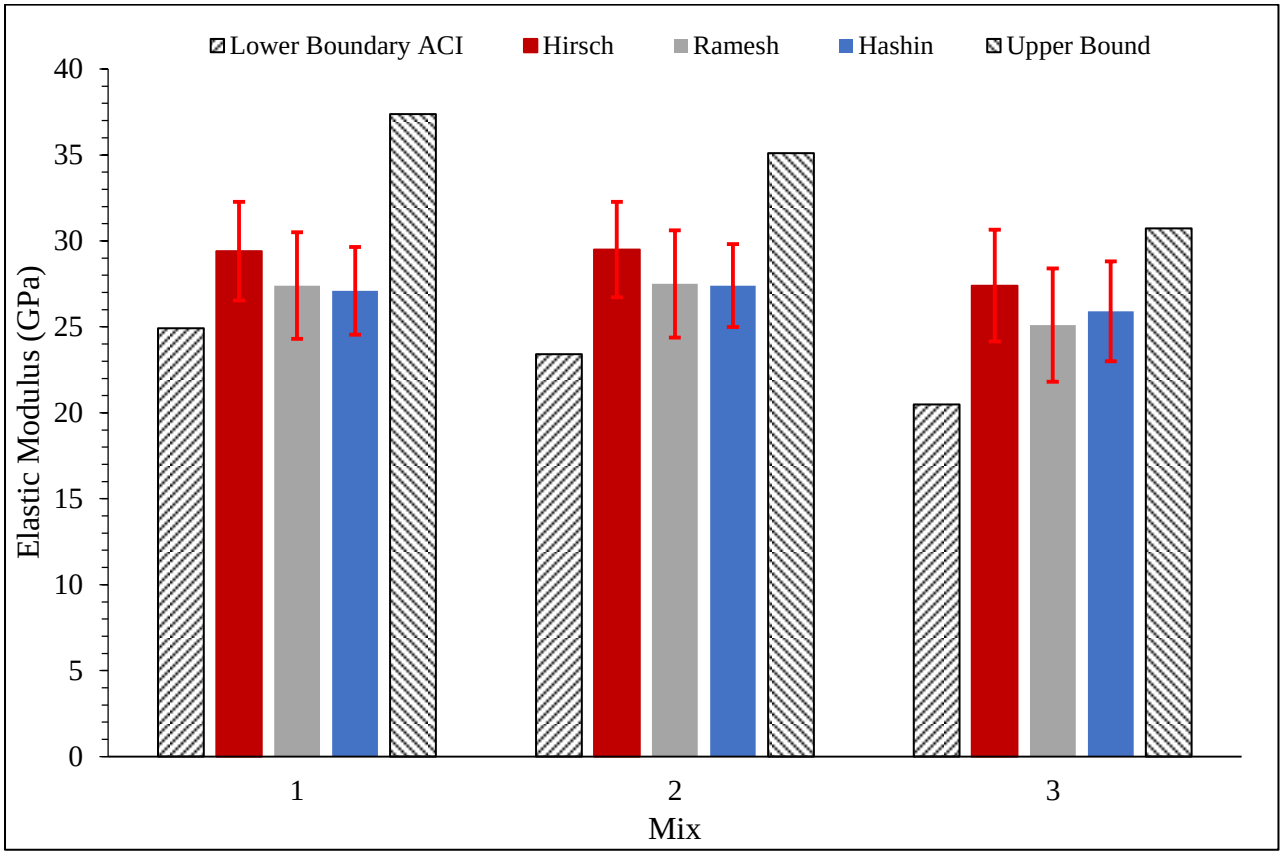

Figure 7.4: Comparison of the predicted elastic modulus with the bounds provided by ACI 318.

CHAPTER 8

CONCLUSION AND FUTURE WORK

This study presented a probabilistic tool for estimating the elastic modulus of concrete using Digital Image Processing techniques. It also studied the effect of a representative volume element (RVE) on the volumetric distribution of mortar and aggregates in a concrete mix. In addition, this study investigated the effect of aggregate shape on the elastic modulus and uniaxial strength of concrete. The main findings of this study are:

- The tool presented in this study shows that the elastic modulus of concrete is function of the volumetric fractions of aggregates and mortar and their corresponding elastic properties. The tool proposed can be used in reliability analysis to assess the structural integrity of structures.
- The distributions presented for the elastic modulus of mortar and limestone aggregates show the importance of quantifying the uncertainties associated with the measurement of this value. Further research and experimental work regarding the estimation of the elastic modulus of limestone aggregates shall be done. More samples should be collected from different regions to cover the territories of Lebanon.
- The study shows that the RVE size plays a major role in modelling the volumetric distributions of concrete constituents. Further research could include studying the relationship between the RVE and the maximum aggregate size of aggregate.

- In this study, the effect of flaky aggregates on the elastic modulus of concrete was studied. The higher surface area associated with flaky aggregates shows a potential room for enhancing the elastic modulus of concrete.
- The use of composite models to estimate the elastic modulus of concrete is an efficient approach and the effect of interfacial zone shall be further studied.

REFERENCES

[1] *ASTM C125−15b Standard Terminology Relating to Concrete and Concrete Aggregates*, 2015: ASTM.

[2] J. F. Lamond and J. H. Pielert, *Significance of tests and properties of concrete and concrete-making materials,* West Conshohocken, PA: ASTM , 2006.

[3] S. Al-Oraimi, R. Taha and H. F. Hassan, "The effect of the mineralogy of coarse aggregate on the mechanical properties of high-strength concrete," *Construction and Building Materials,* vol. 20, no. 7, pp. 499-503, 2006.

[4] S. H. Kosmatka, B. Kerkhoff and W. C. Panarese, "Design and Control of Concrete Mixtures," Portland Cement Association, Illinois, USA , 2002.

[5] D. M. Suchorski, "Aggregates for Concrete," *ACI Education Bulletin E1-07, ACI commite E-701, Materials for Concrete Construction. ,* 2007.

[6] J. F. Lamond and J. H. e. Pielert, Significance of tests and properties of concrete and concrete-making materials, West Conshohocken: ASTM International, 2006.

[7] J.-j. Zheng, Y.-f. Wu, X.-z. Zhou, Z.-m. Wu and X.-y. Jin, "Prediction of Young's Modulus of Concrete with Two Types of Elliptical Aggregate," *ACI Materials Journal,* pp. 603-611, 2014.

[8] A. H. Gandomi, A. H. Alavi, M. G. Sahab and P. Arjmandi, "Formulation of elastic modulus of concrete using linear genetic programming," *Journal of Mechanical Science and Technology,* pp. 1273-1278, 2010.

[9] M. Jedidi and M. Kaouther, "Destructive and Non-destructive Testing of Concrete Structures," *Jordan Journal of Civil Engineering,* pp. 432-441, 2014.

[10] A. D7012-14, "Standard Test Methods for Compressive Strength and Elastic Moduli of Intact Rock Core Specimens under Varying States of Stress and Temperatures," ASTM International, West Conshohocken, PA, 2014.

[11] *BS 1881-121:1983, Method for determination of static modulus of elasticity in compression,* British Standards, 1983.

[12] J. S. Popovics, J. Zemajtis and I. Shkolnik, "A study of static and dynamic modulus of elasticity of concrete," ACI-CRC, 2008.

[13] "Guidebook on non-destructive testing of concrete structures," International Atomic Energy Agency , Vienna , 2002.

[14] S. K. Verma, S. S. Bhadauria and S. Akhtar, "Review of Nondestructive Testing Methods for Condition Monitoring of Concrete Structures," *Journal of Construction Engineering*, p. Article ID 834572, 2013.

[15] T. Plachy, P. Padevet and M. Polak, "Comparison of two experimental techniques for determination of Young's modulus of concrete specimens," in *5th WSEAS International Conference on Applied and Theoretical Mechanics*, 2009.

[16] *BS 1881-209:1990 Testing Concrete: Recommendations for the measurement of dynamic modulus of elasticity*, BSI, 1990.

[17] *ASTM C215-14 Standard Test Method for Fundamental Transverse, Longitudinal, and Torsional Resonant Frequencies of Concrete Specimens*, ASTM , 2014.

[18] *BS EN 12504-4:2004 Testing Concrete: Determination of ultrasonic pulse velocity*, BSI , 2004.

[19] *ASTM C597-09 Standard Test Method for Pulse Velocity Through Concrete*, ASTM , 2009.

[20] S. Han and W. Park, "Investigation of dynamic and static elastic modulus based on in-situ concrete cores," in *2nd International Symposium on Service Life Design for Infrastructure*, Delft, The Netherlands, 2010.

[21] D. Shen and X. Lu, "Experimental Study on Dynamic Compressive Properties of Microconcrete Under Different Strain Rate," in *The 14th World Conference on Earthquake Engineering*, Beijing, China, 2008.

[22] N. C. f. B. Standardization, *Concrete Structure Design Rules NS 3473 E.*, Stockholm, 1992.

[23] A. C. 363, "State-of-the-Art Report on High-Strength Concrete," American Concrete Institute, 1992.

[24] *Eurocode 2: Design of concrete structures - Part 1-1: General rules and rules for buildings,* The British Standard Institution, 2014.

[25] L. J. Parrott, "The Production and Properties of High-Strength Concrete," *Concrete,* vol. 3, no. 11, pp. 443-448, 1969.

[26] Comite Euro-International Du Beton, "CEB-FIP Model Code," Thomas Telford, London, 1990.

[27] A. C. 318, Building Code Requirement for Structural Concrete (ACI 318-11) and Commentary, American Concrete Institute , 2011.

[28] W. Voigt, "Uber die beziehung zwischen den beiden elastizitatkonstanten isotroper korper," *Wiedemanns Annalen der Physik and Chemie,* vol. 38, pp. 573-587, 1889.

[29] A. Reuss, "Berechnung der fliessgrenze von mischkristallen auf grund der plastizitatsbedingung fur einkristalle," *Zeitschrift fur Angewandte Mathematik und Mechanik* , vol. 9, pp. 49-58, 1929.

[30] I. Yaman, H. M. Aktan and N. Hearn, "Active and non-active porosity in concrete part II: evaluation of existing models," *Materials and Structures* , pp. 110-116, 2002.

[31] R. Chamrova, *Modelling and Measurement of Elastic Properties of Hydrating Cement Paste,* Suisse: Ecole Polytechnique Federale de lausanne , 2010.

[32] T. J. Hirsch, "Modulus of Elasticity iof Concrete Affected by Elastic Moduli of Cement Paste Matrix and Aggregate," *ACI Materials Journal* , vol. 59, no. 3, pp. 427-452, 1962.

[33] U. J. Counto, "The effect of the elastic modulus of the aggregate on the elastic modulus, creep and creep recovery of concrete," *Magazine of Concrete Research* , vol. 16, no. 48, pp. 129-138, 1964.

[34] Z. Hashin and S. Shtrikman, "A variational approach to the theory of the elastic behaviour of multiphase materials," *Journal of the Mechanics and Physics of Solids,* vol. 11, no. 2, pp. 127-140, 1963.

[35] G. Xotta, *Mesoscale Modelling Of Concrete As a Multiphase Material,* Italy : University Of Padova , 2012.

[36] G. Ramesh, E. D. Sotelino and W. Chen, "Effect of Interface on Elastic Moduli of Concrete Material," Purdue University , West Lafayette, Indiana.

[37] C. Qian, H. Dong and Y. Liu, "Comparisons of ITZ characteristics of marble and sandstone aggregates," *Magaine of Concrete Research,* pp. 609-615, September 2010.

[38] E. J. Garboczi and D. P. Bentz, "Analytical formulas for interfacial transition zone properties," *Advanced Cement Based Materials* , vol. 6, no. 3-4, pp. 99-108, 1997.

[39] E. Garboczi and D. P. Bentz, "The Effect of the Interfacial Transition Zone on Concrete Properties: The Dilute Limit," in *Proceedings of the Fourth Materials Conference*, Washington, DC , 1996.

[40] Z. Chunsheng, L. Kefei and M. Fu, "Numerical and statistical analysis of elastic modulus of concrete as a three-phase heterogeneous composite," *Computers and Structures*, vol. 139, pp. 33-42, 2014.

[41] E. H. Barhdadi, P. Lipinski and M. Cherkaoui, "Four Phase Model: A New Formulation to Predict the Effective Elastic Moduli of Composites," *Journal of engineering materials and technology*, vol. 129, no. 2, pp. 313-320, 2007.

[42] Z. Hashin and P. Monteiro, "An inverse method to determine the elastic properties of the interphase between the aggregate and the cement paste," *Cement and Concrete Research* , vol. 32, no. 8, pp. 1291-1300, 2002.

[43] G. De Schutter and L. Taerwe, "Random particle model for concrete based on Delaunay triangulation," *Materials and Structures,* vol. 26, pp. 67-73, 1993.

[44] P. Stroeven and S. Martjin, "Dynamic Computer Simulation of Concrete on Different levels of the micro-structure," *Image Anal Stereol,* vol. 22, no. 1, pp. 1-10, 2003.

[45] E. Masad and M. E. Kutay, "Characterization of the Internal structure of Asphalt Mixtures," *Transportation Research Circular Number E- C161,* pp. 2-16, January 2012.

[46] H. Zhi-Yi, W. Xin-fei, Z. Xing-Yi and L. Zhuo, "Application of digital image processing technique to simulate the maco-mechanical behavior of asphalt concrete," *Geotechnical Special Publication,* vol. 212, pp. 167-174, 2011.

[47] A. Carlos, I. Masumi, M. Hiroaki, M. Maki and O. Takahisa, "The effects of limestone aggregate on concrete properties," *Construction and Building Materials* , pp. 2363-2368, 2010.

[48] I. B. Muhit, S. Haque and a. M. R. Alam, "Influence of crushed coarse aggregates on properties of concrete," *American Journal of Civil Engineering and Architecture,* pp. 103-106, 2013.

[49] A. Shamsad and S. A. Alghamdi, "A study on effect of coarse aggregate type on concrete performance," *Arabian Journal for Science and Engineering,* vol. 37, no. 7, pp. 1777-1786, 2012.

[50] P. C. Aitcin and P. K. Mehta, "Effect of Coarse Aggregate Characteristics on Mechanical Properties of High-Strength Concrete," *Materials Journal,* pp. 103-107, 1990.

[51] B. Hamad, G. Khoury and H. Khatib, "Petrographic, mechanical and chemical properties of major coarse aggregate resources in Lebanon, eastern Mediterranean," *Bulletin of Engineering Geology and the Environment,* pp. 297-305, 2001.

[52] A. Palmstrom and E. Broch, "Use and misuse of rock mass classification systems with particular reference to the Q-system," *Tunnelling and underground space technology,* vol. 21, no. 6, pp. 575-593, 2006.

[53] *Standard Test Method for determining Rock Quality Designation (RQD) of Rock Core,* ASTM International , 2008.

[54] W. G. Pariseau, Design Analysis in Rock Mechanics, Second Edition, Taylor & Francis, 2011.

[55] T. Ramamurthy, Engineering In Rocks For Slopes Foundations And Tunnels, PHI Learning Private Limited, 2015.

[56] Z. T. Bieniawski, *Tunnel design by rock mass classifications,* PENNSYLVANIA STATE UNIV UNIVERSITY PARK DEPT OF MINERAL ENGINEERING, 1990.

[57] D. Deere and R. Miller, "Engineering Classification and Index Properties For Intact Rock," Air Force Weapons Laboratory, Kirtland AFB, New Mexico, 1966.

[58] V. Palchik, "On the Ratios between Elastic Modulus and Uniaxial Compressive Strength of Heterogeneous Carbonate Rocks," *Rock Mechanics and Rock*

Engineering, vol. 44, no. 1, p. 121–128, 2011.

[59] Z. Chunsheng, L. Kefei and M. Fu, "Numerical and statistical analysis of elastic modulus of concrete as a three-phase heterogeneous composite," *Computers and Structures*, pp. 33-42, 2014.

[60] N. A. Al-Shayea, "Effects of testing methods and conditions on the elastic properties of limestone rock.," *Engineering Geology* , pp. 139-156, 2004.

[61] V. Palchik and Y. Htazor, "Crack damage stress as a composite function of porosity and elastic matrix stiffness in dolomites and limestones," *Engineering Geology*, pp. 233-245, 2002.

[62] P. Turgut, M. I. Yesilnacar and H. Bulut, "Physico-thermal and mechanical properties of Sanliurfa limestone, Turkey," *Bulletin of Engineering Geology and the Environment*, pp. 485-490, 2008.

[63] J. MayCrespo, P. Quintana, J. Alvarado-Gil, B. A. Juárez de la Rosa, A. MayPat and F. Avilés, "Physical, Petrographic, and Mineralogical Properties of Limestone Rocks from the Peninsula of Yucatán," *MRS Proceedings*, 2012.

[64] T. Lam, D. Martin and D. McCreath, "Characterising the geomechanics properties of the sedimentary rocks for the DGR excavations," in *Canadian Geotechnical Conference*, Ottawa, 2007.

[65] L. X. M. Zhang, AiHong and Lu, "Experimental study on the mechanical properties of rocks at high temperature," *Science in China Series E: Technological Sciences*, pp. 641-646, 2009.

[66] D. O'HANDLEY and W. GREEN, "Recent developments in digital image processing at the image processing laboratory at the jet propulsion laboratory," *Proceedings of the IEEE*, vol. 60, no. 7, pp. 821 - 828, 1972.

[67] M. S. Robinson and B. L. Jolliff, "Apollo 17 landing site: Topography, photometric corrections, and heterogeneity of the surrounding highland massifs," *Journal of Geophysical Research*, vol. 107, no. E11, pp. 20-30, 2002.

[68] "The Nobel Prize in Physiology or Medicine 1979," Nobelprize.org, [Online]. Available: http://www.nobelprize.org/nobel_prizes/medicine/laureates/1979/. [Accessed 3 Sep 2016].

[69] B. Basavaprasad and M. Ravi, "A study on the importance of image processing and its applications," *International Journal of Research in Engineering and Technology*, pp. 155-160, 2014.

[70] K. H. Moon, A. C. Falchetto, M. P. Wistuba and J. H. Jeong, "Analyzing Aggregate Size Distribution of Asphalt Mixtures Using Simple 2D Digital Image Processing Techniques," *Arabian Journal for Science and Engineering* , vol. 40, no. 5, pp. 1309-1326, 2015.

[71] T. Reida and J. Harrison, "A semi-automated methodology for discontinuity trace detection in digital images of rock mass exposures," *International Journal of Rock Mechanics and Mining Sciences*, vol. 37, no. 7, pp. 1073-1089, 2000.

[72] S. Chen, Z. Q. Yue and L. G. Tham, "Digital image-based numerical modeling method for prediction of inhomogeneous rock failure," *International Journal of Rock Mechanics and Mining Sciences*, vol. 41, no. 6, pp. 939-957, 2004.

[73] I. S. Bessa, V. T. Castelo Branco and J. B. Soares, "Evaluation of different digital image processing software for aggregates and hot mix asphalt characterizations," *Construction and Building Materials*, vol. 37, pp. 370-378, 2012.

[74] K. H. Moon and A. C. Falchetto, "Microstructural Investigation of Hot Mix Asphalt (HMA) Mixtures using Digital Image Processing (DIP)," *KSCE Journal of Civil Engineering*, vol. 19, no. 6, pp. 1727-1737, 2015.

[75] N. R. Sefidmazgi, *Defining Effective Aggregate Skeleton In Asphalt Mixture Using Digital Imaging (Dissertation)*, Madison: UNIVERSITY OF WISCONSIN – MADISON, 2011.

[76] E. Masad, B. Muhunthan, N. Shashidhar and T. Harman, "Quantifying Laboratory Compaction Effects on the Internal Structure of Asphalt Concrete," *Transportation Research Record: Journal of the Transportation Research Board*, vol. 1681, pp. 179-185, 1999.

[77] S. Arasan, E. Yenera, F. Hattatoglu, S. Hinislioglua and S. Akbuluta, "Correlation between Shape of Aggregate and Mechancial Properties of Asphalt Concrete: Digital Image Processing Approach," *Road Materials and Pavement Design* , vol. 12, no. 2, pp. 239-262, 2011.

[78] L. Bruno, G. Parla and C. Celauro, "Image analysis for detecting aggregate gradation

in asphalt mixture from planar images," *Construction and Building Materials* , vol. 28, no. 1, pp. 21-30, 2012.

[79] A. Arshadi and H. Bahia, "Development of an image-based multi-scale finite-element approach to predict mechanical response of asphalt mixtures," *Road Materials and Pavement Design,* vol. 16, pp. 214-229, 2015.

[80] Z. Wu, H. Rong, J. Zheng, F. Xu and W. Dong, "An experimental investigation on the FPZ properties in concrete using digital image correlation technique," *Engineering Fracture Mechanics,* vol. 78, no. 17, p. 2978–2990, 2011.

[81] C. Başyiğit, B. Çomak, Ş. Kılınçarslan and İ. S. Üncü, "Assessment of concrete compressive strength by image processing technique," *Construction and Building Materials,* vol. 37, pp. 526-532, 2012.

[82] A. P. C. Duarte, B. A. Silva, N. Silvestre, J. de Brito and E. Julio, "Mechanical characterization of rubberized concrete using an image-processing/XFEM coupled procedure," *Composite Part B,* vol. 78, pp. 214-226, 2015.

[83] J. Sachs, Digital Image Basics, Digital Light & Color, 1996-1999.

[84] "ASTM D7012-14 - Standard Test Methods for Compressive Strength and Elastic Moduli of Intact Rock Core Specimens under Varying States of Stress and Temperatures," ASTM International, West Conshohocken, PA, 2014.

[85] P. M. Santi, J. E. Holschen and R. W. Stephenson, "Improving elastic modulus measurements for rock based on geology," *Environmental & Engineering Geoscience,* pp. 333-346, 2000.

[86] K. J. Bathe, *Automatic Dynamic Incremental NonLinear Analysis,* Watertown, MA 02472, USA, 1986.

[87] C. F. Goble and M. D. Cohen, "Influence of Aggregate Surface Area on Mechanical Properties of Mortar," *ACI materials journal,* vol. 96, no. 6, pp. 657-662, 1999.

[88] N. S. Klein, A. Aguado, B. M. Toralles-Carbonari and L. V. Real, "Prediction of the water absorption by aggregates over time: Modelling through the use of value function and experimental validation," *Construction and Building Materials,* vol. 69, pp. 213-220, 2014.

[89] H. Yu and S. Shen, "Impact of aggregate packing on dynamic modulus of hot mix asphalt mixtures using three-dimensional discrete element method.," *Construction and Building Materials.,* 2012.

[90] I. B. Topcu, T. Bilir and A. R. Boga, "Estimation of modulus of elasticity of slag concrete by using composite materials.," *Construction and Building Materials.,* 2010.

[91] H. Tobbi, A. S. Farghaly and B. Benmokrane, "Strength Model for Concrete Columns Reinforced with Fiber-Reinforced Polymer Bars and Ties.," *ACI Structural Journal ,* pp. 1-6, 2014.

[92] M. M. Salman and A. H. Al-Amawee, "The Ratio between Static and Dynamic Modulus of Elasticity in Normal and High Strength Concrete," *Journal of Engineering and Development ,* pp. 163-174, 2002.

[93] F. Richart, A. Brandtzaeg and R. Brown, "A study of the failure of concrete under combined compressive stresses.," *Bulletin 185, Univ. of Illinois Engineering Experimental Station, Champaign, III,* 1928.

[94] J. P. Patel, "Broader use of steel slag in concrete," Cleveland State University, 2008.

[95] E. M. Palmeira, F. Tatsuoka, R. J. Bathurst, P. E. Stevenson and J. G. Zornberg, "Advances in Geosynthetics Materials and Applications for Soil Reinforcement and Enviromental Protection Works.," *Electronic Journal of Geotehnical Engineering, Spec Issue State of the Art in Geotech Eng,* pp. 1-38, 2008.

[96] T. Mang, Y. Liu and D. Brown, "Modulus of elasticity, creep and shrinkage of concrete," Transportation Research Board, Florida, 2005.

[97] Y. Liu, *Strength, Modulus of Elasticity, Shrinkage and Creep of Concrete,* Florida: University of Florida, 2007.

[98] J. Kupec and A. McGown, "The Biaxial Load-Strain Behaviour of Biaxial Geogrids," in *Proceedings of the 3rd Asian Regional Conf. on Geosynthetics,* 2004.

[99] H. Klee, "World Business Council for Sustainable Development," July 2009. [Online]. Available: www.wbcsdcement.org/recycling. [Accessed January 2015].

[100] H. He, P. Stroeven, M. Stroeven and L. J. Sluys, "Influence of particle packing on elastic properties of concrete.," *Magazine of Concrete Research,* 16 12 2011.

[101] N. C. Hawkins, R. W. Patterson, J. Mogge and T. F. Yosie, "Building a Sustainability Road Map for Engineering Education," *ACS Sustainable Chemistry & Engineering*, pp. 340-343, 2013.

[102] B. Haranki, "Strengt, Modulus of Elasticity, Creep and Shrinkage of Concrete Used in Florida," University of Florida, Flroida, 2009.

[103] R. P. S. -. Engineer, February 1996. [Online]. Available: http://www.omafra.gov.on.ca/english/engineer/facts/95-089.htm.

[104] F. El Meski and G. Chehab, "Flexural Behavior of Concrete Beams Reinforced with Different Types of Geogrids," *Journal of Materials in Civil Engineering*, 2013.

[105] J. Drexhage and D. Murphy, "Sustainable development: from Brundtland to Rio 2012," *United Nations Headquarters, New York* , pp. 9-13, 2010.

[106] S. B. Dhule, S. Valunjkar, S. Sarkate and S. Korrane, "Improvement of Flexible Pavement With Use of Geogrid," *Electronic Journal of Geotech Engineering*, pp. (16) 269-279, 2011.

[107] C. J. Desha, K. C. Hargroves, M. H. Smith and P. Stasinopoulos, "The Importance of Sustainability in Engineering Education: A Toolkit of Information and Teaching Material," in *Engineering Training & Learning Conference*, 2003.

[108] A. De Luca, F. Nardone, F. Matta, A. Nanni, G. P. Lignola and A. Prota, "Structural Evaluation of Full-Scale FRP-Confined Reinforced Concrete Columns," *Journal of Composites for Construction*, pp. 112-123, 2010.

[109] D. W. Christensen, T. Pellien and R. F. Bonaquist, "Hirsch Model for Estimating the Modulus of Asphalt Concrete.".

[110] H. Beushausen and T. Dittmer, "The influence of aggregate type on the strength and elastic modulus of high strength concrete," *Construction and Building Materials* , pp. 132-139, 2015.

[111] S. A. Arhin, R. Madhi and W. Khan, "Optimal Mix Designs for Pervious Concrete for an Urban Area," *International Journal of Engineering Research & Technology (IJERT)*, pp. 42-50, 2014.

[112] *CEB CEB/FIP Model MC90, (1997). European Standard for Design of Concrete*

Structures, p. 348..

[113] *BS EN 1992-1-1:2004 Design of concrete structures. General rules and rules for buildings,* British Standards, 2004.

[115] C. Aquino, I. Masumi, M. Hiroaki, M. Maki and O. Takahisa, "The effects of limestone aggregate on concrete properties," *Construction and Building Materials* , vol. 24, no. 12, pp. 2363-2368, 2010.

[116] S. K. Oraimi, R. Taha and H. F. Hassan, "The effect of the mineralogy of coarse aggregate on the mechanical properties of high-strength concrete," *Construction and Building Materials,* vol. 20, no. 7, p. 499–503, 2006.

APPENDIX A

PROBABILITY DISTRIBUTIONS OF AGGREGATE MORTAR VOID AND INTERFACIAL ZONE VOLUMETRIC FRACTION

Aggregate Mix 2

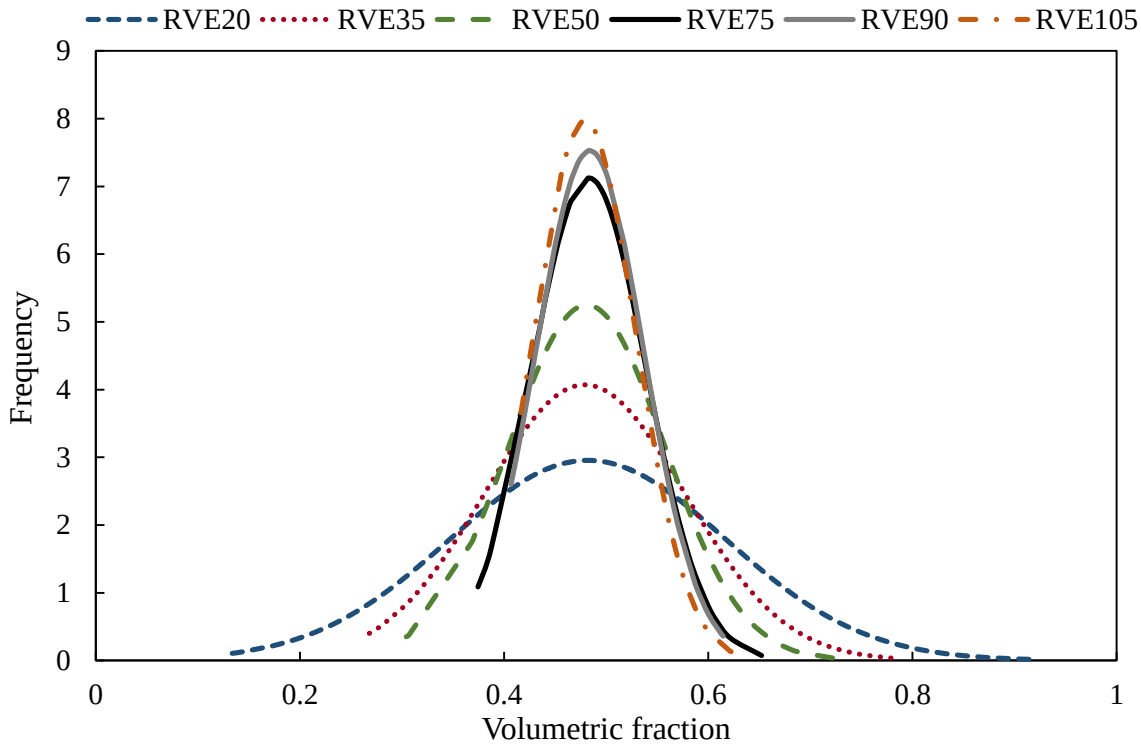

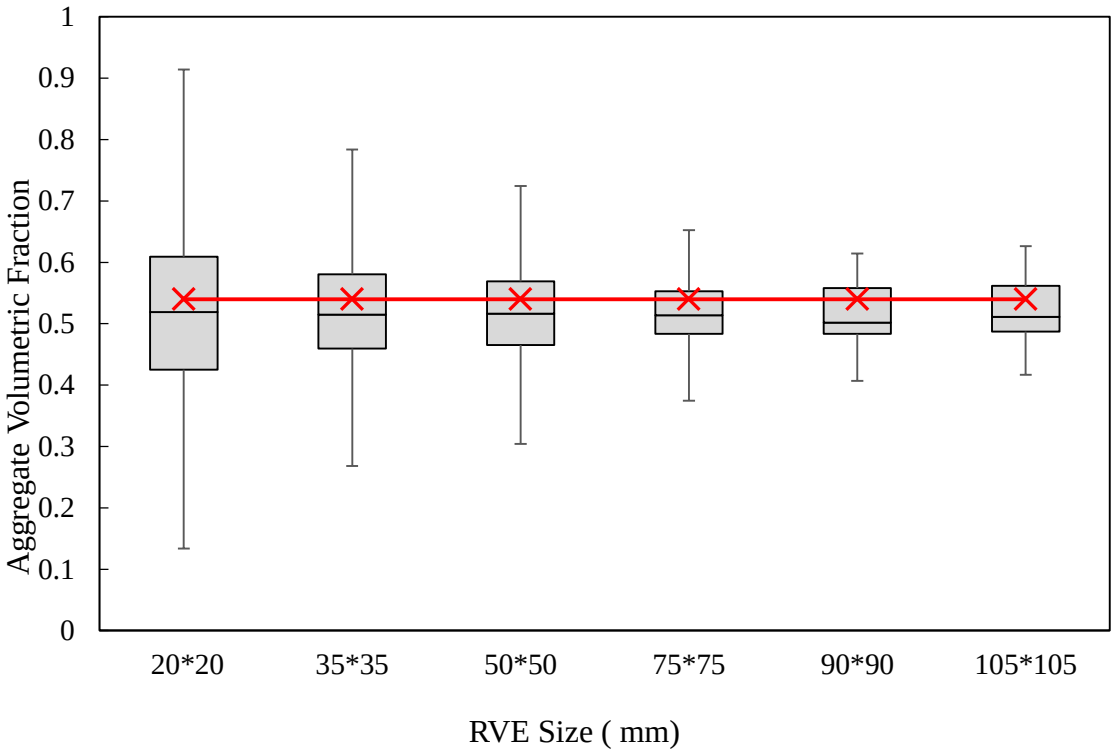
Aggregate Volumetric Fraction
1
0.9
0.8
0.7
0.6
0.5
0.4
0.3
0.2
0.1
0
20*20
35*35
50*50
75*75
90*90
105*105
RVE Size (mm)

Mortar Mix 2

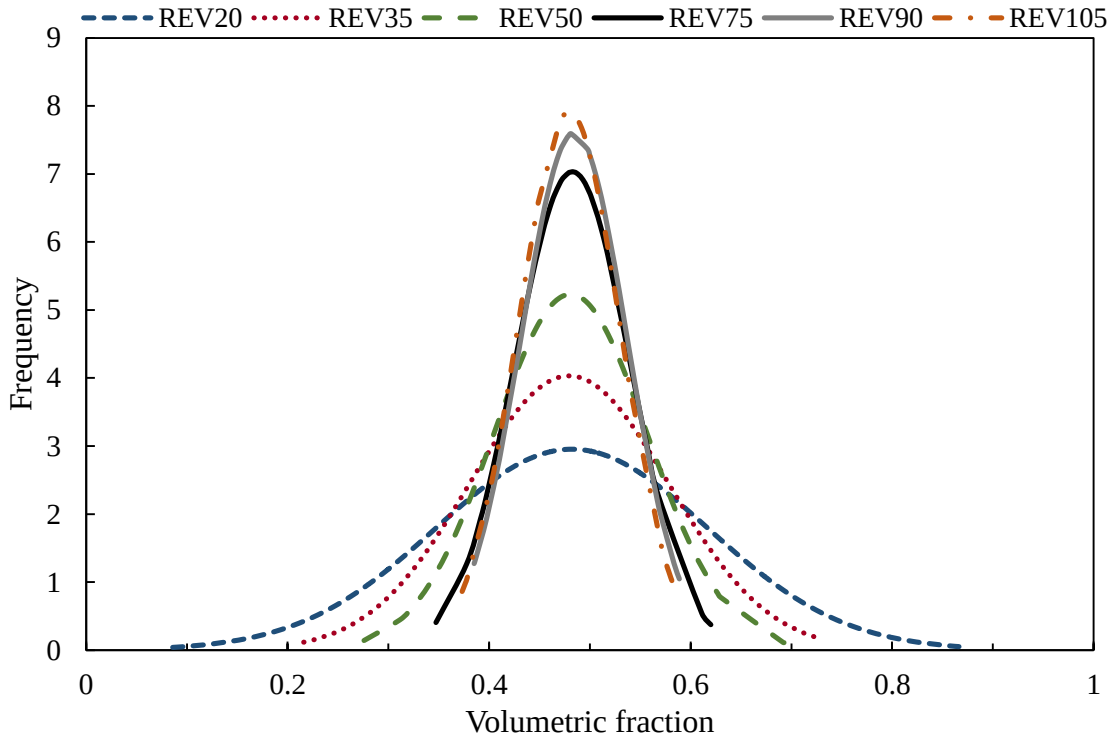
REV20
REV35
REV50
REV75
REV90
REV105
Frequency
9
8
7
6
5
4
3
2
1
0
0
0.2
0.4
0.6
0.8
1
Volumetric fraction

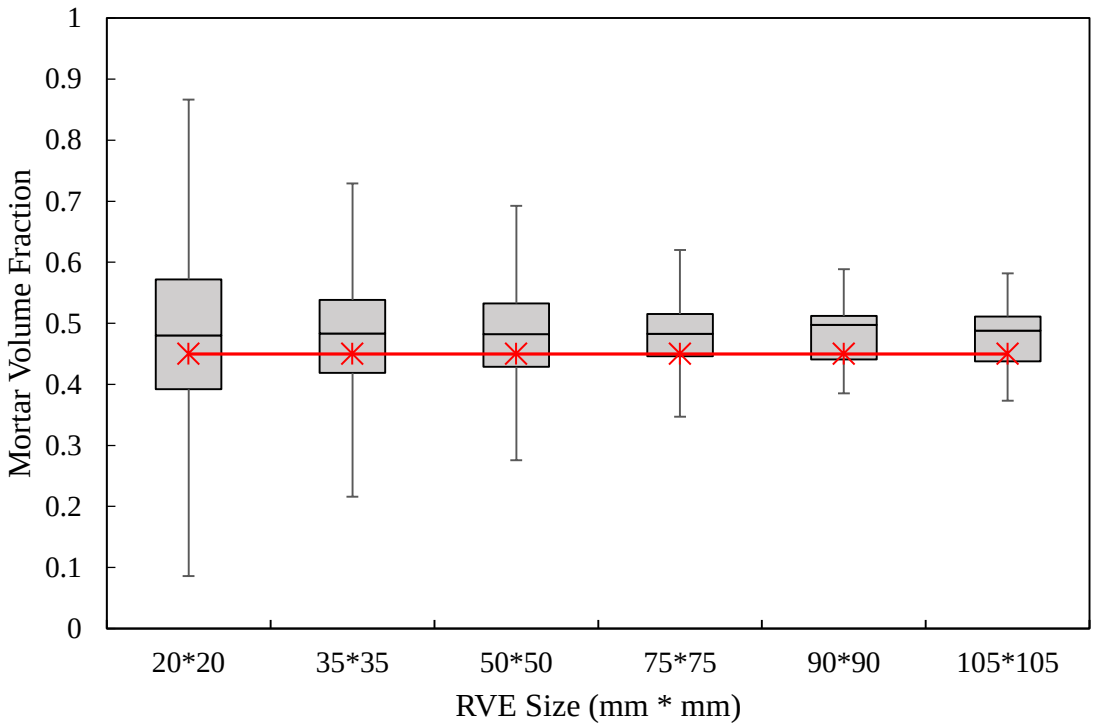
Mortar Volume Fraction
1
0.9
0.8
0.7
0.6
0.5
0.4
0.3
0.2
0.1
0
20*20
35*35
50*50
75*75
90*90
105*105
RVE Size (mm * mm)

Aggregate Mix 3

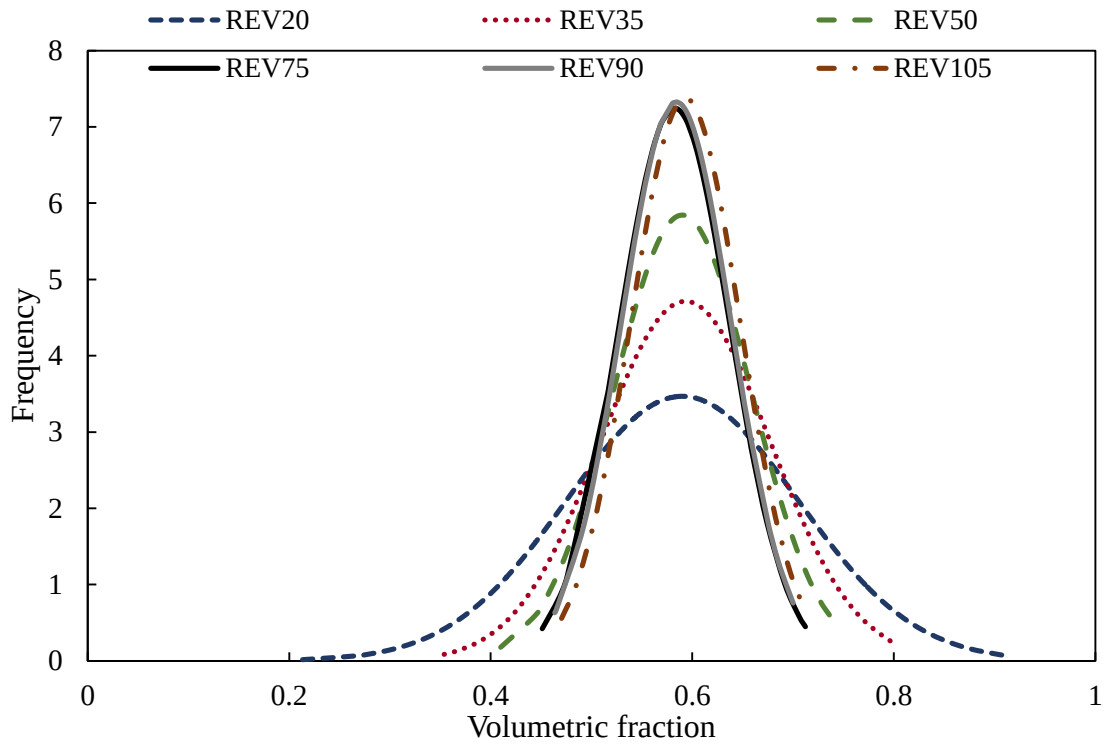

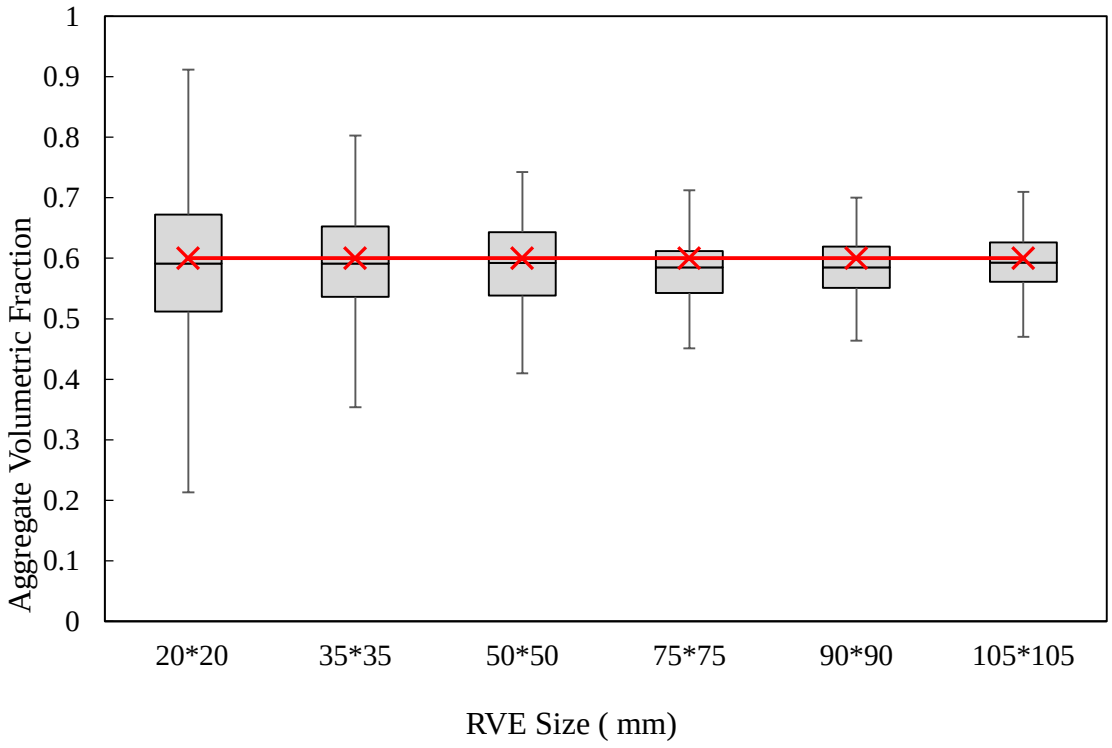

Mortar Mix 3

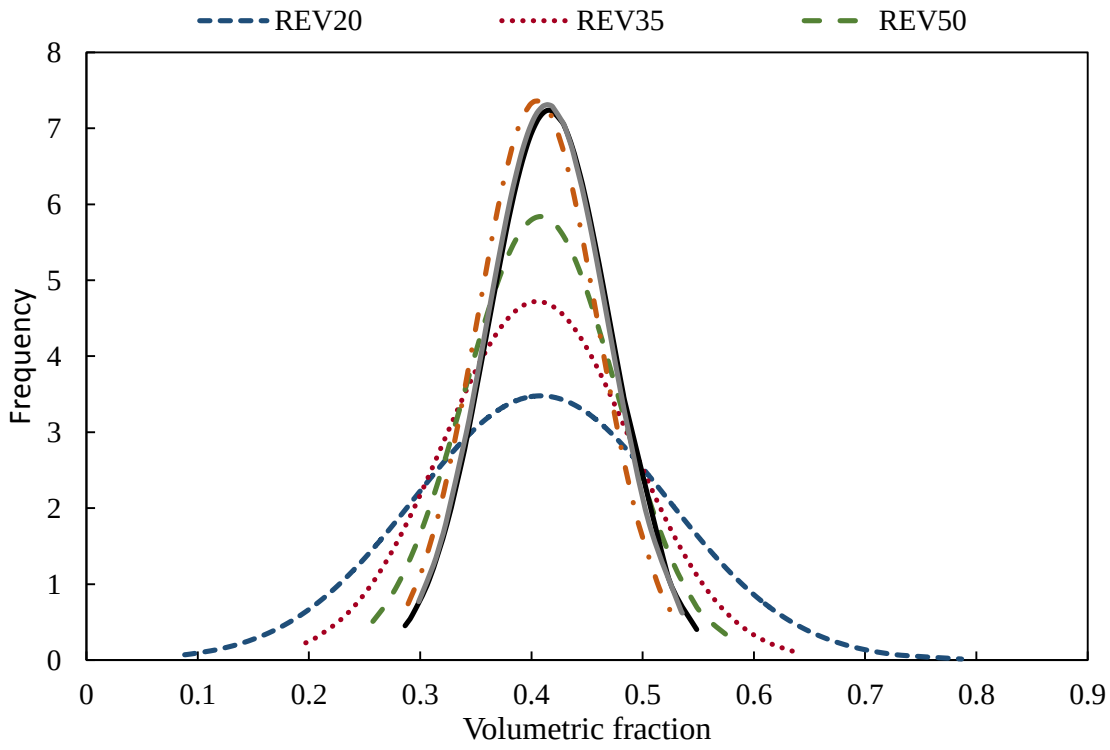
REV20
REV35
REV50
Frequency
Volumetric fraction
0
1
2
3
4
5
6
7
8
0
0.1
0.2
0.3
0.4
0.5
0.6
0.7
0.8
0.9

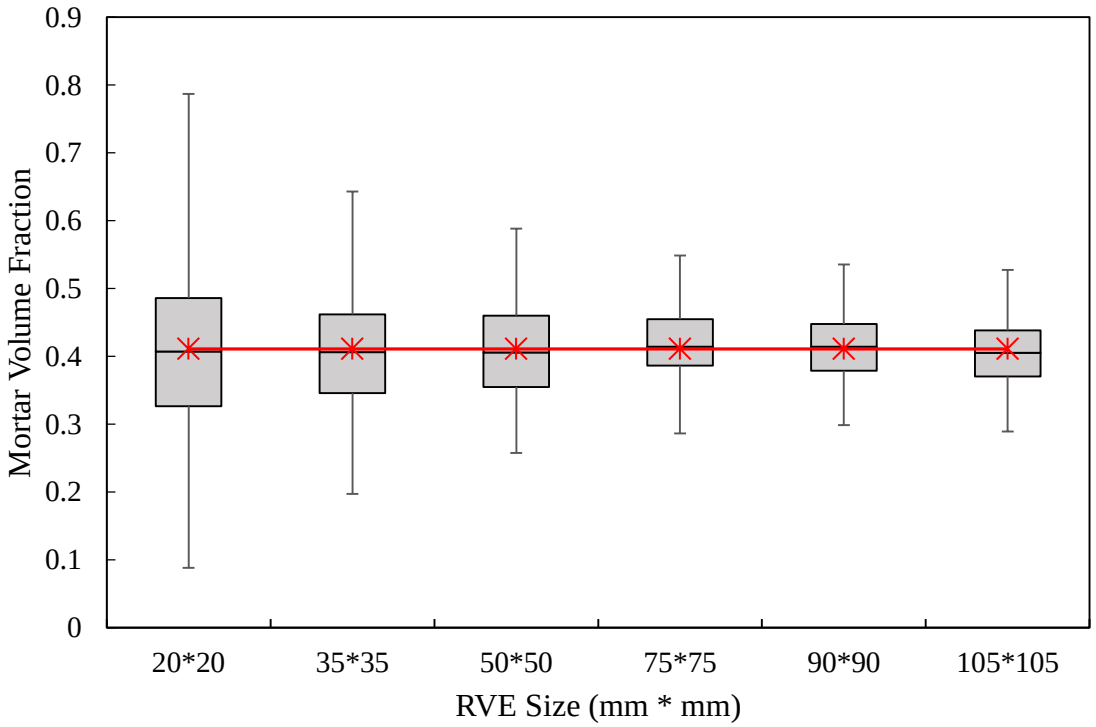
Mortar Volume Fraction
RVE Size (mm * mm)
0
0.1
0.2
0.3
0.4
0.5
0.6
0.7
0.8
0.9
20*20
35*35
50*50
75*75
90*90
105*105

ITZ- Mix1

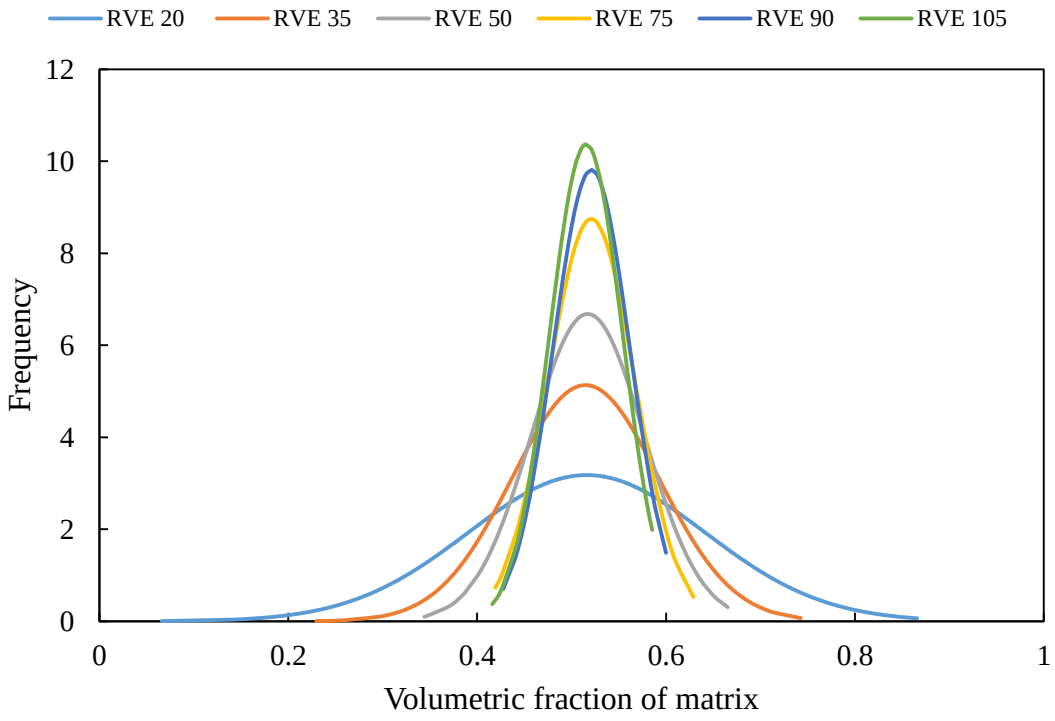
RVE 20
RVE 35
RVE 50
RVE 75
RVE 90
RVE 105
12
10
8
6
4
2
0
Frequency
0
0.2
0.4
0.6
0.8
1
Volumetric fraction of matrix

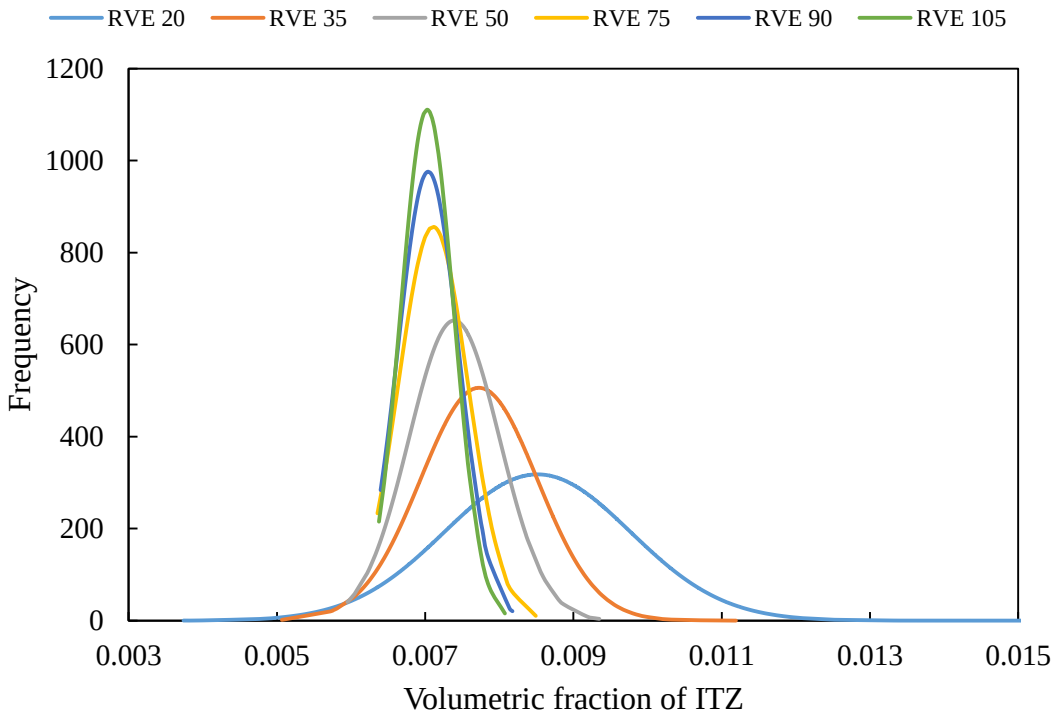
RVE 20
RVE 35
RVE 50
RVE 75
RVE 90
RVE 105
1200
1000
800
600
400
200
0
Frequency
0.003
0.005
0.007
0.009
0.011
0.013
0.015
Volumetric fraction of ITZ

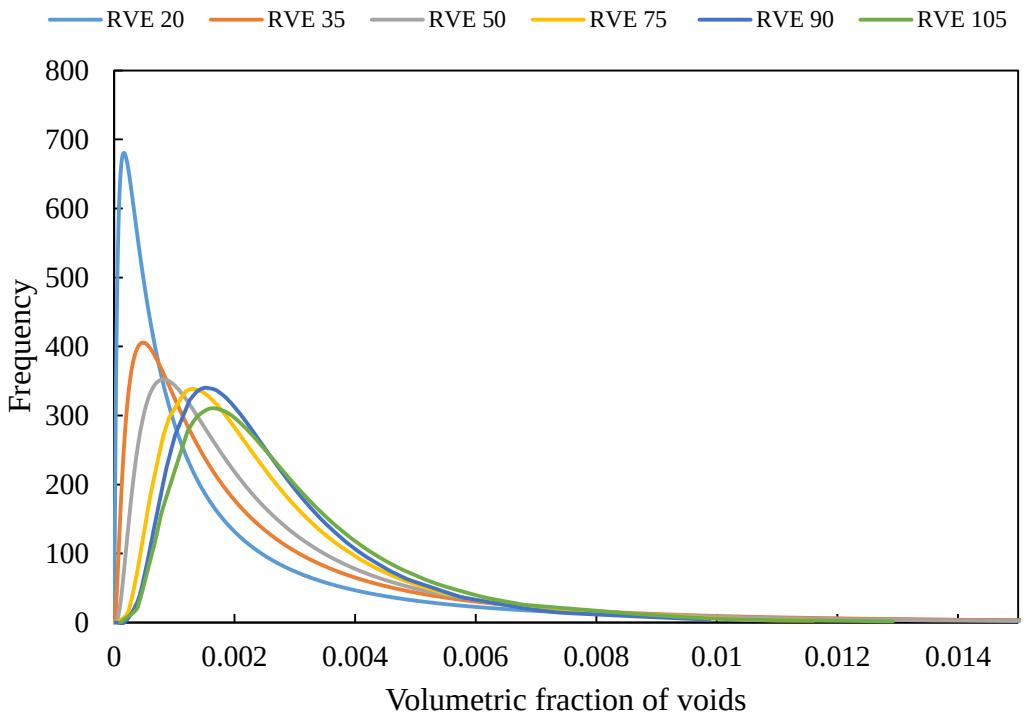
RVE 20
RVE 35
RVE 50
RVE 75
RVE 90
RVE 105
800
700
600
500
400
300
200
100
0
Frequency
0
0.002
0.004
0.006
0.008
0.01
0.012
0.014
Volumetric fraction of voids

Mix2

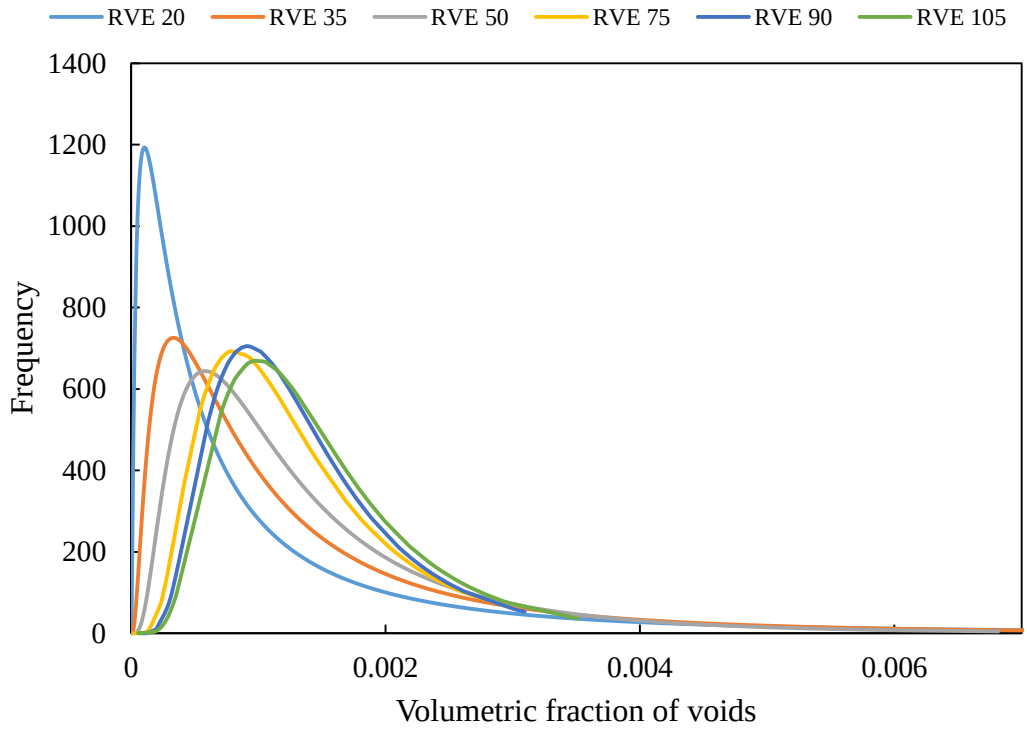
RVE 20
RVE 35
RVE 50
RVE 75
RVE 90
RVE 105
1400
1200
1000
800
600
400
200
0
Frequency
0
0.002
0.004
0.006
Volumetric fraction of voids

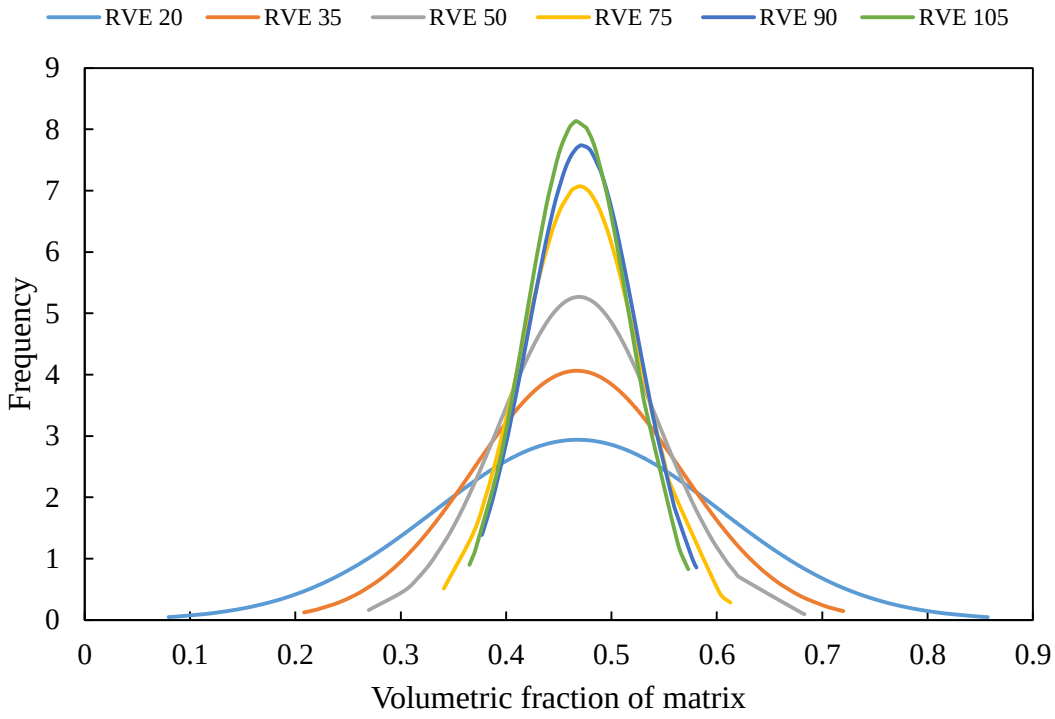
RVE 20
RVE 35
RVE 50
RVE 75
RVE 90
RVE 105
9
8
7
6
5
4
3
2
1
0
Frequency
0
0.1
0.2
0.3
0.4
0.5
0.6
0.7
0.8
0.9
Volumetric fraction of matrix

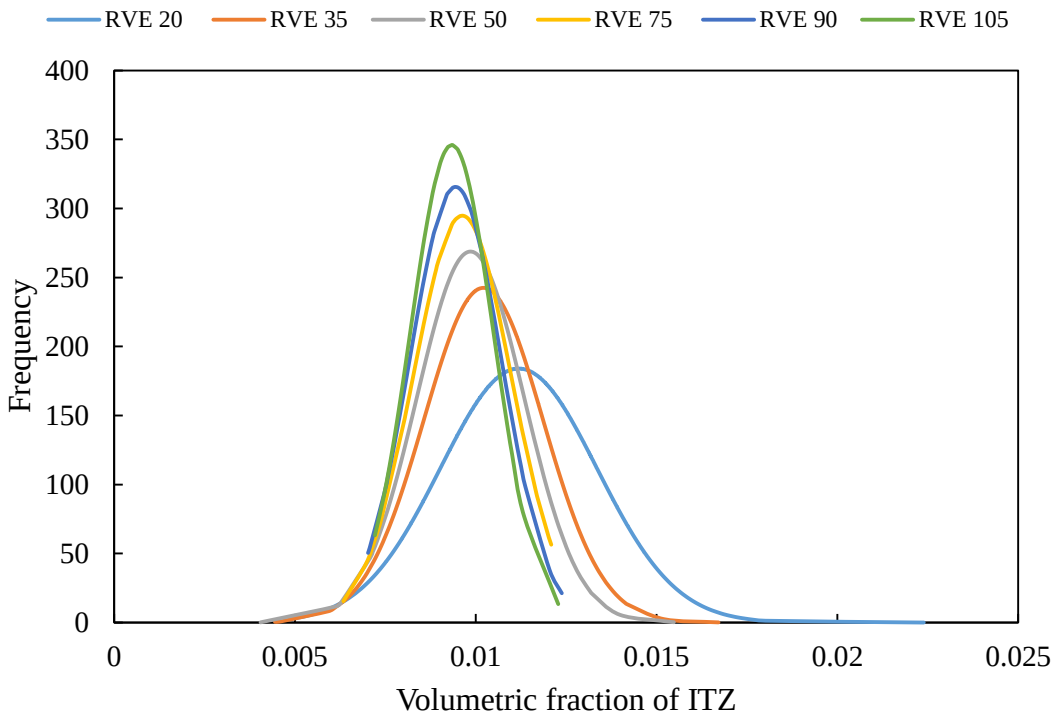
RVE 20
RVE 35
RVE 50
RVE 75
RVE 90
RVE 105
400
350
300
250
200
150
100
50
0
Frequency
0
0.005
0.01
0.015
0.02
0.025
Volumetric fraction of ITZ

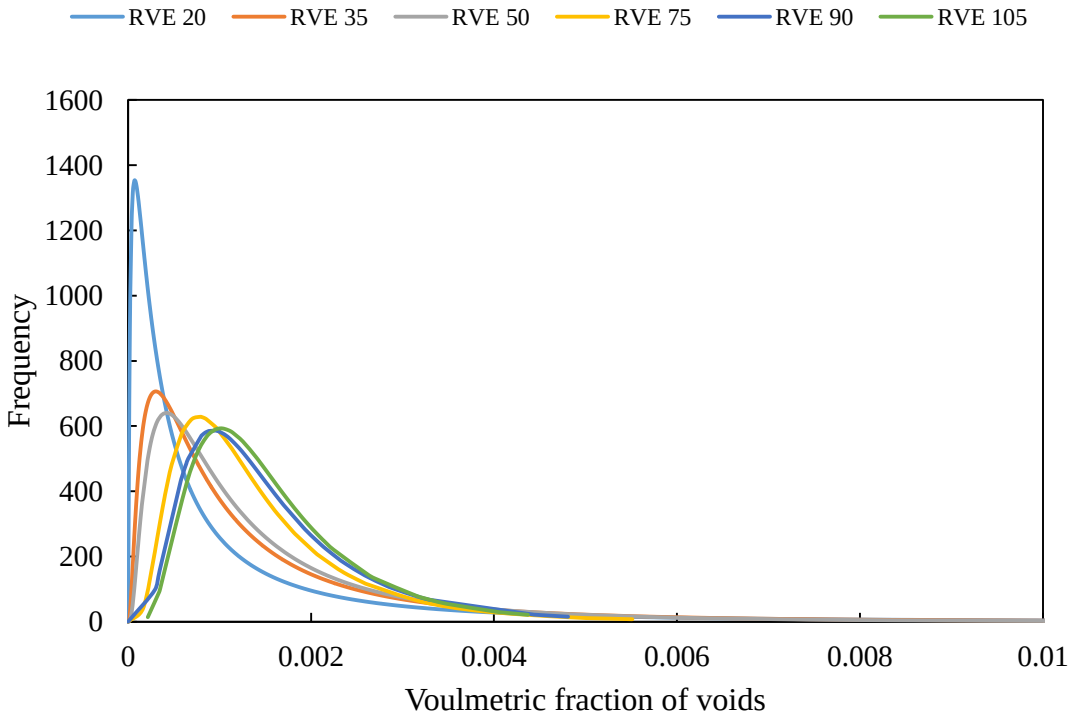
RVE 20
RVE 35
RVE 50
RVE 75
RVE 90
RVE 105
1600
1400
1200
1000
800
600
400
200
0
Frequency
0
0.002
0.004
0.006
0.008
0.01
Voulmetric fraction of voids

Mix 3

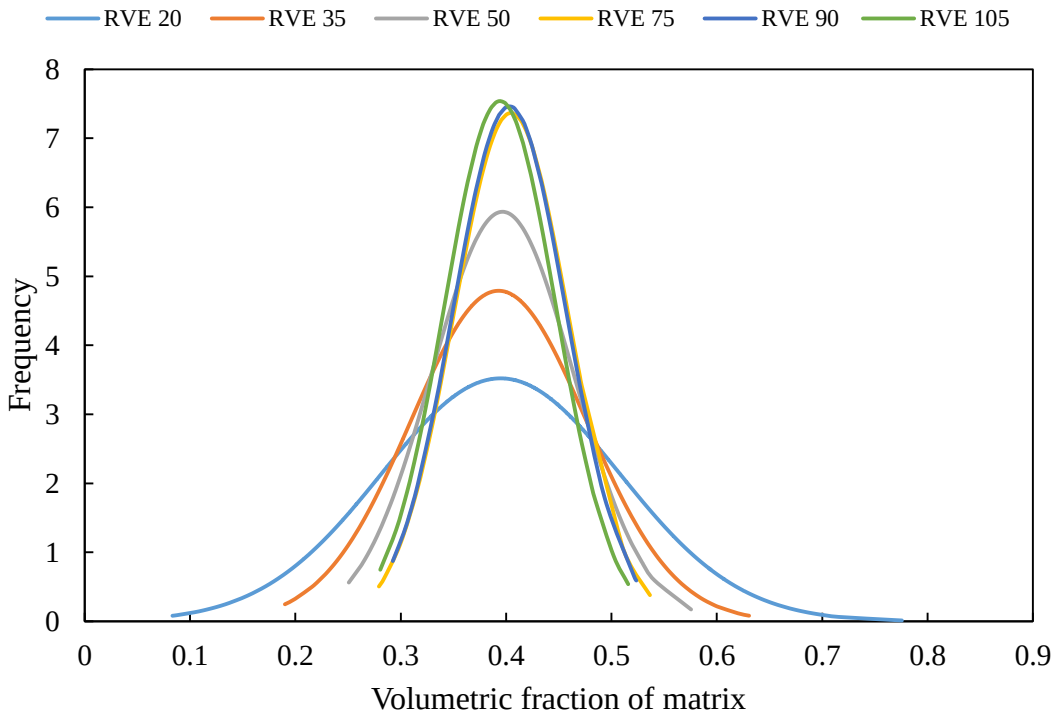
RVE 20
RVE 35
RVE 50
RVE 75
RVE 90
RVE 105
Frequency
0
1
2
3
4
5
6
7
8
0
0.1
0.2
0.3
0.4
0.5
0.6
0.7
0.8
0.9
Volumetric fraction of matrix

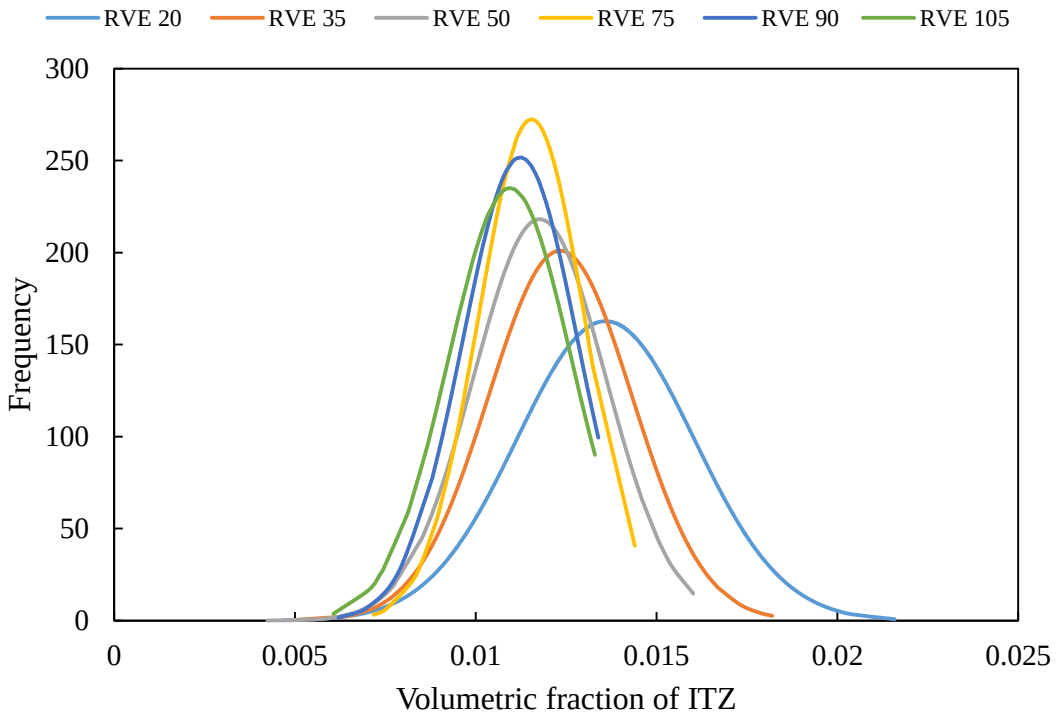
RVE 20
RVE 35
RVE 50
RVE 75
RVE 90
RVE 105
Frequency
0
50
100
150
200
250
300
0
0.005
0.01
0.015
0.02
0.025
Volumetric fraction of ITZ

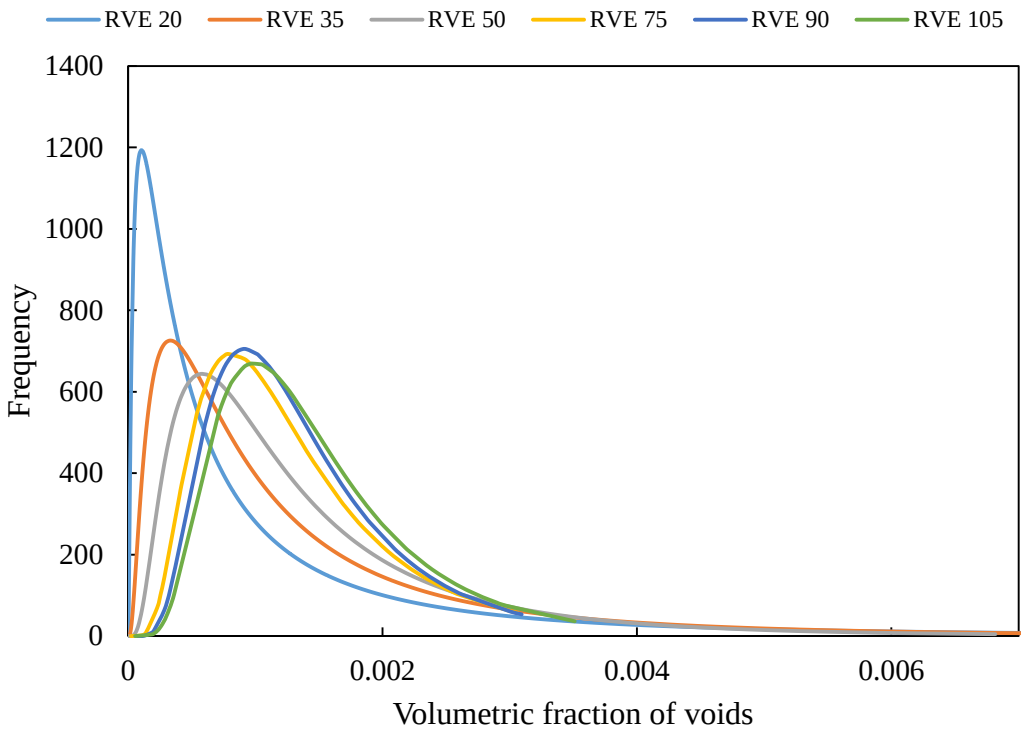
RVE 20
RVE 35
RVE 50
RVE 75
RVE 90
RVE 105
1400
1200
1000
800
600
400
200
0
Frequency
0
0.002
0.004
0.006
Volumetric fraction of voids